Brandenburgische Technische Universität Cottbus - Senftenberg

# Behaviour of Water Drop on the Insulator Surface and Study of Electric Field Distribution on Parallel Insulators under DC

Von der Fakultät für Maschinenbau, Elektrotechnik und Wirtschaftsingenieurwesen der Brandenburgischen Technischen Universität Cottbus-Senftenberg zur Erlangung des akademischen Grades eines Doktors der Ingenieurwissenschaften genehmigte Dissertation


Vorgelegt von

Master Ingenieur

Naresh Kumar Challagondla

Geboren am 02. June 1985 in Sriramgiri, Indien


Vorsitzender: Prof. Dr.-Ing. Harald Fien

Gutachter 1: Prof. Dr.-Ing. Harald Schwarz

Gutachter 2: Prof. Dr.-Ing. Dr. h. c. Heinz-Helmut Schramm

Tag der mündlichen Prüfung: 16. Februar 2015

# Acknowledgements

This work is carried out at the department of Energy Distribution and High Voltage Engineering at Brandenburg University of Technology Cottbus- Senftenberg.

First and foremost, I would like to express my special appreciation and thanks to my PhD advisor Prof. Dr.-Ing. H. Schramm for providing me with the opportunity to complete my PhD thesis. He has been supportive since the days I began working on insulators. I am very grateful for his patience, motivation, enthusiasm and immense knowledge in high voltage engineering. He has been actively interested in my work and has always been available to advise me.

I would like to thank Dr. Kynast from Siemens AG for his encouragement, constructive suggestions and interesting discussions. The financial support is provided by Siemens AG. This is gratefully acknowledged.

My sincere thanks to Prof. Harald Schwarz and Prof. Harald Fien for initiating the graduate program at TU Cottbus, participating in my dissertation committee and spending time to review my dissertation.

I thank my parents and brother for providing me support whenever I needed it. My hard working parents have given up many things for me to be in Germany. I would not have made it this far without them. In final year of my PhD I married the best person out there for me. She has been a true and great supporter. I truly thank my wife for sticking to my side, even when I was irritable and depressed.

# Abstract

With the recent developments in electrical transmission system, HVDC transmission for long distances has become feasible. With this development, many insulators are being used in HVDC system. Different kinds of insulators are situated at different places (example: desert, near to sea, agriculture area, etc.) so they will get expose to different types of pollution. Pollution affects the behavior of insulation in terms of breakdown and withstand capability. The application experience of insulators under HVDC conditions is limited. There is a necessity to understand the flashover performance and to recognize key parameters in the design and dimensioning of insulators used under HVDC conditions. This dissertation presents the difference between the analysis of partial breakdowns at AC and DC.

The dissertation explains the behavior of a water drop on insulator shed surface energized with DC. It deals with the moving water drop and hanging drop at the edge of the shed.

There are many situations where insulator structure should be in parallel. For example, the structure of insulators in vertical disconnector equipment often is parallel. If insulators are arranged in parallel, then the behavior of the electric field is totally different. It is important to know the behavior of these insulators used in HVDC system. This report also explains the pollution and non-pollution behavior of parallel insulators energized with DC.

The results can be a source of information to optimize the design and dimensioning of HVDC insulators, especially in pollution conditions.

Key words: HVDC, High-Voltage insulators, pollution performance, water drop behavior, parallel insulators, Ansys Maxwell.

# Kurzfassung

Mit den neuen Entwicklungen im Bereich der elektrischen Übertragungsnetze wurde die HGÜ für große Entfernungen ermöglicht. Durch diese Entwicklungen werden viele Isolatoren im HGÜ-System verwendet. Unterschiedliche Arten von Isolatoren werden an verschiedenen Orten eingesetzt (z.B.: in der Wüste, in der Nähe vom Meer, im landwirtschaftlichen Bereich, etc.), wodurch sie auch unterschiedlicher Verschmutzung ausgesetzt werden. Die Verschmutzung beeinflusst das Verhalten der Isolation in Bezug auf ihre Belastbarkeit und ihr Versagen. Die praktischen Erfahrungen mit Isolatoren unter HGÜ-Bedingungen sind begrenzt. Es ist erforderlich das Überschlagverhalten zu verstehen und die wichtigen Parameter für die Auslegung und Dimensionierung von Isolatoren unter HGÜ Bedingungen zu erkennen. Diese Dissertation stellt den Unterschied zwischen Teilentladungen bei AC und DC dar.

Die Dissertation erklärt das Verhalten eines Wassertropfens auf der Schirm Oberfläche des Isolators bei angelegter DC Spannung. Sie befasst sich mit bewegten Wassertropfen und hängenden Tropfen am Rand des Schirms.

Es gibt viele Situationen, in denen eine parallele Isolator-Struktur erforderlich ist. Zum Beispiel kommt in vertikalen Trennschaltern eine parallele Struktur der Isolatoren vor. Wenn Isolatoren parallel angeordnet sind, ist das Verhalten des elektrischen Feldes völlig unterschiedlich. Es ist wichtig, das Verhalten der Isolatoren in der HGÜ-Anlage zu kennen. Dieser Bericht erklärt auch das Verhalten bei der Verschmutzung und im verschmutzungsfreien Zustand von parallelen Isolatoren unter DC Spannung.

Die Ergebnisse können als Informationsquelle verwendet werden, um die Auslegung und Dimensionierung von HGÜ-Isolatoren, insbesondere bei Verschmutzung, zu optimieren.

Schlüsselwörter: HGÜ, Hochspannungsisolatoren, Verhalten bei Verschmutzung, Verhalten bei Wassertropfen, parallele Isolatoren, Ansys Maxwell.

# Contents

# 1 Introduction

## 1.1 General Information

We know that there has been a need for electrical insulation since the time of discovery of electricity. The electric power demand is increasing day by day due to more consumption of power in the private and the industrial sectors. As the voltage level gets higher, the problem of finding suitable insulation becomes more complex and critical. As the level of transmission voltage is increased, switching and lightning impulse voltages as well as withstand ability of the insulator under polluted conditions are important factors which determine the insulation level of the system. The reliability of the system mainly depends on the environmental and weather conditions which cause flashover on polluted insulators leading to system outages.

It is generally recognized that the main events leading to flashover of polluted insulators under service voltage are caused by adverse environmental conditions, as some pollution layer is deposited on the insulator surface. A wet conducting path is formed due to dew deposition of light rain and then leakage current begins to flow on the insulator surface. The surface layer is heated which causes an increase in the conductivity and the leakage current. The heating results in local drying of the surface layer, and so called ‘’dry bands’’ occur. Partial arcs bridge the dry bands on the insulators. The partial discharges increase with a number of streamer discharges and glows occur across those dry bands having the highest potential gradient. These discharges also cause audible noise. Finally the partial streamer discharges (partial flashovers) are connected in series, and a complete flashover occurs. Because of this effect, pollution monitoring on the insulator surface is important for the proper design of the insulators for establishing adequate maintenance systems, and for defining effective countermeasures against pollution flashover.

As the advantages for HVDC transmission are higher than those of HVAC for long distances, a large amount of the power is transmitted through HVDC and UHVDC links. Many of the insulators in converter stations and transmission lines are under HVDC

stress. Examples which use HVDC connections for transmission of electrical power from generating station to power distribution station are shown below. Figure 1.1 shows the ±800 kV UHVDC which is the world's longest transmission link between Xiangjiaba and Shanghai in China.


Figure 1.1: ±800 kV UHVDC transmission line in China

Figure 1.2 shows the ±500kV HVDC line from Mundra in Gujarat to Mohindergarh near New Delhi in the power deficit state of Haryana.

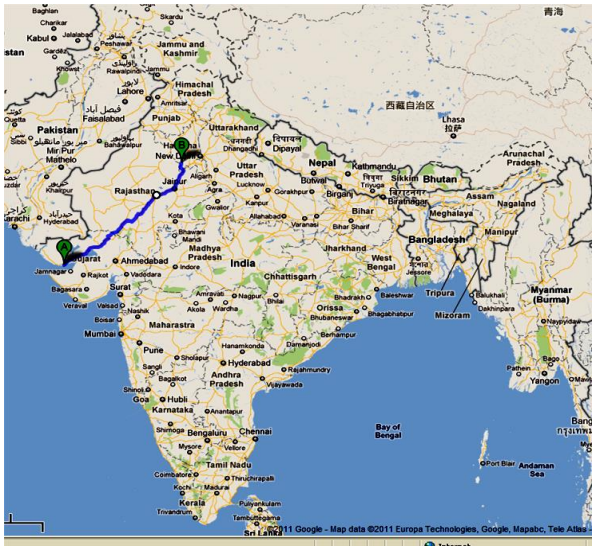


Figure 1.2: ±500kV HVDC line in India

Figure 1.3 shows the large scale offshore wind farm cluster in the North Sea to the Germany power grid. It helps Germany towards its target of 35 percent renewable electricity by 2020.

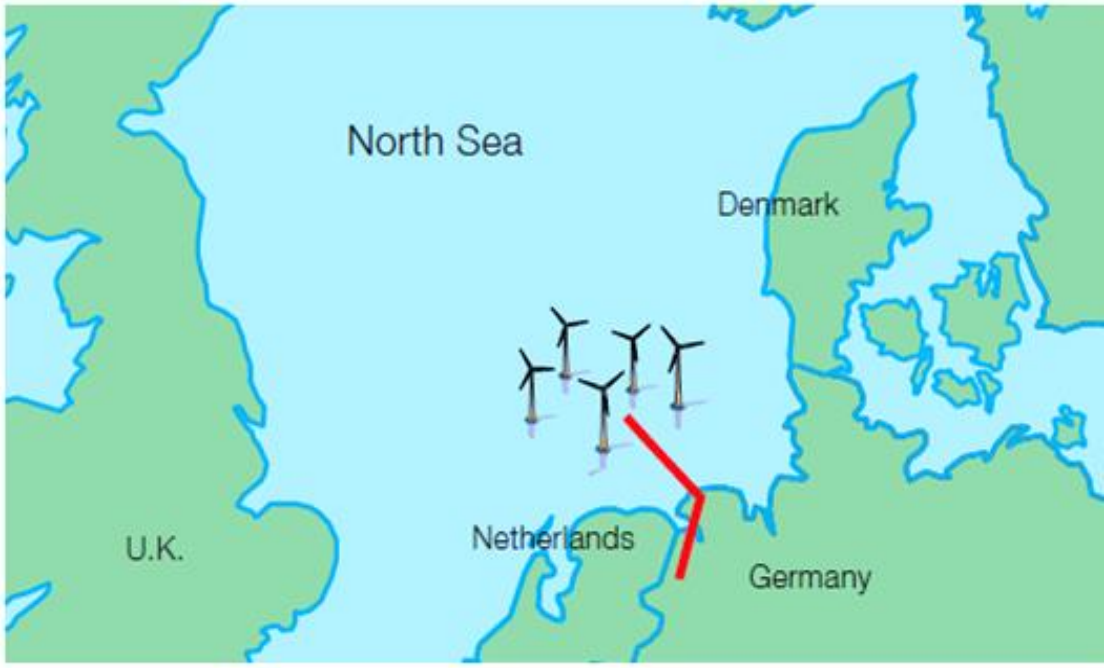


Figure 1.3: HVDC link between offshore wind farms to Germany grid

Pollution behavior of insulators under HVDC stress is different from HVAC stress because of large contamination due to electrostatic forces and long duration of partial arcs. It is very important to know this behavior because the flashover of polluted insulators can cause power outage of long duration over a large area. Pollution flashover is playing an important role in the design of transmission lines and converting stations, especially used in DC system.

There is still so much research work to be done on the polluted insulators to know the behavior of them under HVDC stress. There are many issues to discuss about polluted insulators. There are also some cases where insulator structures are in parallel. This can be on transmission lines or in substation equipment. Some examples which show parallel insulator structures are displayed in figures 1.4-1.7.

Figure 1.4: Parallel insulators used in transmission line

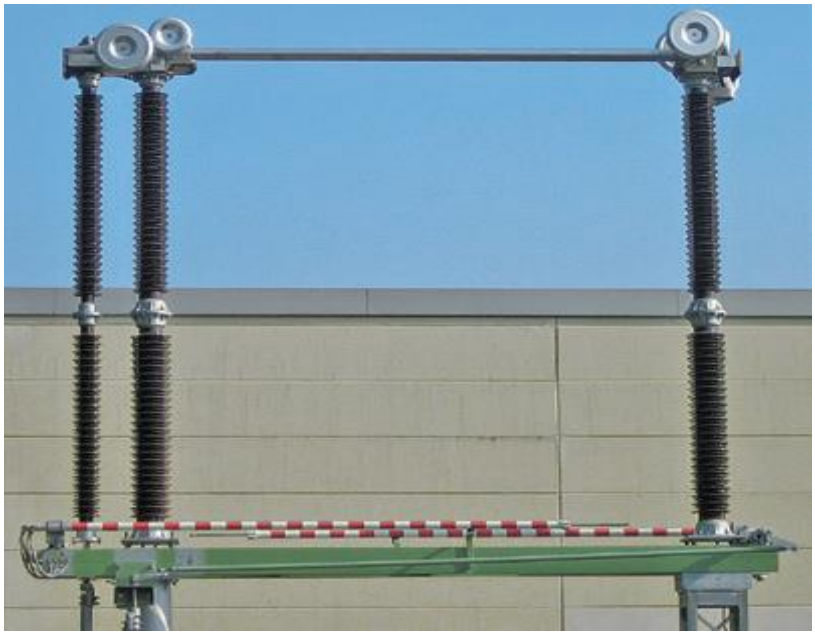

Figure 1.5: Vertical break disconnector

Figure 1.6: Pantograph disconnectors

Figure 1.7: Knee type disconnectors

No research on the insulators when they are in parallel under HVDC has been done. This is one of the issues discussed in this report. This dissertation concentrates mainly on two issues. One is the behavior of a water drop on the insulator surface under DC stress, and the other issue is the behavior of parallel insulators under DC stress. Simulation work has been done on those two problems. The theory regarding water drop behavior and flashover mechanism is also explained in the dissertation.

## 1.2 Organization of Work

Extensive work has been carried out in the last few decades to know the behavior of polluted insulators under AC stress. There are only few literature sources available which tried to explain the behavior of polluted insulators under DC stress. Also there are some literatures available to explain the behavior of water drops on the insulator surface under AC stress. However, there is no description for the behavior of a water drop on the insulator shed surface under DC stress. This dissertation explains the behavior of a moving water drop on porcelain and composite insulator sheds. It also shows the effect of a hanging water drop at the end of an insulator shed.

There has been no research done on the polluted insulators when two insulators are in parallel. This dissertation shows the behavior of parallel polluted insulators under DC stress. A simple model for parallel insulators has been created and explains the electric field between and outside of the two insulators.

Introduction and the brief description of insulators and pollution environments are explained in chapter 1 and 2. A detailed theory about the software considered for the simulation and the important parameters considered in the software are explained in chapter 3.

The characteristic of partial discharges under AC is well known. There are so many publications about the detection and evaluation of partial discharge parameters at AC voltage. However, there is a little knowledge about characteristics of partial discharge at DC voltage. The theory part of the partial discharges at DC voltage which is different from the partial discharges at AC voltage is explained in chapter 4.

In chapters 5 and 6, the behavior of a water drop under DC stress and simulation results on a water drop placed on the porcelain and composite insulator sheds are presented.

Chapter 7 demonstrates the behavior of parallel insulators with and without pollution. The difference in performance of parallel insulators when compared to a single insulator is explained in chapter 7.1. Electric field performance on the surfaces of parallel insulators is discussed in chapter 7.2. Then chapter 7.3 illustrates the study of the electric field on parallel insulators with and without pollution. The critical position between the parallel insulators is shown in chapter 7.4. Finally some conclusions are briefly given in chapter 7.5.

Results, discussions and recommendations for future work are illustrated in chapters 8.

# 2 Basic Knowledge

This chapter deals with the insulators and the problems encountered with them.

## 2.1 Types of Insulators

Based on the usage there are two types of insulators available. They are line insulators and post insulators. There is a clear explanation in the following chapters.

### 2.1.1 Line Insulators

Line insulators are used to insulate the tower or pole from the live electrical line. These line insulators may consist of a string of insulator units, depending on the insulator types and application. Generally if the line voltage increases, more insulator units are used in the string.

The overhead line insulators are mostly made of the following materials
1) Porcelain insulators, which are ceramic materials made by heating raw materials, generally including clay in the form of kaolin, in an oven up to temperatures between 1,200°C (2,192°F ) and 1,400°C (2,552 °F). Some insulators made of porcelain are shown in following figures (figures 2.1 to 2.3)

Figure 2.1: 10 kV insulator

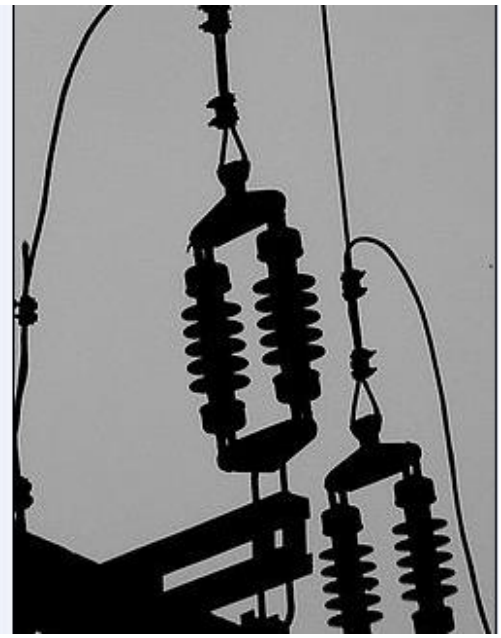

Figure 2.2: Porcelain insulators for power line

Figure 2.3: Porcelain insulator at railways

2) Glass insulators, which are used for disc and pin types. Thermal stability of this material is consistent up to 538°C. Insulator made of glass is shown in figure 2.4

Figure 2.4: Suspended glass disk insulator unit used in cap and pin insulator strings for high voltage transmission lines

3) Composite polymer insulators, which may be a combination of fiberglass, plastic and resin. These are sometimes used for the long rod and post type insulators and have been in service for more than 25 years. A modern composite insulator core consists of glass fibers in a resin based matrix to achieve maximum tensile strength.

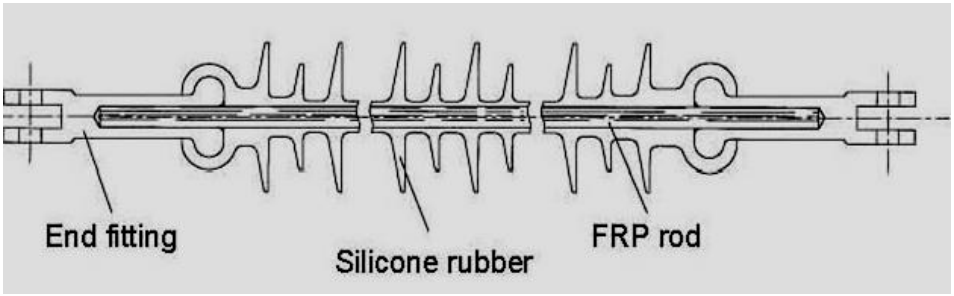


Figure 2.5: Synthetic composite insulator

To strengthen the structure of insulator, we use a FRP rod (fiber reinforced polymer). The housing in figure 2.5 that encloses silicon rubber also forms the weather sheds and may be hydrophobic (water repellent), which helps to reduce leakage current. Some housings are designed to remain hydrophobic when polluted, giving composite

synthetics a distinct advantage over porcelain types. Some composite insulators which are used for distribution overhead power lines and transmission overhead power lines are shown in figure 2.6.

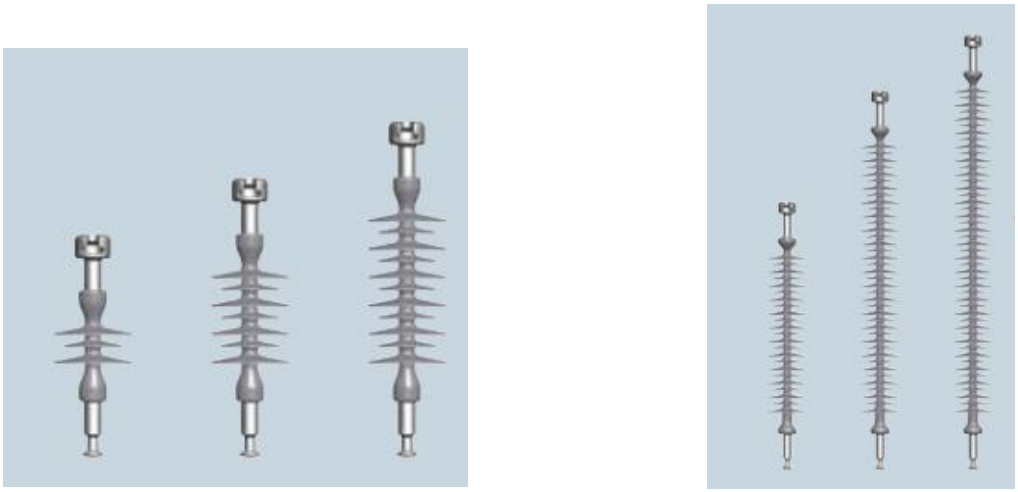

Figure 2.6: Long rod insulators for distribution and transmission overhead power lines

4) Plasticized wood insulators also referred to as polymer concrete has been used for medium voltage line insulators. These are shown in figure 2.7. Although uncommon, there are a number of insulator styles made from wood. The best known and most desirable wood insulators are made from the dense wood lignum vitae for the San Francisco trolley system. Since these designs utilize organic material, there have been concerns about material life span [FRE 2000].

Figure 2.7: Insulators made up of wood

### 2.1.2 Post Insulators

Most of the post insulators are used in electrical substations and they are manufactured from porcelain or composite insulating materials. Post insulators have metal bolts which are made of aluminum alloy. These are called flanges. Mainly post insulators are used in substations to insulate high voltage switchgear and transformers. Some examples of post insulators are shown in figures 2.8 and 2.9.

Figure 2.8: Post insulators made of porcelain

Figure 2.9: Post insulator made of composite materials

## 2.2 Classes of Pollution

According to IEC standards [IEC 2008], there are two main basic types of insulator pollution which may lead to flashover. Those two types are type A and type B which are explained below.

**Type A (Solid Pollution)**

Solid pollution with non-soluble components deposited on the insulator surface. A wet conducting path is formed when moisture is present due to dew deposition or light rain and leakage current begins to flow on the insulator surface. This type of pollution can be characterized by ESDD/NSDD (equivalent salt deposit density/ non soluble deposit density) and DDGIS/DDGIN (dust deposit gauge index soluble/ dust deposit gauge index non soluble). The ESDD of a solid pollution layer may also be evaluated by surface conductivity under controlled wetting conditions.

Type A pollution is most often associated with inland, desert or industrially polluted areas. It can also arise in coastal areas in cases where a dry salt layer builds and then rapidly becomes wetted by dew, mist, fog or drizzle.

Type A pollution has two main components, namely soluble pollution that forms a conductive layer when wetted, and non-soluble pollution that forms a binding layer for soluble pollution. These are described in the following paragraph.

Soluble pollution is subdivided into high solubility salts (e.g. salts which dissolve readily into water) and low solubility salts (e.g. hardly soluble salts). Soluble pollution is measured in terms of equivalent salt deposit density (ESDD) in $mg/cm^2$. Examples of non soluble pollutions are dust, sand, clay, oil, etc. Non soluble pollution is measured in terms of non-soluble deposit density (NSDD) in $mg/cm^2$.

**Type B (Liquid Pollution)**

Liquid electrolytes deposited on the insulator with very little or no non-soluble components. This type of pollution can be best characterized by conductance or leakage current measurements.

Type B pollution is most often associated with coastal areas where salt water or conductive fog is deposited onto the insulator surface. Other sources of type B pollutions are crop spraying, chemical mists and acid rain.

## 2.3 Types of Environments

Environments are described by the following five types. These types are describing the typical pollution characteristics for a region. Examples of the type of pollution (A or B) for a particular environment are explained below. In practice most polluted environments comprise more than one of these types, for example coastal regions with sandy beaches. In these cases it is important to determine which pollution type (A or B) is dominant.

**Desert type environments**

These are areas which are characterized by sandy soils with extended periods of dry conditions. The pollution layer in these areas normally comprises salts that dissolve slowly in combination with a high NSDD level (type A). The insulators are polluted mainly by wind borne pollution. Natural cleaning can occur under the infrequent periods of rain or by “sand blasting” during strong wind conditions. Infrequent rain combined with the slow dissolving salts causes natural cleaning to be less effective. Critical wetting,

which poses a risk for insulator flashover, can occur frequently in the form of dew on the insulators.

In recent publications, there have been reports of contamination levels as much as 1.4 $mg/cm^2$ at measuring sites in desert places [INM 2014]. Such contamination levels fall beyond the typical ranges considered in the relevant international standard [IEC 2008]. Application of ceramic insulators with the specific creepage distance provided in recent standards (i.e. 31 mm/kV phase-to-phase voltage or 53.7 mm/kV phase-to-ground) has proven insufficient in many of these problematic service areas.

**Coastal type environments**

These areas are typically in the direct vicinity of the coast, but in some cases, depending on topography, they can be as far as 50 km inland. Pollution is deposited onto the insulators mainly by spray, wind and fog. The pollution build-up is generally rapid, especially during spray or conductive fog conditions (type B). A build-up of pollution over a longer term can also occur through a deposit of wind-borne particles, where the pollution layer on the insulators consists of quick dissolving salts with a degree of inert component (type A) which depends on the local ground characteristics. Natural cleaning of the insulators is typically effective as the active pollution consists mainly of fast dissolving salts

**Industrial type environments**

These are areas located in close proximity to an industrial pollution source, and may effect only few installations. The pollution layer may constitute conductive particulate pollution, such as coal, metallic deposits; or dissolved gasses, such as NOx, SOx (type B); or pollution that dissolves slowly, such as cement, gypsum (type A). The pollution layer may have a medium to high inert component (medium to high NSDD) (type A). The effectiveness of natural cleaning in industrial areas can vary greatly depending on the type of pollution present. The pollution often consists of heavy particles which settle on horizontal surfaces.

**Agriculture type environments**

These are areas which are situated in the vicinity of agricultural activity. Typically there will be areas subjected to ploughing (type A) or crop spraying (type B). The pollution layer on the insulators consists mostly of fast or slowly dissolving salts such as chemicals, bird droppings or salts present in the soil. The pollution layer will normally have a medium to high inert component (medium to high NSDD). Natural cleaning of the insulators can be quite effective depending on the type of salt deposited. The pollution often consists of heavy particles which settle on the horizontal surface. But it may also be wind borne pollution.

**Inland type environments**

Areas with a low level of pollution without any clearly identified sources of pollution.

## 2.4 Necessities for the Study of Polluted Insulators under DC

There are many literatures which explain the behavior of polluted insulators under AC. Only few literature sources explain the behavior of polluted insulators under DC stress. DC energized insulators gather more pollution because of the electrostatic attraction of pollution particles under the unidirectional electric field. This is even dominated by an aerodynamic profile of the insulator. On the other hand, there is little or no attraction of pollutants by the alternating electric field on the insulators energized with AC. Research measurements suggest that the ratio of DC to AC pollution deposition in the same service environment can vary significantly - in some cases as much as factor 10 [INMR 2014]. The difference in flashover voltage (FOV) for AC and DC with respect to pollution is shown in below figure 2.10.

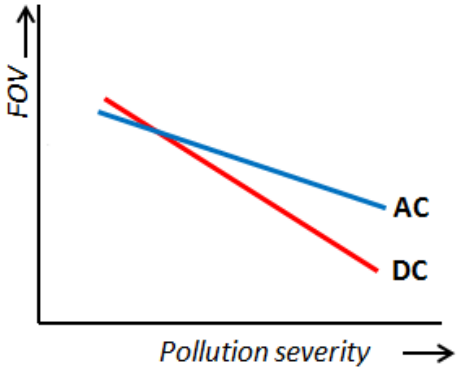


Figure 2.10: Relative AC versus DC pollution flashover voltage (FOV) as a function of pollution severity

There is no voltage zero in DC therefore dry band arcing under DC stress is more likely to grow into flashover. In case of AC, dry band arcs must reignite after each voltage zero. DC dry band arcs are also more mobile and likely to leave the insulator surface and can propagate through air [CWG 2012]. It is shown in figure 2.11. This causes an easy ionization of air which leads to streamer discharges. There are important differences between the developments of pollution flashover under DC energization when compared with AC energization. For AC systems the insulator design depends on lightning or switching performance of the line or substation. In case of DC systems, the important parameter for insulation design is the pollution performance. Therefore, it is very significant to study the polluted insulators under DC.

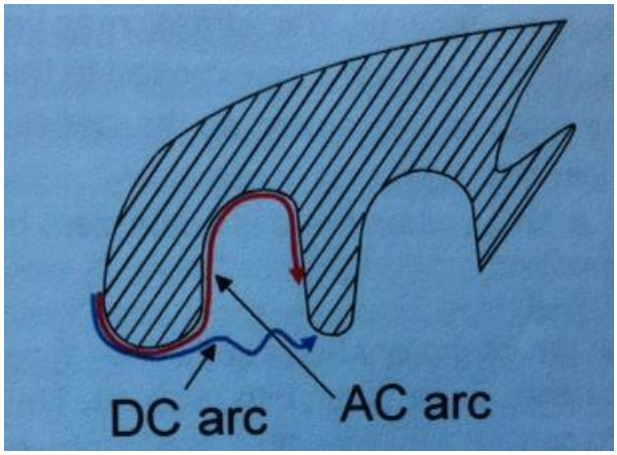


Figure 2.11: Schematic representation of arc propagation under DC and AC voltage

# 3 Modeling and Simulation Tools

This chapter explains the simulation software, Mesh and boundary settings in the software for the simulation.

## 3.1 Simulation Software

There are different kinds of electrical simulation software available in the market. All the available software calculation methods can be classified into two: integral equation methods and differential methods. The integral equation methods include the charge simulation method (CSM) and the boundary element method (BEM). The differential methods comprise the finite element method (FEM) and the finite difference method (FDM) [SIN 1995]. This is shown in the flow chart (figure 3.1).

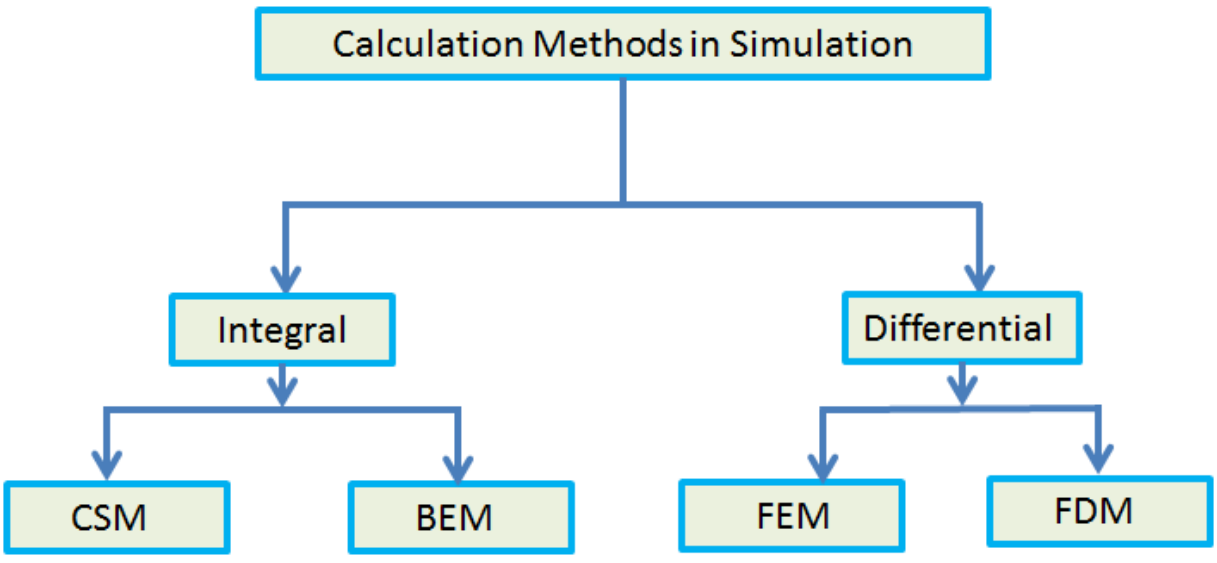


Figure 3.1: Representation of flow chart for calculation methods used in simulation

In the integral methods fictitious charge distributions are either positioned inside the electrodes or on the electrode boundaries. In these methods only the boundary surfaces are discretized and they are, therefore, suggested for three dimensional problems with unbounded space. The differential methods involve the total solution space to be

subdivided into triangular elements and are therefore preferably suited to boundary problems [SIN 1995]. BEM and FEM have become the two dominant numerical techniques in computer-aided engineering (CAE). In the differential method, FEM is the most common calculation method used by many software. The basic difference between BEM and FEM is that BEM is needed to solve for unknowns on the boundaries, whereas FEM solves for unknowns in the volume. In this project the Ansys Maxwell software which uses FEM method is used to get the simulation results on insulators. For a given design, the FEM needs the entire geometry, including the surrounding region to be modeled with finite elements. These finite elements are explained in the chapter 3.1.2. A system of linear equations is generated to calculate the potential distribution at the nodes of each element. The main reason to use the FEM is its ability to solve quite simply problems that are distinct on complex geometries.

### 3.1.1 Ansys Maxwell & Solver Types

Ansys is one of the electrical simulation software available in the market. It uses the finite element method to calculate the simulation results. In the commercial FEM package Ansys Maxwell is used to analyze the water drops and pollution layer over the insulators. Ansys Maxwell is based on the following Maxwell equations (equations 3.1 to 3.4) to solve the electromagnetic fields in the solving region.

$$\nabla \times H = J + \frac{\partial D}{\partial t} \qquad (3.1)$$

$$\nabla \times E = -\frac{\partial B}{\partial t} \qquad (3.2)$$

$$\nabla \cdot D = \rho \qquad (3.3)$$

$$\nabla \cdot B = 0 \qquad (3.4)$$

Where

E is the electric field

D is the electric displacement

B is the magnetic flux density

H is the magnetic field intensity

J is the conduction current density

$\rho$ is the charge density

This software has different solution types for different kind of problems. The solvers available for 2D are shown in figure 3.2.

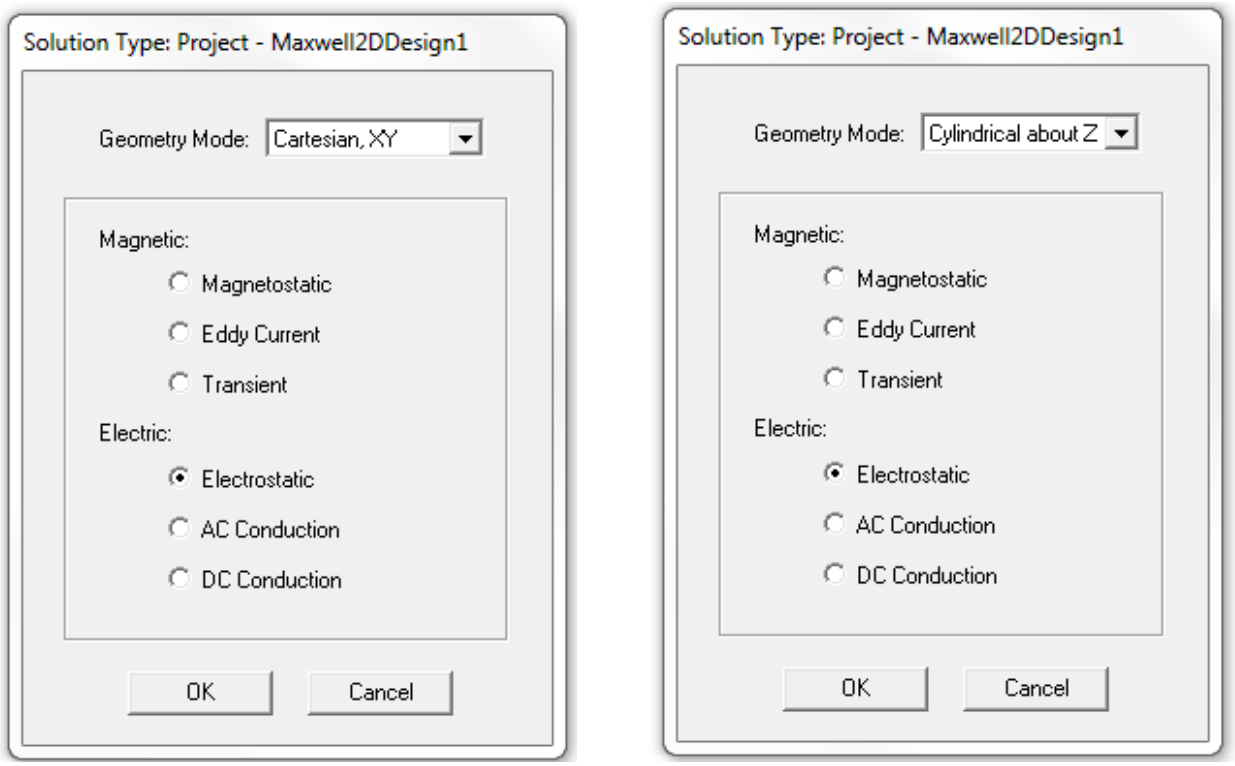


(a) (b)

Figure 3.2: Solver types for Cartesian (a) and cylindrical (b) geometry in Ansys Maxwell 2D

An electrostatic solver is helpful to know the voltage and electric field distributions over an insulator. AC conduction and DC conduction solvers are useful to know the behavior of a pollution layer (with certain conductivity) accumulated on the insulator surface and to understand the behavior of insulators under AC and DC voltages. Here one can observe that there are two types of geometries available in the solvers. One is the Cartesian XY and the other is the Cylindrical about Z. For normal insulators or bushings it is better to use “Cylindrical about Z” as the insulator or bushing is a cylindrical structure and has rotational symmetry with an axis Z. It assumes that the insulator model sweeps 360° around the z- axis of a cylindrical coordinate system. When it comes to solver types for three dimensional (3D) models, Ansys Maxwell has the following solvers shown in figure 3.3.

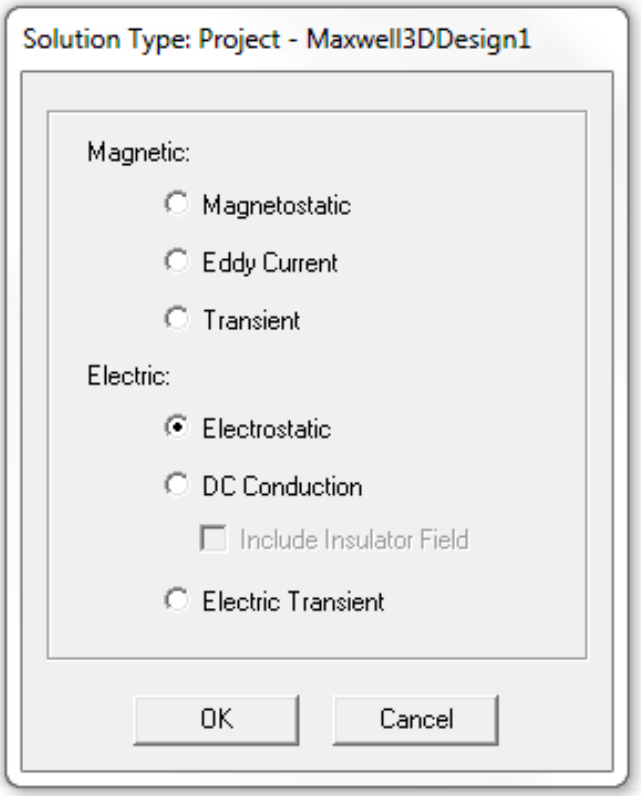


Figure 3.3: Solver types for 3D models

After observing 2D and 3D solvers (from figures 3.2 and 3.3) one could say that there is no “AC Conduction” for 3D models and there is no “Electric Transient” for 2D models. Moreover there is no option of “Including insulator field” for a “DC Conduction” solver in 2D. Generally conduction solvers (AC conduction and DC conduction) are used to simulate the conductive layers. Example: to simulate a thin pollution layer (with conductivity more than 0) over the insulator surface. There is no possibility to compare AC and DC results for 3D models as the solver “AC conduction” is not available for 3D. This is the main drawback in Ansys Maxwell. The simulation of a water drop on the insulator surface and simulation of the parallel insulators have been done using the solver “DC Conduction” with the option “Including insulator field”. It is shown in figure 3.4.

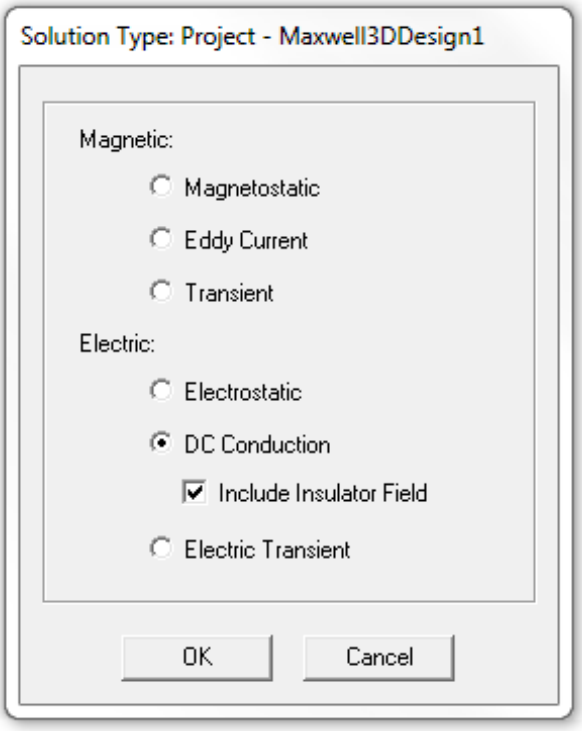


Figure 3.4: Solver used for the simulation

The solver “DC Conduction” computes the electric fields on insulators due to the applied potentials. The quantity for which the electric conduction field simulator resolves is the electric potential. The electric field and the current density are spontaneously calculated from the potential. The resistance matrix, a derived quantity, may be calculated from these basic field quantities. The theory of DC conduction is as follows.

When a material with a non-zero conductivity is subjected to a potential difference, conduction current flows in that material. At all points in the problem space the current density (J) will be proportional to the electric field (E) that is established due to the potential difference (equation3.5).

$$J(x,y) = \sigma E(x,y) = -\sigma \nabla \varphi(x,y) \qquad (3.5)$$

Where

$J(x,y)$ is the current density

$E(x,y)$ is the electric field

$\sigma$ is the conductivity

$\varphi$(x,y) is the electric potential

The equation that the DC conduction field simulator solves is based on the fact that, under steady state conditions, the amount of charge leaving any infinitesimally small region must equal the charge flowing into that region.

$$\nabla \cdot J = -\frac{\partial \rho}{\partial t} = 0 \qquad (3.6)$$

The field quantity that DC conduction actually solves for is the electrical potential $\varphi$ in the following equation

$$\nabla \cdot (\sigma \nabla \varphi) = 0 \qquad (3.7)$$

Note that -$\sigma \nabla \varphi = J$

An example for a plot of the electric potential computed by the “DC Conduction” solver is shown in figure 3.5.

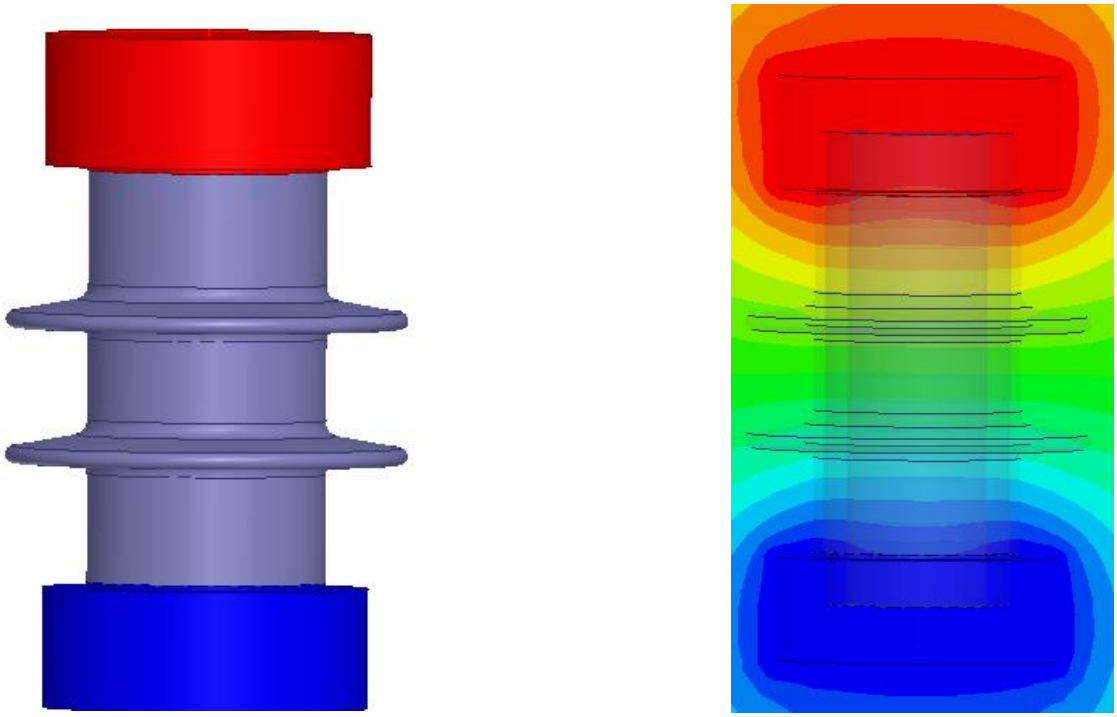

(a) (b)

Figure 3.5: Insulator model (a) and potential deviation plot (b) with “DC conduction” solver

### 3.1.2 Mesh & Boundary Settings

Finite element analysis is a numerical method for approximating the solution of linear partial differential equations (some nonlinearity can be accommodated). To predict the

degree of freedom of the values throughout a model, the spatial domain of a model is broken down into a finite number of elements. Individual elements are defined by points in space called nodes. Elements connect to each other via shared nodes in space. Finite elements can fit distorted geometries.

The degree of freedom values at an individual element's nodes are related to loads on the element by a set of linear algebraic equations. The equations are based on assumed interpolation functions (shape functions) for the degree of freedom values inside an element as a function of values at nodes, spatial coordinates and consideration of material properties of the model domain. Just as the elements fit together via shared nodes to form the spatial shape of a model, the linear algebraic equations are linked together into a large global set of linear algebraic equations for the behavior of the entire model. Methods for solving these simultaneous linear equations in a computer include direct methods by decomposition, and iterative methods that iteratively improve an approximation of the solution. The solution method choice is influenced by the element type and model size.

Ansys Maxwell mesh creator can create a mesh according to predefined mesh operations. A mesh operation defines one or more conditions for some selected objects for mesh maker to create meshes that satisfy the conditions. Maxwell generates an initial mesh, which includes surface approximation. If necessary, the mesher will automatically perform any repairs needed to recover an accurate mesh representation of the model. The solution profile will indicate when mesh repairs have been made, and the results of these repairs will be displayed per object in the mesh statistics window. In this process any mesh operations that were defined are used to refine the mesh.

Using the resulting mesh, Maxwell computes the electromagnetic fields that exist inside the structure based on the assigned excitations. If any error occurs in the process, Maxwell recomputes the error and the iterative process repeats until the convergence criteria are satisfied or the maximum number of adaptive passes is completed. The elements and nodes are important in the calculation process. The discretization of a solid into elements is shown in figures 3.6 and 3.7.

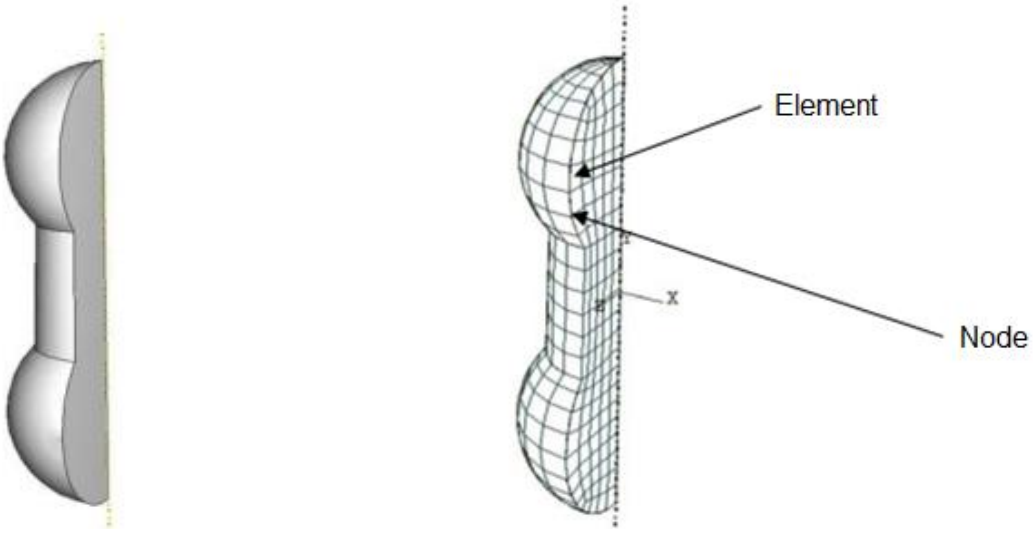


(a) A solid object (b) Mesh of the solid object

Figure 3.6: Example for a solid object (a) and Mesh (b) for the solid object model

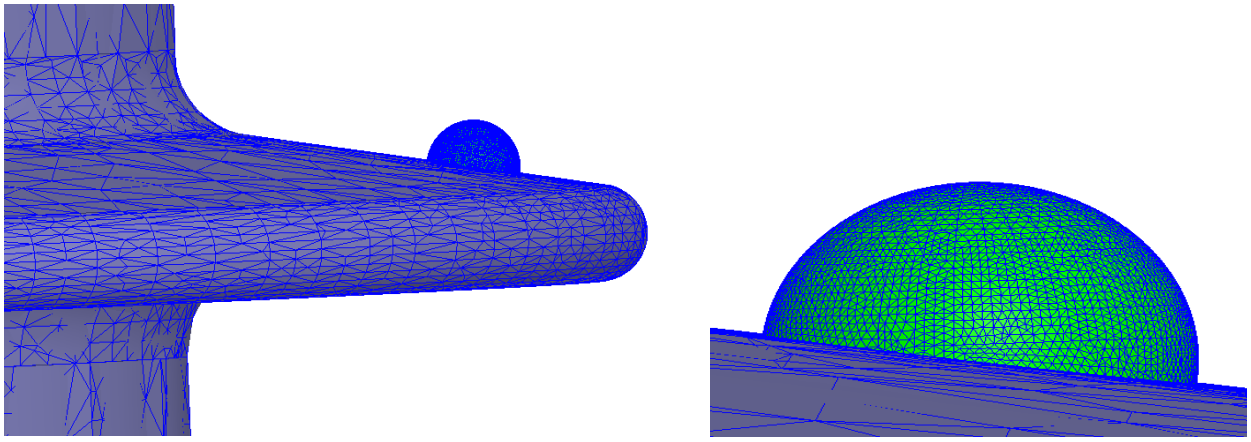

Figure 3.7: Examples for mesh creation on insulator shed surface with water drop

The calculation procedure involving in solution process of Ansys Maxwell is shown in the flow chart (figure 3.8).

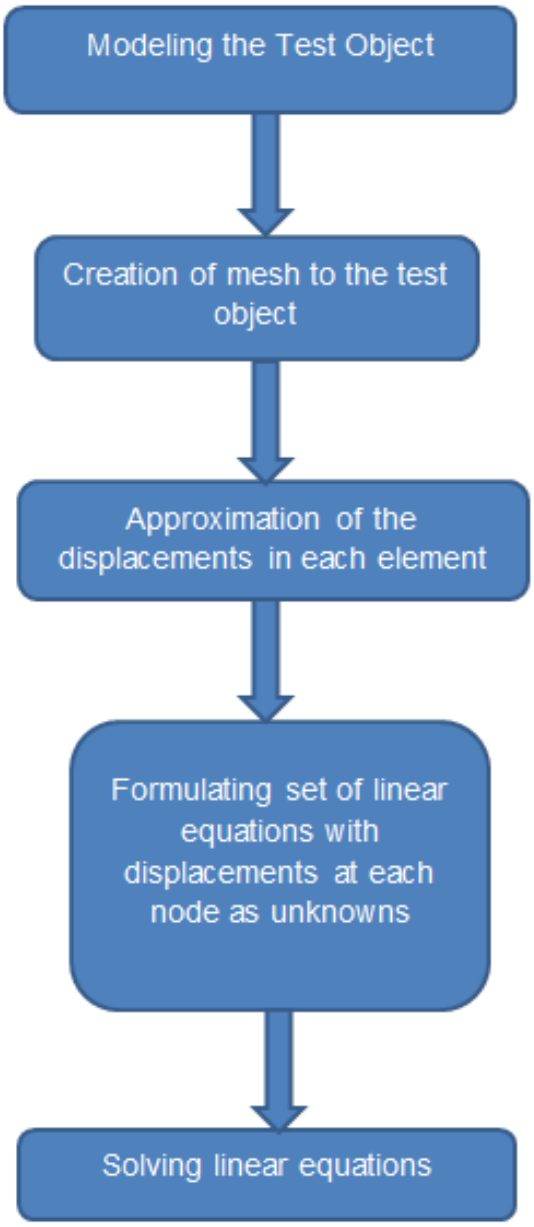


Figure 3.8: Flow chart for the solution process in Ansys Maxwell

The solution of any field problem is only possible if appropriate boundary conditions have been set. Boundary conditions define the behavior of the electric or magnetic field at object interfaces or edges of the problem region. They are always necessary in order to ensure the uniqueness of the electromagnetic field calculation. They can also be used

- To simulate structures that are magnetically isolated, electrically insulated, or electrically isolated.

- To set the electric or magnetic potential at a surface to a constant value or a function of position, in order to define the behavior of the electric or magnetic field on that surface.
- To simulate the field patterns that would exist in a structure while modeling only part of it. To do this, we can define planes of symmetry where electric or magnetic fields are either tangential to or normal to the direction and magnitude (or opposite direction) of the field on another surface.
- To simulate the field patterns produced by thin resistive layers on conductors or eddy currents with very tiny skin depths in conductors.

Boundary conditions are always necessary from a mathematical perspective in order to ensure the uniqueness of the solution calculated by Maxwell. Boundary conditions represent a convenient way of modeling different ideal situations. For example, in order to model the field in a dielectric sandwiched between two very thin conducting objects, only the two respective surfaces need to be modeled on either side of the dielectric object. In the setup, those top and bottom surfaces carry appropriate boundary conditions, and the field in the dielectric is correctly simulated without having to draw the respective conductors.

Different boundaries available in DC conduction solver of Ansys Maxwell are shown in the table 1[ANS 2014].

| Boundary Type | E-Field Behavior | Used to model |
|---|---|---|
| Default Boundary Conditions (Natural and Neumann) | Field behaves as follows:<br><br>• Natural boundaries — The normal component of **D** changes by the amount of surface charge density. No special conditions are imposed.<br><br>• Neumann boundaries — **E** is tangential to the boundary. Flux cannot cross a Neumann boundary. | Ordinary E-field behavior on boundaries. Object interfaces are initially set to natural boundaries; outer boundaries are initially set to Neumann boundaries. |
| Insulating | Same as Neumann, except that current cannot cross the boundary. An insulating boundary is **only** available for electrostatic solutions that include a DC conduction analysis. | Thin, perfectly insulating sheets between touching conductors. |
| Symmetry | Field behaves as follows:<br><br>• Even Symmetry (Flux Tangential) — **E** is tangential to the boundary; its normal components are zero.<br><br>• Odd Symmetry (Flux Normal) — **E** is normal to the boundary; its tangential components are zero. | Planes of geometric and electrical symmetry. |
| Matching (Master and Slave) | The E-field on the slave boundary is forced to match the magnitude and direction (or the negative of the direction) of the E-field on the master boundary. | Planes of symmetry in periodic structures where **E** is oblique to the boundary. |

Table 1: Different types of boundaries in “DC conduction” solver

In the simulation of water drop on the composite insulator shed, a region with the Natural and Neumann boundary is considered. This boundary is selected as we are interested to see the electric field near the drop and the electrical flux available should not cross the boundaries of the region. The same boundary conditions are applied while knowing the behavior of parallel insulators with and without pollution. Boundary regions used in the simulation are shown in figure 3.9.

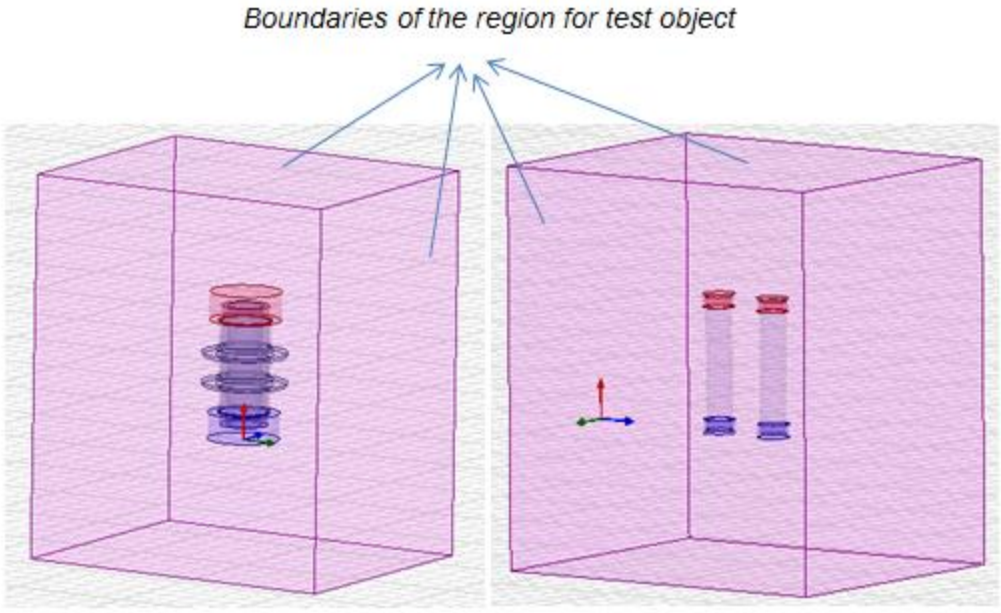


Figure 3.9: Boundaries used in the simulation of test objects

The advantage of Ansys Maxwell is, if we try to create a region that does not contain all of the objects in our model, the region is automatically expanding to cover all objects. The region also updates automatically as our geometry changes. A refined mesh has been created all over the space inside the region so that it could be possible to see the electric field behavior surrounding the test object up to the boundaries of the region.

# 4. Partial Breakdown (PD) at DC

The first step for a dielectric leading to breakdown is the occurrence of partial discharges. It is the consequence of a local electric stress concentration, mainly caused by the defect of the insulation or at the electrodes because of the surface roughness and sharp edges. When pollution is accumulated over the surface of the insulator there will be a high stress between the wet regions of the surface which leads to partial breakdown. In case of water drop on the insulator surface partial breakdown is the consequence of electric stress concentration near the droplet.

Partial discharge is the incomplete breakdown phenomena. Only a part of the insulation fails. An example is when non uniform pollution accumulates over the surface of the insulator only at some parts a partial discharge or breakdown occurs. The other part of the insulation can withstand the electric field stress. The occurrence of such a breakdown is a partial discharge.

It is obvious that the majority of the work on partial discharges has always been focused on AC applications. Full review of partial discharges occurring at AC voltage was published by Bartnikas [BAR 2002]. The effects of DC partial discharges are still being studied. This chapter explains the measurement and analysis of partial discharges at DC voltage. Before trying to understand this concept it is better to know some basics about partial discharge which are explained in the following subchapters.

## 4.1 Classification of Partial Discharges at DC

According to the place of discharge, there are three types of partial discharges which are explained in the following chapters.

### 4.1.1 Internal Discharges

This type of discharge occurs in insulations of low dielectric strength. It can occur in the form of gas filled cavities or oil filled cavities or other foreign particles. Internal partial discharges are shown in the figure 4.1.

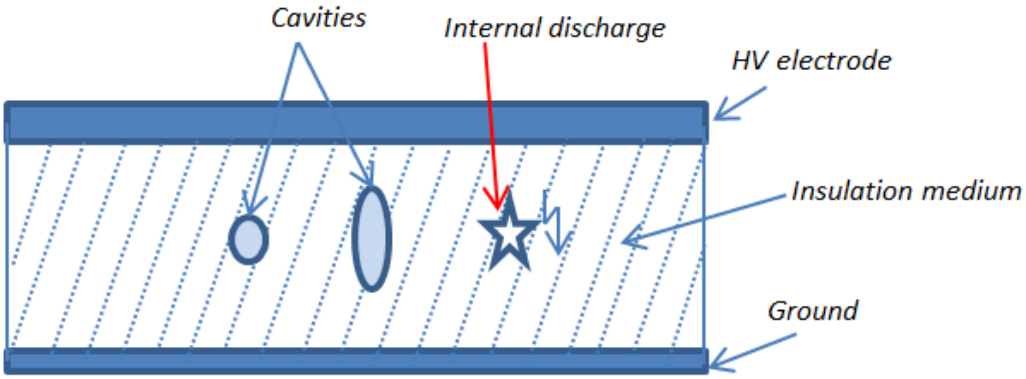


Figure 4.1: Internal discharges

### 4.1.2 Surface Discharges

Surface discharges occur when the edge of a high voltage electrode is placed on the surface of a dielectric medium. This type of discharge may occur in bushings or at the end of cables and at any point on insulator surfaces between a high voltage electrode and ground electrode. The pollution or water drops on the insulator surface may cause the surface discharge. Example for surface discharge is shown in figure 4.2.

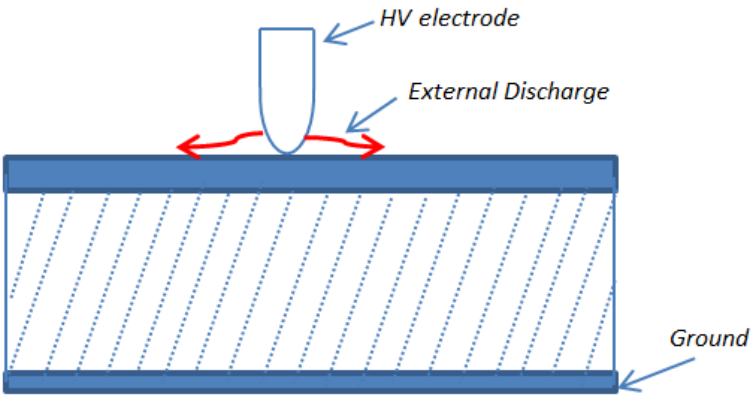


Figure 4.2: Surface discharges

### 4.1.3 Corona Discharges

Corona discharges are caused by the ionization of the medium surrounding the conductor. This discharge causes a luminous glow near to the conductors or at the points where the breakdown field stress exists. This type of discharge is shown in figure 4.3. The discharge occurs near the water drop on the insulator is corona discharge.

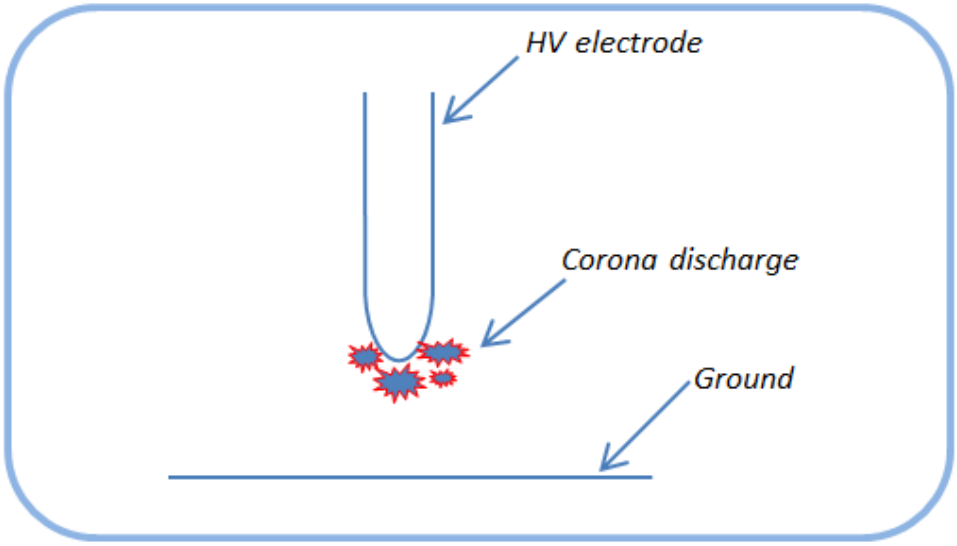


Figure 4.3: Corona discharge

## 4.2 Analysis of Partial Breakdown at DC Voltage

In order to start a PD two conditions must be satisfied.

1. The condition of minimum breakdown voltage $V_{min}$must be fulfilled.
2. A free electron must be present to start the ionization process. In this research, this situation happens near a water drop and near to pollution layer which is deposited on the insulator surface.

The generation of a starting electron is a stochastic process and is governed by a statistical time lag $t_L$. During this time lag the electric field near the water drop or pollution layer may exceed to the electric field $\nabla E$ and the partial discharge starts at $E_{min} + \nabla E$. This process is schematically represented in the figure 4.4.

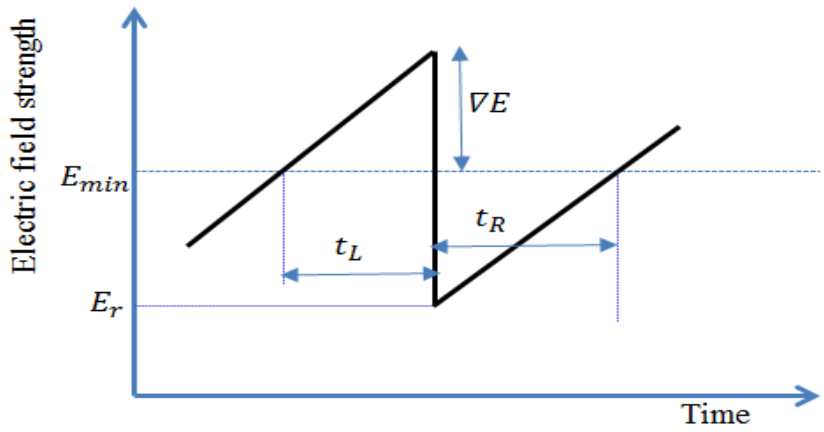


Figure 4.4: The electric field strength at the partial discharge location

After the discharge the electric field drops to $E_r$. It is a residual electric field. Once again the electric field strength increases from $E_r$ to $E_{min}$ after a certain time $t_R$. This time is known as recovery time. The process of discharge is strongly affected by the extra electric field strength $\nabla E$ which occurred at the time of discharge. At DC voltages $\nabla E$ is considerably smaller than at AC voltages [MOR 2005].

AC partial discharges are resolved from the recorded quantities of discharge magnitude q and phase position ∅. As DC does not have a phase angle, partial discharges at DC are resolved from the recorded quantities of discharge magnitude q and the time of occurrence $t_i$ or the time $\Delta t_i$ between discharges. These parameters are shown in the figure 4.5.

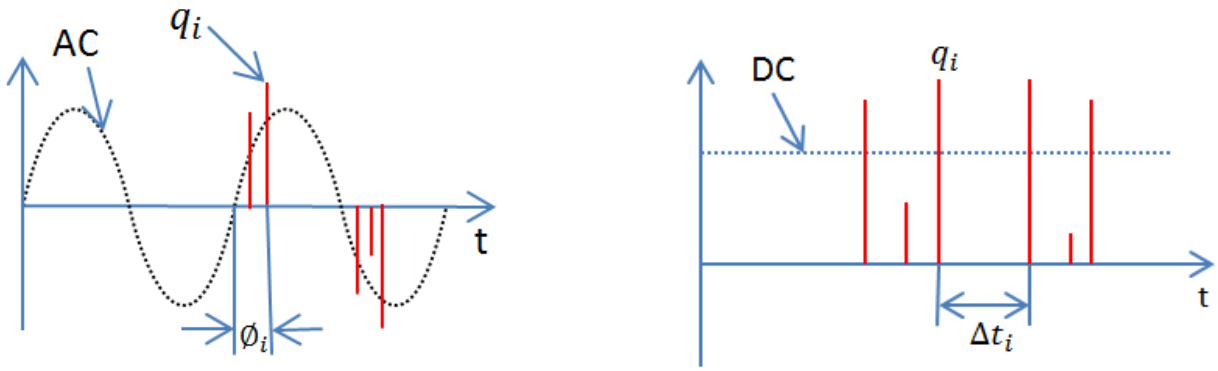


a) PD at AC voltage

b) PD at DC voltage

Figure 4.5: Partial discharge constraints for AC (a) and DC voltage (b)

The most important derived quantity for a DC partial discharge is the time $\Delta t_i$ between the consecutive discharges. It is related to the discharge physics. After the occurrence of a partial discharge it takes a certain time until the voltage drop caused by the partial discharge has disappeared and before another discharge can occur. A more detailed theory of possible discharge distributions and behavior are described by Fromm [FRO 1995]. Most systems measure the histogram H (q, ∅) (number of discharges depending on the discharge magnitude q and on the phase angle ∅ ) for partial discharges at AC voltage. There is no accepted standard yet for partial discharge at DC voltage. Some displayed data are used in different literatures. Some of these are the time functions of discharge frequency [SHI 1972] and the apparent discharge current [MÜL 1976], the distribution functions for discharge magnitude [SAL 1966] [MAL 1987], time [MAC 1990], conditioned distributions [VAN 1992] or a 3-dimensional H (q, $\Delta t_{suc}$) distribution [FRO 1995].

### 4.2.1 Measurement System for Partial Breakdown at DC

A partial discharge causes a discharge current at the discharge location. This current can be measured as a voltage impulse across measuring impedance which is shown in figure 4.6. Generally a discharge detector measures an apparent charge which can be calculated from an integration of the discharge current. Finally the magnitude of the apparent charge is shown by the detector. The same measuring circuit can be used for AC and DC partial discharges. The primary difference is in the analysis of the measured data.

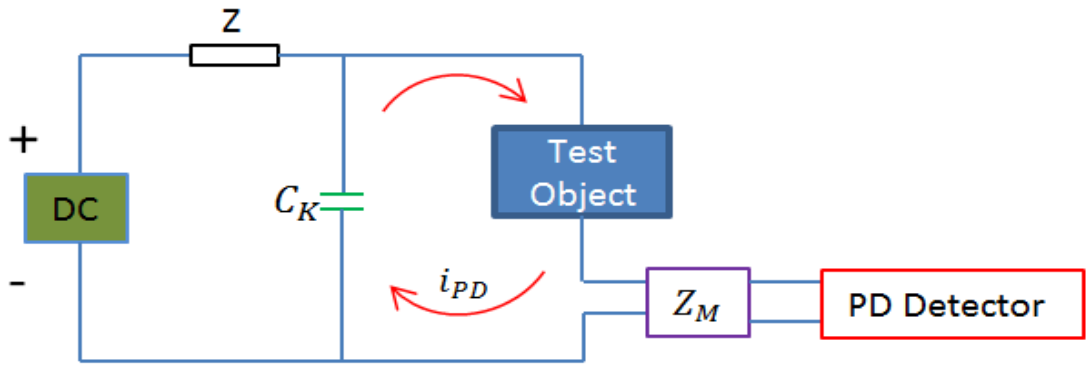


Figure 4.6: Partial discharge measurement circuit

In the measuring circuit Z is the blocking impedance, $C_K$ is the coupling capacitor and $Z_M$ is the measuring impedance. The coupling capacitor should be optimized according to the test object capacitance ($C_p$), usually $C_K \cong 0.1\, C_P$ is recommended [WOL 2010]. The blocking impedance (Z = 10…..100 mH) reduces noise signals penetrating via the test voltage generator into the measuring circuit.

The DC measurement system should have a good noise rejection to avoid misinterpretation. It should have automatic on-line recording over long periods (e.g. hours, days). This is required for the dielectric properties (space charge, conduction channel) to reach a stable state. The discharge process is stochastic. For every single discharge its magnitude and time of occurrence recorded within a given time interval are called basic quantities which are measured by a PD detector. Quantities describing the discharge process are called deduced quantities which are derived from the basic quantities. The main task in measuring PD is to reduce the large amount of basic quantities to a few deduced quantities which are sufficient for an evaluation. The flow chart for the conventional discharge detection is shown in figure 4.7.

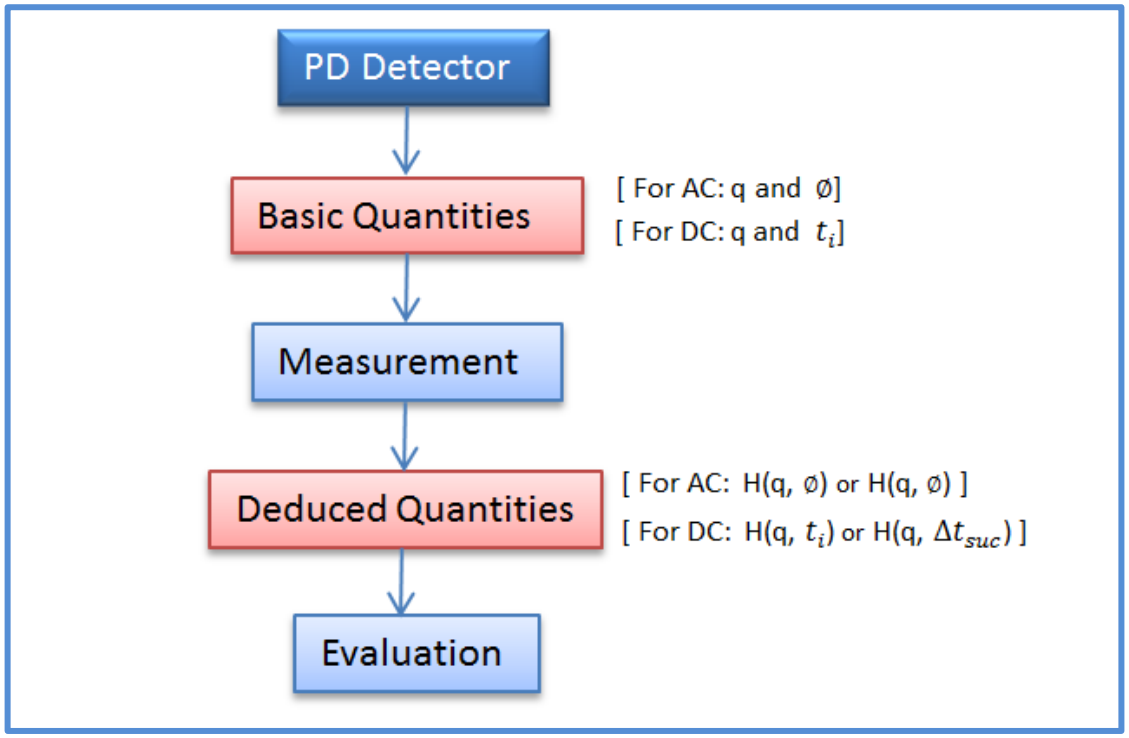


Figure 4.7: Flow chart for the partial discharge detection

The measuring system should have the facility of storing basic quantities and of off-line calculation of the deduced quantities. The deduced quantities can be evaluated by a computer using basic quantities which are stored. For DC voltage less work has been done to separate discharge quantities containing information from the quantities which don't have sufficient information. It is therefore worthwhile to store all accessible basic quantities for a DC discharge. Mr. Fromm presented the time lag/recovery model which describes the stochastic discharge process [FRO 1995].

All the following parameters are necessary to study and to find the behavior of the DC discharge process:

The time lag $t_L$

The recovery time $t_R$

The time to previous discharge $\Delta t_{pre}$

The time to successive discharge $\Delta t_{suc}$

The time lag of previous $t_{L,pre}$ & successive $t_{L,suc}$ discharges

The recovery time of previous $t_{R,pre}$ and successive $t_{R,suc}$ discharges

All these parameters are shown in the figure 4.8.

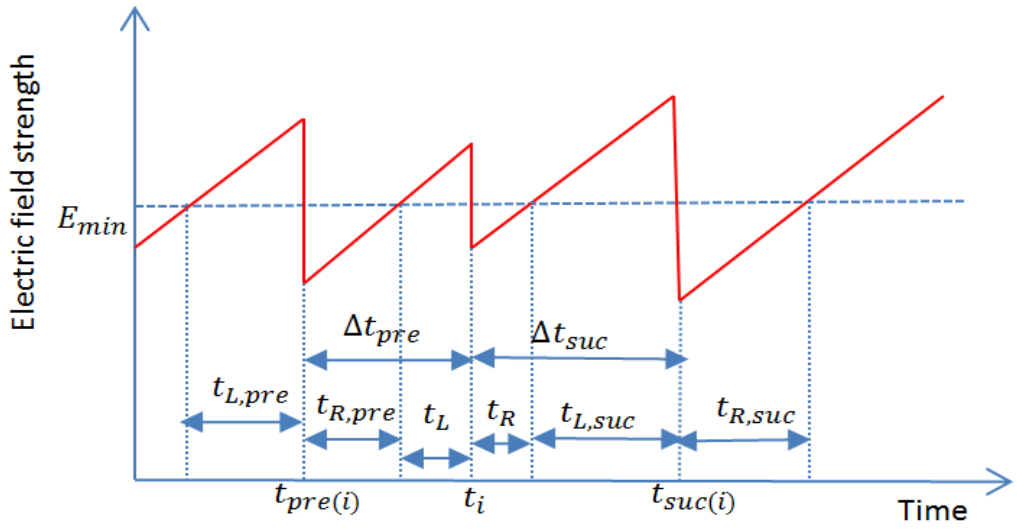


Figure 4.8: The relationship between all the timings in DC discharge process

### 4.2.2 Representation and Investigation of Partial Breakdown at DC

The partial discharge pattern generated for each defect varies. Each defect shall produce a certain type of distribution. The partial discharge of a test object should be measured and it should be compared with a finger print.

A database of the different kind of discharge patterns generated by different defects is recorded and a finger print is created by different authors [MOR 2005] [FRO 1995]. Any measured unknown pattern is compared with the fingerprint to recognize the type of defect.

The partial discharge magnitude can be shown as simple charge time diagrams or through different representations of histograms in 2D or 3D. Some of the statistical histograms are shown in figures 4.9 to 4.11.

- **PD magnitude as function of time q(t):**

The measured PD data is represented as a function of the discharge magnitude (pC) vs time (min).

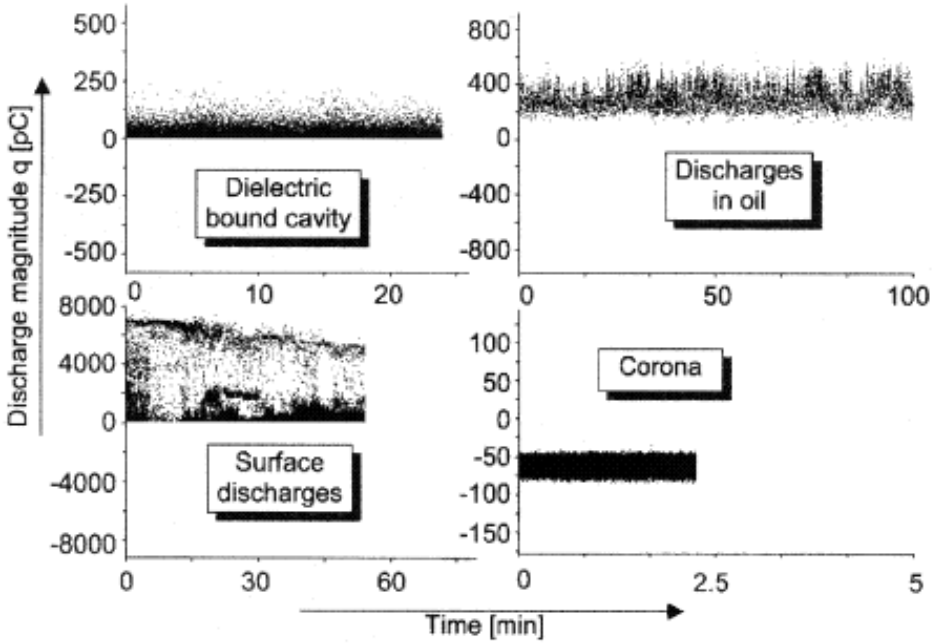


Figure 4.9: Plot of the DC discharge magnitude vs time for four different defects [MOR 2005]

- **Density function magnitude as function of time:**

The data are represented in a graph of the probability density function H(q) and discharge magnitude q.

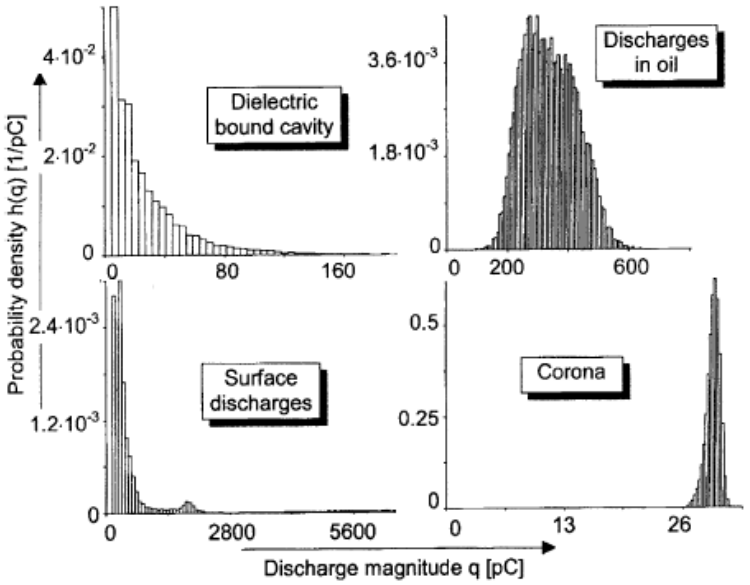


Figure 4.10: Histogram of PD at DC discharges [MOR 2005]

- **Probability density function H as a function of q and $\Delta t_{suc}$**

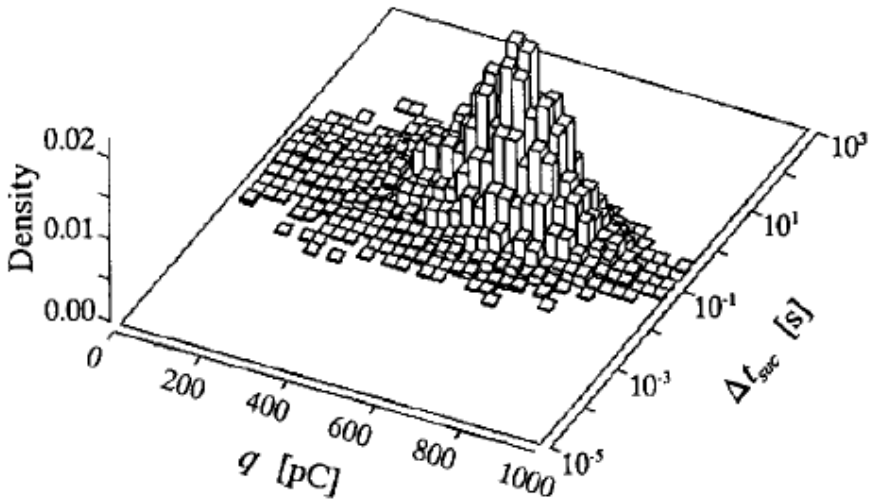


Figure 4.11: Example for 3D histogram of DC corona discharge [FRO 1995]

## 4.3 PD Monitoring Systems for Polluted Insulators

Partial discharge measurement on polluted insulators always depends on the pollutants deposited on the surface of the insulators. Several methods have been proposed in the literatures [MON 2004] [MAT 1999] [IWA 1998] [CHA 1999] [IEC 1993] to measure the quantity of pollutants deposited on an insulator surface. Following are examples of these methods.

- Measurement of equivalent salt deposit density (ESDD)
- Determination of non-soluble deposit density (NSDD)
- Measurement of surface resistance (SR)

All these methods necessitate to transport the insulators from the field to the laboratory for measurement of the amount of the surface pollutants. When insulator sheds of overhead line or post insulators are exposed to polluted environments due to humidity there will be partially conductive wet and dry regions on the insulator surface. The presence of conductive regions leads to the flow of a leakage current. This causes initially partial discharges which in turn generate a flashover. Partial discharges occurred on the insulators used in transmission lines are shown in figure 4.12.

Figure 4.12: Discharge on polluted insulators of a 400kV line [CIG 2012]

The magnitude of the leakage current depends on the level of contamination, as well as on the wetting of the insulator. It is not difficult to measure the leakage current on an insulator surface. Attributes in the current waveform from the leakage current measurement can be correlated with the pollution layer and then together with the intensity of humidity it is possible to get the information about the pollution level. The setup of PD monitoring system to be used on polluted insulators is shown in figure 4.13. The advantage of the leakage current measurement on polluted insulators is the availability of online monitoring system.

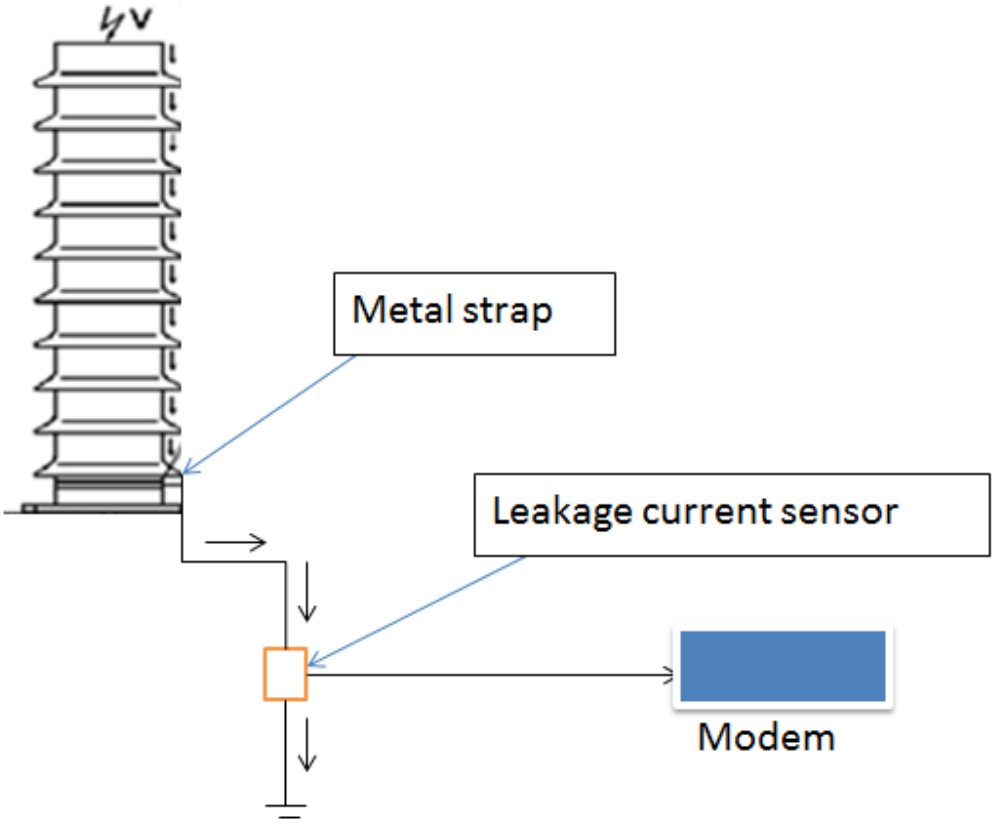


Figure 4.13: PD monitoring system on insulators

The modem connected to the leakage current sensor should be able to detect, amplify and store the principle characteristics of the leakage current signal. There is no standard comparison of leakage current to the pollution level under DC conditions. It is important to store all the data for future reference.

# 5 Behavior of Water Drop on Insulating Surface under DC

Water drop behavior under electric field stress is a typical problem on polluted insulators. The initial research work in this field was started at the beginning of the past century. In 1931 Mr. Macky described the appearance of water drop deformations and discharges [MAC 1931]

There is no electric field if it is considered that water drops are uncharged. All molecules in a water drop tend to attain a low energy state. As per physics, liquid always tries to reduce its surface area. The surface of the water drop leads to surface tension forces. There are two kinds of forces. One acts tangentially and other acts normal to the surface. Tangential components cancel each other. So the remaining components are normal. Finally the surface of a water drop leads to net components of surface tension forces acting normal to the center of the water drop. In order to compensate these forces, pressure forces must be equal to the surface tension forces. The resulting is known as Young- Laplace equation if all forces are balanced. It is a nonlinear differential equation that describes the pressure difference across the interface between two fluids, such as water and air.

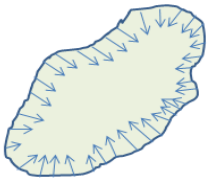

Figure 5.1: Arbitrary shaped surface

Let us consider some arbitrary shaped surface as shown in figure 5.1. If this arbitrary shape tends to reduce its surface it is necessary that all the molecules at the edges should move towards the center. This is because something at higher energy level wants to go to a lower energy level. Liquid has a highly prominent tendency to reduce

surface tension. Therefore molecules at the surface experience a force that reduces the surface area. This can be represented in formulas 5.1 and 5.2.

$$dF \propto dL \quad (5.1)$$

$$dF = S.dL \quad (5.2)$$

Here

dF - force at surface

dL - small length of the surface, where the force is experienced.

S is a constant

The constant S is the property of the interface.

The pressure difference can be expressed in following equation

$$P_d = \gamma\left(\frac{1}{R_1} + \frac{1}{R_2}\right) \quad (5.3)$$

Here

$P_d$ - Pressure difference over an interface

$\gamma$ - Surface tension

$R_1$ and $R_2$ - Radii of curvatures

The fluid volume will have a sphere form until the surface tension forces are lower than the cohesive forces. Then $R_1 = R_2 = R$, and $P_d$ become

$$P_d = 2.\frac{\gamma}{R} \quad (5.4)$$

In our case the water drop is surrounded by the air atmosphere. The differential pressure $P_d$ will contribute to the increase of the water drops internal pressure

$$P_i = P_e + P_d \quad (5.5)$$

Where

$P_i$ - Internal pressure

$P_e$- External pressure

## 5.1 Effect of Electric Field Stress on the Water Drop

When high voltage is applied on the insulator flange, there will be an electric field stress on the water drop which is accumulated on the insulator surface. Due to the big difference between the relative permittivity of water and air (water: 81, air: 1) an electrostatic force will act on the water drop surface. In case of an interface between two dielectrics, the tensile stress in the material of smaller permittivity can be expressed in the following way [KÜP 1990]

$$\sigma = \frac{1}{2} \times (\varepsilon_2 - \varepsilon_1)\left(E_{tan1}^2 + \frac{\varepsilon_1}{\varepsilon_2} * E_{n1}^2\right) \qquad (5.6)$$

Where

$\sigma$ - Tensile stress

$\varepsilon_1, \varepsilon_2$ - Permittivity of the materials

$E_{tan1}$-Tangential component of the electric field in material 1

$E_{n1}$ - Normal component of the electric field in material 1

Because of the water drop deformation, only the normal component of the electric field will influence the tensile stress, and by considering the water permittivity($\varepsilon_2$) to be greater than the air permittivity ($\varepsilon_1$) the expression 5.6 of tensile stress becomes

$$\sigma = \frac{1}{2}.\varepsilon_1.E_{n1}^2 \qquad (5.7)$$

Therefore the tensile stress of the water drop surface is proportional to the square of the normal component of the electric field. It is not compulsory that the normal component of the electric field on the surface of a water drop is constant all over the surface. The equilibrium condition of a water drop is shown in figure 5.2.

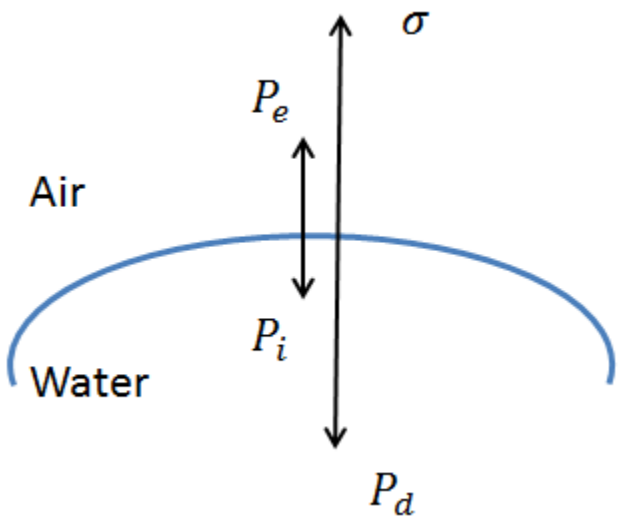


Figure 5.2: Equilibrium condition of a point on the surface of a water drop

In order to fulfil the equilibrium condition of water drop stability, the following condition must be valid at each and every point of a water drop surface [BRA 1971].

$$\sigma = P_d - (P_i - P_e) \qquad (5.8)$$

A higher differential pressure $P_d$ must be compensated by high tensile stress caused by the normal component of the electric field at poles of a water drop. This is possible only if the radius of curvature of a water drop becomes smaller. Therefore a normal water drop will change the form under the influence of the electric field. The degree of deformation can be calculated by using high speed cameras. Generally a water drop may take an ellipsoid shape under the stress of the electric field [TAY 1964]. There is an increase in the deformation with the increase in the electric field. There will be a limit for stable deformation. In any case the electric stress should not exceed this limit. If it happens that the equilibrium condition is not fulfilled the free drop becomes unstable. Taylor and Sherwood found experimentally and theoretically that an uncharged water drop becomes unstable under the following condition [TAY 1964] [SHE 1988].

$$E = c.\sqrt{\frac{\gamma}{\varepsilon_0.r}} \qquad (5.9)$$

Where

E - Critical electric field stress in V/m

r – Radius of the drop before deformation in m

$\gamma$ – Surface tension of the water in N/m

c – Constant

From the previous equation (5.9) it can be concluded that there is an increase in the critical electric field with decreasing radius and increasing surface tension [SHE 1988]. Different authors have estimated the value of the constant c with some differences. These values are shown in the table 2. Dr. Kamra measured water drops falling at their maximum velocity in a horizontal electric field [KAM 1993]. Therefore, water drops must have deformed in the horizontal direction before the electric field is applied. His measured value of the constant c is lower than the values offered by other writers.

| **Writer** | **Value of constant 'c'** | **Process** |
|---|---|---|
| Kamra[KAM 1993] | 0,273 | Experimental |
| Nolan[NOL 1926] | 0,414 | Experimental |
| Macky[MAC 1931] | 0,420 | Experimental |
| Sherwood[SHE 1988] | 0,454 | Theoretical |
| Wilson[WIL 1925] | 0,455 | Experimental |
| Taylor[TAY 1964] | 0,461 | Theoretical |

Table 2: Values of constant c given by different authors

Taylor's theoretical calculations are based on the assumption that the water drop is spheroid before its disintegration [TAY 1964]. This might be the reason that his constant value c is larger than the values from other authors. Nolan made experiments with free

falling water drops in a horizontal electric field [NOL 1926]. Macky used free falling water drops in a vertical electric field rather than a horizontal electric field [MAC 1931]. Wilson used soap bubble on a wet aluminum plate in a vertical electric field [WIL 1925]. The behavior of water drops on a hydrophobic surface is similar to the water drops in the free space. Therefore the electrodynamic behavior of water drops in a free space can be simulated by water drops on a hydrophobic surface [WIN 1994].

## 5.2 Discharge Process near the Water Drop

Before starting the simulation work it is important to know the theory of the discharge mechanism near the water drop. According to theory the discharge process starts at the triple point junction. In our case this point is the connecting point of water droplet, air and insulator surface. The water–air boundary on the insulating surface under the influence of the electric field can be the starting point of the discharge process. The water drop becomes unstable when the electric field reaches its critical value. The water drop instability can be characterized by the following way:

- Conical tips formation near the poles of the water drop
- Splitting of a single drop into two or more small drops

The development of a discharge near the water drop was described by Macky, W.A [MAC 1931]. He made a statement that the discharge starting from conical tips of the water drop is comparable with a discharge at a metal tip having positive or negative polarity.

### 5.2.1 Breakdown in Non-Uniform Electric Field

The electric field distributions can be categorized into two forms. One is “uniform electric fields” and the other is “nonuniform electric fields”. In a uniform electric field the electric potential is linearly distributed. The electric field intensity is constant everywhere in the space between the two electrodes [RAV 2011]. In uniform electric fields the insulator breakdown occurs without any partial discharge within the dielectric. In practice it is not

possible to have uniform electric fields. This can be achieved only for experimental purposes in research laboratories.

In the case of discharge near the water drop or pollution on the insulator we should consider the case of non-uniform electric fields. In general insulator flanges in atmospheric air having nonuniform fields are more common than flanges having uniform electric fields. Figure 5.3 shows the non-uniform fields near flange and a water drop.

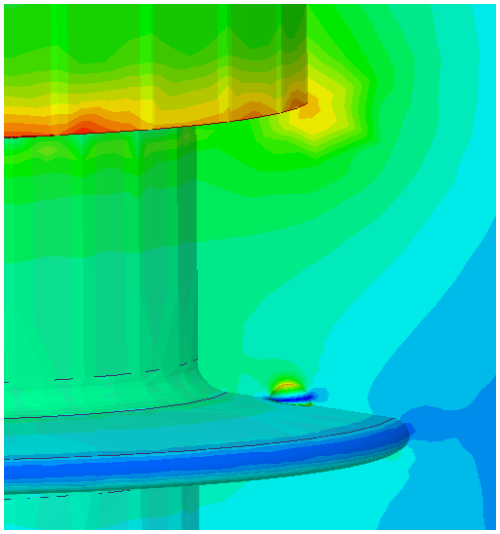

Figure 5.3: Nonuniform electric field in case of composite insulator

The electric field configuration on the composite insulator when a water drop is present on the shed surface is shown in figure 5.4. There is no constant color of the electric field simulation which means it is a non-uniform electric field configuration.

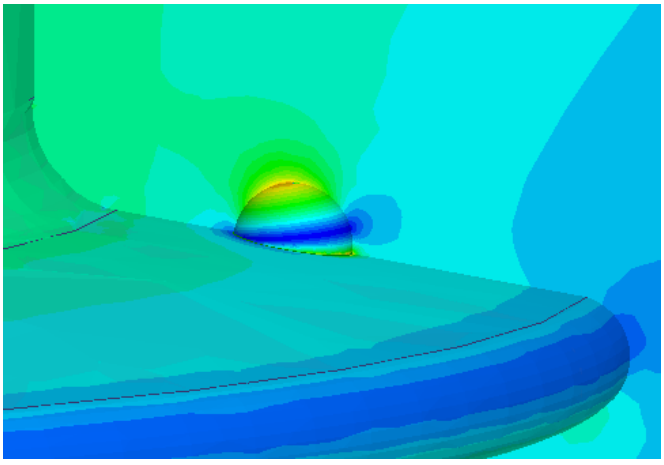

Figure 5.4: Electric field configuration near the water drop on the insulator shed

There could be a possibility of discharge between the flange of the insulator and a water drop present on the shed. It is shown in the figure 5.5.

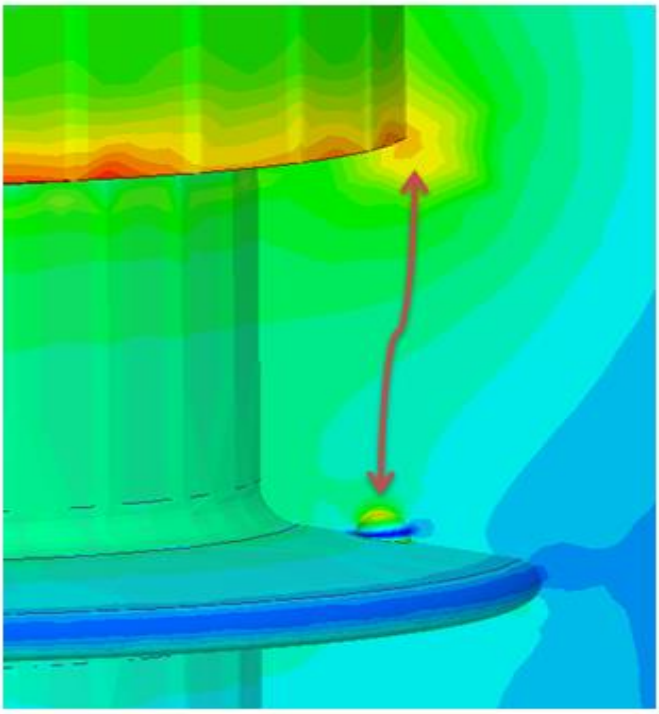

Figure 5.5: Discharge possibility between the flange and water drop

### 5.2.1.1 Avalanche Discharge

The discharge process starts with the growth of avalanche and streamer progression. The flange has an asymmetrical electrode configuration and resembles a needle electrode at the edge. The applied voltage to the top flange is a positive DC voltage. If we consider that a discharge starts at the conical tips of the water drop this configuration is analogues to the discharge at a metal tip having positive polarity, which is explained in the following chapters.

### 5.2.1.2 Ionization Coefficient

By increasing the applied voltage on the top flange, the electric field intensity near a water drop increases. After reaching breakdown voltage, the air near water drop loses its insulating properties and an avalanche discharge starts. This approach uses ionization coefficients, which are dependent on the field to evaluate the breakdown condition. The applied electric field in this case might decrease close to the electrode tip. It can happen after a short distance that the electric field strength may fall below the minimum filed value required for impact ionization $E_i$. If this happens, avalanches are not able to extend beyond certain length $\Delta x$. In this type of situations the magnitude of the electric field intensity E depends strongly upon the location. If there is a sufficient amount of kinetic energy $\Delta W$ that the molecule is ionized a further electron is released. The next collision process is successful if $\Delta W$ gains at least the ionization energy $W_i$.

$$\Delta W \geq W_i \qquad (5.10)$$

Where

$\Delta W$ – Kinetic energy

$W_i$ – Ionization energy

The condition for ionization is written in the following way

$$E.\lambda_{m,e} \geq U_{ion} \qquad (5.11)$$

Where

E - Electric field intensity

$\lambda_{m,e}$- Mean free path of the electrons

$U_{ion}$ – Ionization voltage of the air, and it can be calculated by

$$U_{ion} = \frac{W_i}{e} \qquad (5.12)$$

If the ionization condition is satisfied, the multiplication process of the electrons by collision ionization starts. Depending on the electric field intensity new electrons (“dn”) are produced over a distance dx:

$$dn = \alpha.n(x).dx \qquad (5.13)$$

Where

$\alpha = \alpha(E)$, ionization coefficient of the electrons

The number of electrons generated in a non-uniform electric field can be written in the following formula 5.14:

$$n(X) = n_o . \exp \int_0^x \alpha dX \quad (5.14)$$

The avalanche is the exponential increase of the number of electrons. When a positive DC voltage applied to the electrode is increasing progressively, the ionization process is enhanced. There are high numbers of carriers at the head of an avalanche and these carriers can cause great concentration of electric field lines. A further progress of the avalanche is possible only when there is a drift of charge carriers away from the electrode. In general the real free paths $\lambda_v$ of the electron establish a statistical distribution. Consequently $\lambda$ is the mean value by description. The ionization coefficient is expressed in the following equation:

$$\frac{\alpha(E)}{p} = A . \exp(-B \frac{p}{E}) \quad (5.15)$$

Where

A and B are constants

p - Pressure

Many authors used the ionization coefficient approach to model the breakdown in non-uniform geometries. This chapter summarizes the work done by the different authors who tried to model the breakdown phenomena in non-uniform electric fields. Some common references for breakdown in non-uniform electric field are [NAS 1971], [RAI 1997], [KUN 1983], [LAG 1994], [MEE 1978], [ENG 1965], [LLE 1957], [LLE 1967], [FRA 1960], [KUF 2000], [COB 1958], [ALS 1968] and [PEE 1915]. At the time of experiments on the polluted insulators or insulators with water drops the partial discharge inception voltage is the parameter which can be measured. Based on the inception voltage the electric field near the water drop can be calculated. Water drops can be deformed under the electric field strength existing near the drop. Therefore, an analytical calculation of the electric field strength is not possible. The electric field values near the water drop can be obtained only from the electric field simulations using simulation software like

Ansys Maxwell or Comsol Multiphysics. To compare the simulation results of the electric field with the measured inception voltage the partial breakdown inception requirements must be fulfilled.

In air, negative ions are formed by the attachment of electrons on a neutral molecule. Generally the collision process over a distance x requires $\eta.n(x)dx$ electrons, where $\eta = \eta(E)$ is the attachment coefficient of electrons. The difference between the ionization coefficient and the attachment coefficient is the effective ionization coefficient.

$$\alpha_e = \alpha - \eta \qquad (5.16)$$

Where

$\alpha$ - Ionization coefficient

$\eta$ - Attachment coefficient

Different writers used different expressions for the ionization coefficient. These expressions are shown in table 3.

| Writer | Ionization coefficient | Remarks |
|---|---|---|
| Friedrich [FRI 1992] | $\frac{\alpha}{p} = \mathrm{C}.[\frac{E}{p} - \left(\frac{E}{p}\right)_M]^2 - A$ | A = 0, 2873 $\frac{1}{mm.bar}$<br>C = 1, 6053 $\frac{1}{mm.bar}$<br>$(\frac{E}{p})_M = 2{,}165\ \frac{kV}{mm.bar}$ |
| Hartmann [HAR 1984] | $\frac{\alpha}{p} = M\{A\left(1 + \frac{C}{N\left(\frac{E}{p}\right)^3}\right).e^{-B.\frac{p}{E}} - 0.\psi\}$ | A = 1,75.10^3 B= 4.10^4<br>C= 1, 15. $10^{12}$ M = 1+$10^{-2}$.H<br>N= 1+3,2× $10^{-2}$.H<br>O = 1+1, 15× $10^{-1}.H^{0,1}$<br>H – water content in g/$m^3$<br>$\psi = \frac{0{,}9}{1{,}49 + e^{-\frac{p}{587}}}$<br>p – pressure at 0°C |
| Korolev [KOR 1998] | $\frac{\alpha}{p} = A.\exp(-\frac{B}{Ep})$ | A = 0,64 $\frac{1}{mm.bar}$<br>B = 19 $\frac{kV}{mm.bar}$<br>$\frac{E}{p}$ = 2,7 – 13,2 $\frac{kV}{mm.bar}$ |
| Meek [MEE 1978] | $E_r = k.\frac{\alpha.e^{\alpha x}}{\sqrt{\frac{x}{p}}}$ | k = 5,6× $10^{-5}$kV.$\left(\frac{mm}{bar}\right)^{0,5}$ |
| Rao & Raju [RAO 1971] | $\frac{\alpha}{p} = C_1.\frac{E}{p}\frac{E}{p} - A_1$ | $A_1 = 80{,}0006\ \frac{1}{mm.bar}$<br>$C_1$ = 16, 7766 $\frac{1}{kV}$ |
| Windmar [WIN 1994] | $\frac{\alpha}{p}$ =exp$\left(\frac{\frac{E}{p}-58{,}2}{4{,}95}\right)$ | $\frac{E}{p} \leq 2{,}625\ \frac{kV}{mm.bar}$ |

Table 3: Expressions of ionization coefficients according to different authors

There is a possibility to calculate the ionization coefficient values based on the expressions shown in the table number 3. To calculate the ionization coefficient it is possible to consider the electric field values obtained from the simulation results. These calculations are worth finding if there are accurate results from practical experiments. For this dissertation no practical experimental results are available. Therefore, the values for the ionization coefficient have not been calculated. For future work it is a good idea to carry out practical experiments on water drops by using the same parameters as in the simulation work.

### 5.2.1.3 Secondary Emission Coefficient

To understand the breakdown mechanism, it is important to know the process of secondary electrons and the related secondary emission coefficient $\gamma$ which depends on the electric field strength and ionization coefficient. This theory has been explained based on the experimental data given in the literatures. Secondary Townsend coefficient can be used as effective secondary emission coefficient (ESEC) [DRA 1996].

According to the Townsend theory the initiation of a gas discharge in a non homogenies field can be expressed as new electrons produced by secondary emission at the cathode. Secondary electrons can be created by incident ions or photons. The number of secondary electrons $n_{sec}$ will be proportional to the number of positive ions $n_+$ incident on a certain region of cathode.

$$n_{sec} = \gamma_s . n_+ \qquad (5.17)$$

Where

$\gamma_s$ - Secondary emission coefficient

$n_+$ - Number of positive ions

Depending on the several experimental conditions the secondary emission coefficient can take values from $10^{-8}$ to $10^{-1}$.

According to the Townsend model, the number of positive ions generated by of initial electrons $n_{eo}$ which are produced in the process of avalanche is given by the following equation.

$$n_{eo}(e^{\alpha s}\text{-}1) \qquad (5.18)$$

Where

$n_{eo}$ - Primary initial number of electrons

$\alpha$ - Ionization coefficient

s - Distance covered by initial electrons

These positive ions strike the cathode and lead to secondary emission. The number of secondary electrons is given by

$$\gamma_s . n_{eo}(e^{\alpha s} - 1) \qquad (5.19)$$

Where

$\gamma_s$ - Secondary emission coefficient

If this number of secondary electrons is higher than the original initial electrons, the current increases promptly in the configuration without any external support. This causes the partial breakdown which finally results in a breakdown on the surface of the insulator. The condition for initiation is given by

$$\gamma_s . (e^{\alpha s} - 1) \geq 1 \quad \text{or} \quad \alpha s = \ln\left(\frac{1}{\gamma_s} + 1\right) \qquad (5.20)$$

Where

$\gamma_s$- Secondary emission coefficient

$\alpha$ - Ionization coefficient

s - Distance covered by initial electrons

The variation in the secondary emission coefficient is very low. Therefore by neglecting it the condition of ignition becomes the following equation [KIN 1985].

$$\alpha s \geq k \qquad (5.21)$$

Where $k \geq 2{,}5$

For inhomogeneous fields the equation becomes

$$\int_0^s \alpha dx \geq k \qquad (5.22)$$

This integration should be done along the expected breakdown path. In any case the ionization coefficient depends on the electric field strength.

### 5.2.1.4 Streamer Discharge

When the number of electrons from the starting avalanche is higher than $10^8$, the electric field varying near the electron avalanche cannot be neglected [KÜC 2005]. It is shown in figure 5.6.

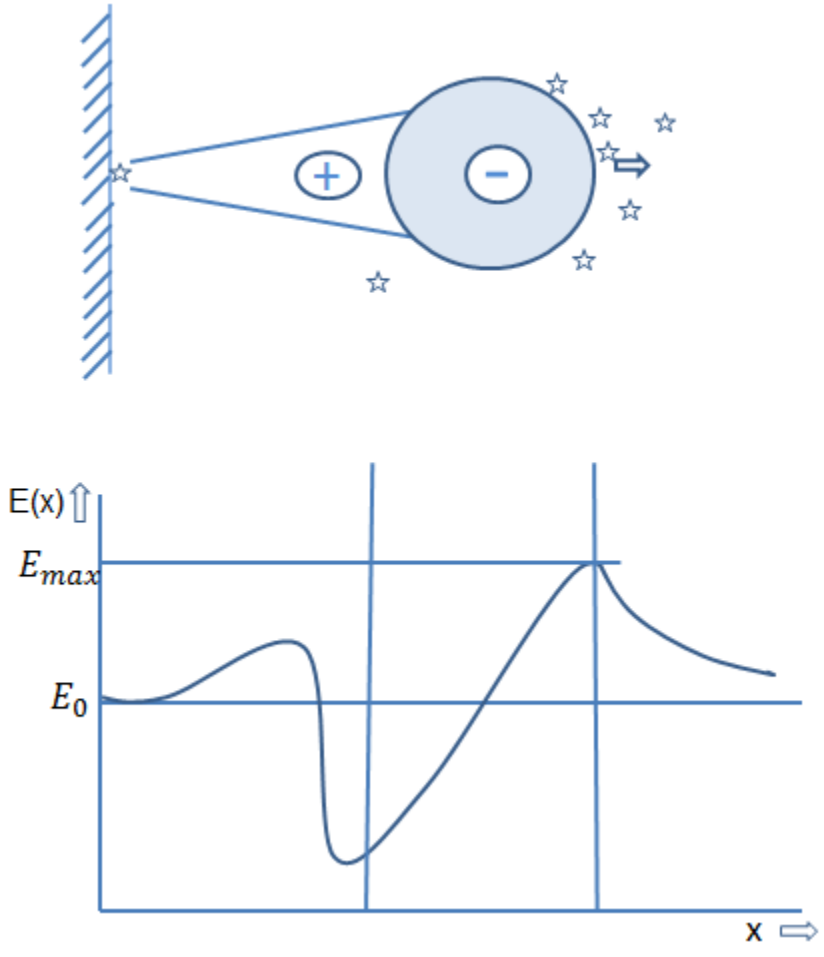


Figure 5.6: Electric field distortion due to the space charge of an electron avalanche

For easiness, the space charge at the head of the avalanche is assumed to have a spherical volume containing negative charges because of the higher number of electrons. At this condition the field becomes enhanced. This situation could happen slightly away from the water drop on the shed surface. This accelerative development of discharge is caused by the photo-ionization process at the speed of light. As shown in figure 5.6 the electric field $E_{max}$ exists at the head of the avalanche. The applied field is $E_0$. The electrons released from the initial avalanche will act as the starting electrons for the secondary avalanches. Because of all these avalanches, a conductive streamer will be developed as shown in the figure 5.7.

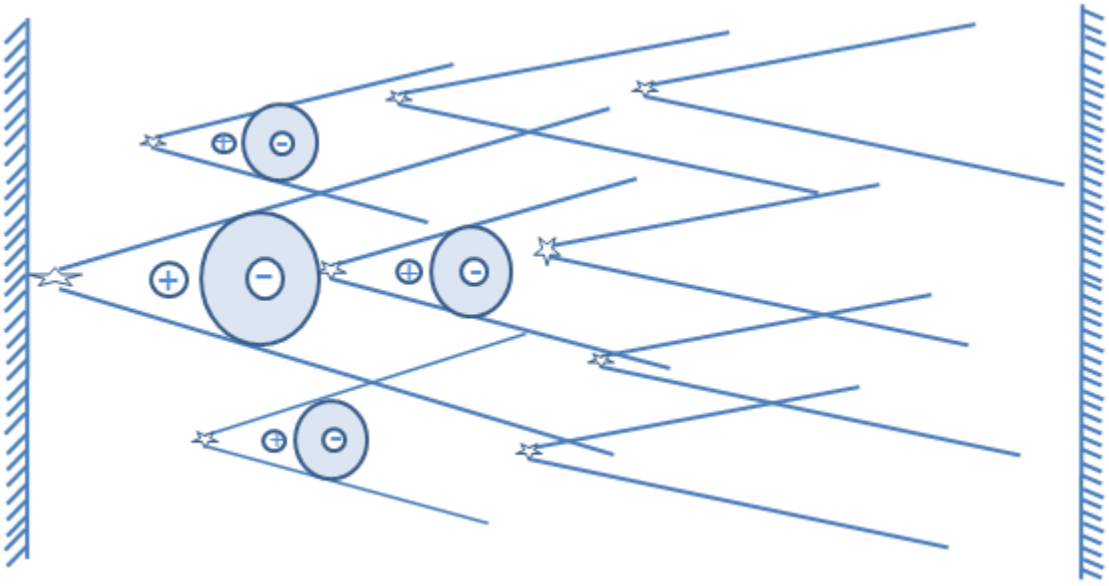

Figure 5.7: Growth of ionization channel

The space charges play an important role in the development of avalanches in the non-uniform electric fields. The transformation from avalanche to streamer occurs when the critical number of electrons $N_{cr}$ is achieved in the avalanche [KÜC 2005].

$$N_{cr} = 10^8 \; or \; \alpha X_c \qquad (5.23)$$

Where

$N_{cr}$ - Critical number of electrons

$\alpha$ - Ionization coefficient

$X_c$ - Length of the avalanche in which secondary electrons are produced

From the above explanation one may understand that the space charge developed in an avalanche can transform the avalanche discharge into streamers which leads to the development of breakdown.

## 5.3 Summary of the Discharge Process

A starting electron will be released in air near the water drop due to existence of the high field stress. A free electron in air gains sufficient kinetic energy for colliding with a neutral molecule. This process develops in a systematic manner and leads to an avalanche. Then there will be new electrons and positive ions. This situation generates the space charge near the water drop. The combined applied field and space charge field causes an intense ionization and excitation of atmospheric air in front of the water drop. The number of electrons depends on the ionization coefficient which is explained in the chapter 5.2.1.2. Instantaneous recombinations of electrons and positive ions release photons which in turn produce further electrons by photo ionization. This happens when the avalanche in the gap reaches a critical size. These electrons develop secondary avalanches under the influence of the field in the gap. In this process photons travel with the velocity of light, and the photo ionization process gives rise to a rapid development of conduction channels across the gap. Finally, this conduction channel leads to the breakdown near the water drop.

# 6 Simulation of a Water Drop on the Insulator Surface under DC

Water droplets play several roles in the pollution flashover and ageing of insulators. The presence of a water drop on the insulator surface increases the electric field flux or intensity along the insulator surface which may lead to an electrical breakdown. As we all know porcelain insulators for distribution and transmission lines have been used for many years. Now the usage of polymer insulators has been increased. Surface corona discharges from water droplets accelerate the aging of the polymer material of the insulator shed and destroy its hydrophobicity. The degradation of hydrophobicity leads to a formation of wet regions causing partial discharges along the surface of the insulator.
The behavior of the insulator when water droplets accumulate on the insulator surface is one of the important parameters to be determined. Conductive particles dissolved in the water change the electric field. The electric field is intensified at the triple point junction between water droplet, air and insulation material. The erosion may take place due to the existing local high electric field. The objective of this work is to study the effect of water drops on the insulator surface under DC stress. This study has been done by investigating electric fields and voltage distributions by changing the position of a water drop on the surface of the insulator sheds.

## 6.1 Water Drop Modeling

In general to model the water drop with different shapes we need special modeling software, for example SOLID WORKS. In Ansys we could create only a simple model. Therefore only a water drop with sphere shape is created and for the modeling of a water drop I assumed fresh water with the following parameters:

Relative permittivity : 81
Conductivity : 0.01 Siemens/m
Diameter of water drop : 5.15 mm

## 6.2 Results of Simulation

Ansys Maxwell software with DC Conduction solver is used to simulate the water drop on the insulator surface. At first the disconnector insulator is modeled in Ansys, and then a water drop is placed on the first shed. Then the drop is moved towards the end of the shed in several steps. This behavior of the electric filed near a water drop is shown in the following sub chapters.

### 6.2.1 2D Results

In order to examine the electric field distribution on an insulator shed surface, an insulator model has been created and started working on the first shed without water drop. A porcelain insulator with following parameters has been used in the simulation.

| | |
|---|---|
| Height of the insulator | : 1215 mm |
| Core diameter | : 100 mm |
| Insulator shed diameter | : 240 mm |
| Distance between two shed | : 24 mm |
| Diameter of the top and bottom flanges | : 140 mm |
| Relative permittivity of the insulator | : 5.7 |
| Conductivity | : 0 Siemens/m |

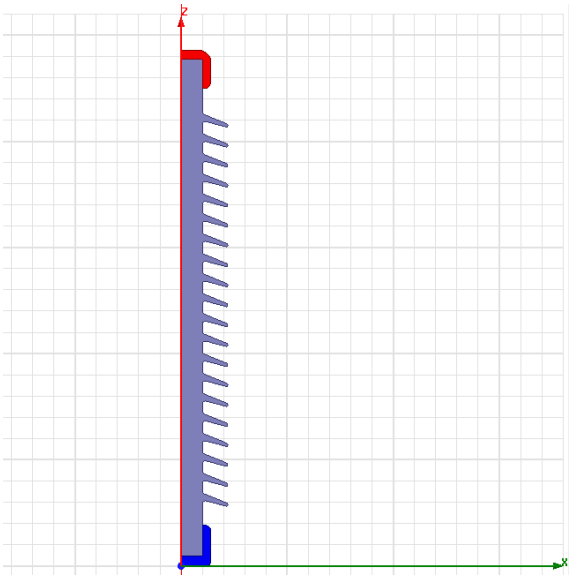


Figure 6.1: Insulator model used for simulation

After using the above model (figure 6.1) in Ansys Maxwell, the results from potential and field simulations are given in figure 6.2.

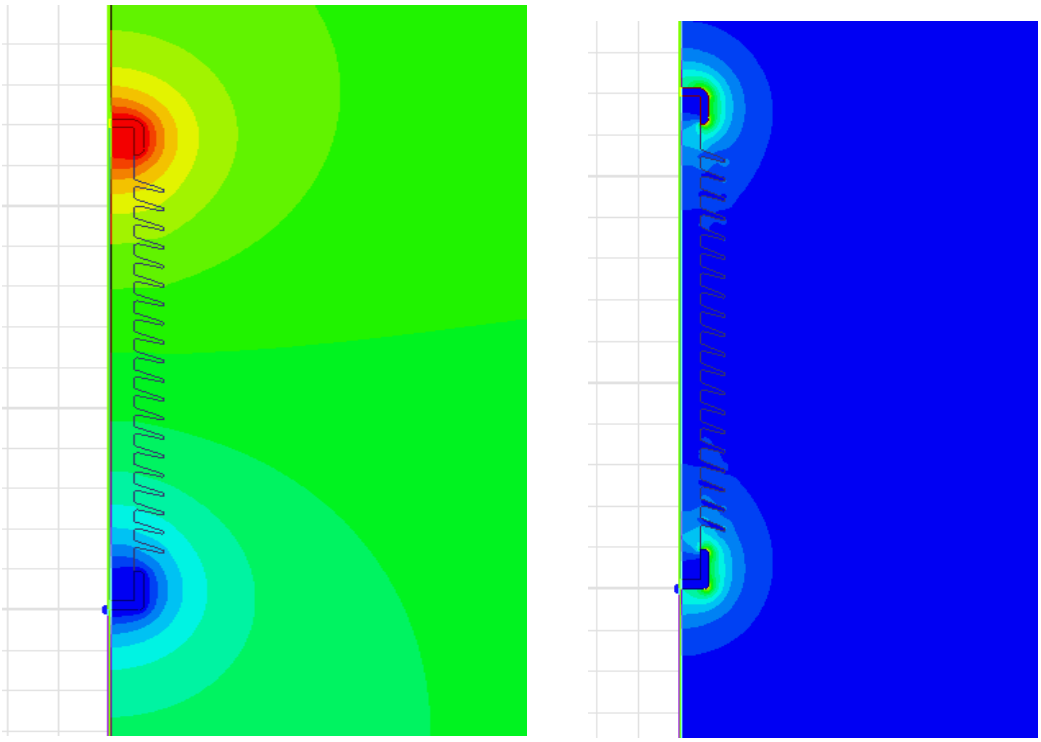

(a) (b)

Figure 6.2: Voltage (a) and electric field (b) distributions on an insulator

For better and easy understanding, I have selected only the first shed and observed the electric field distribution along it. Outer line created on the first shed is shown in figure 6.3.

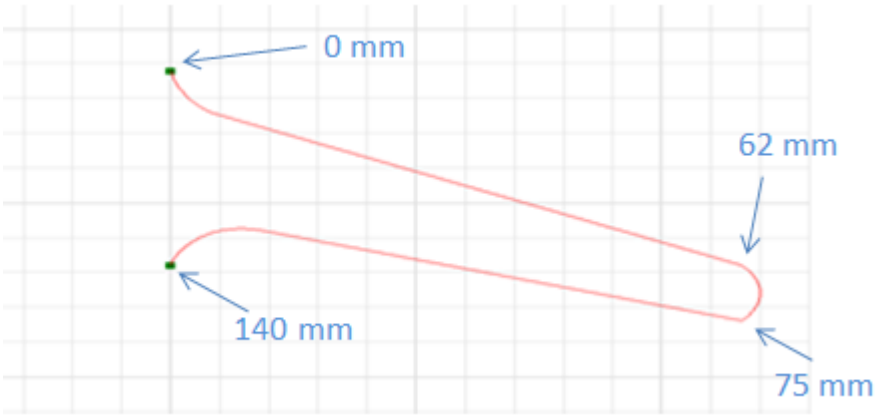


Figure 6.3: Outer line created over the first shed

Electric field values along the first shed between the green points in figure 6.3 have been calculated and drawn in figure 6.4.

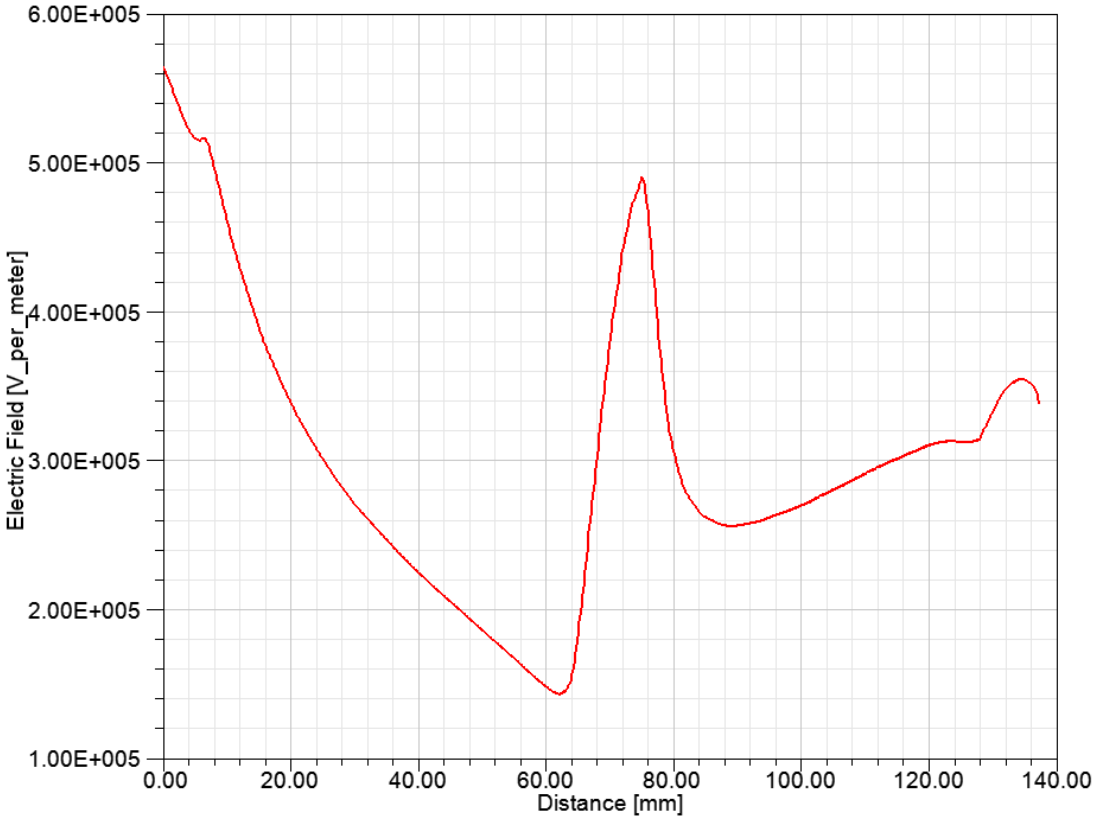


Figure 6.4: Electric field distribution along the reference line

### 6.2.1.1 Water Drop at Different Positions

Now a water drop is placed on the first shed of the insulator and moved towards the end of the shed. The electric field while moving the droplet has been observed. It is shown in figure 6.5.

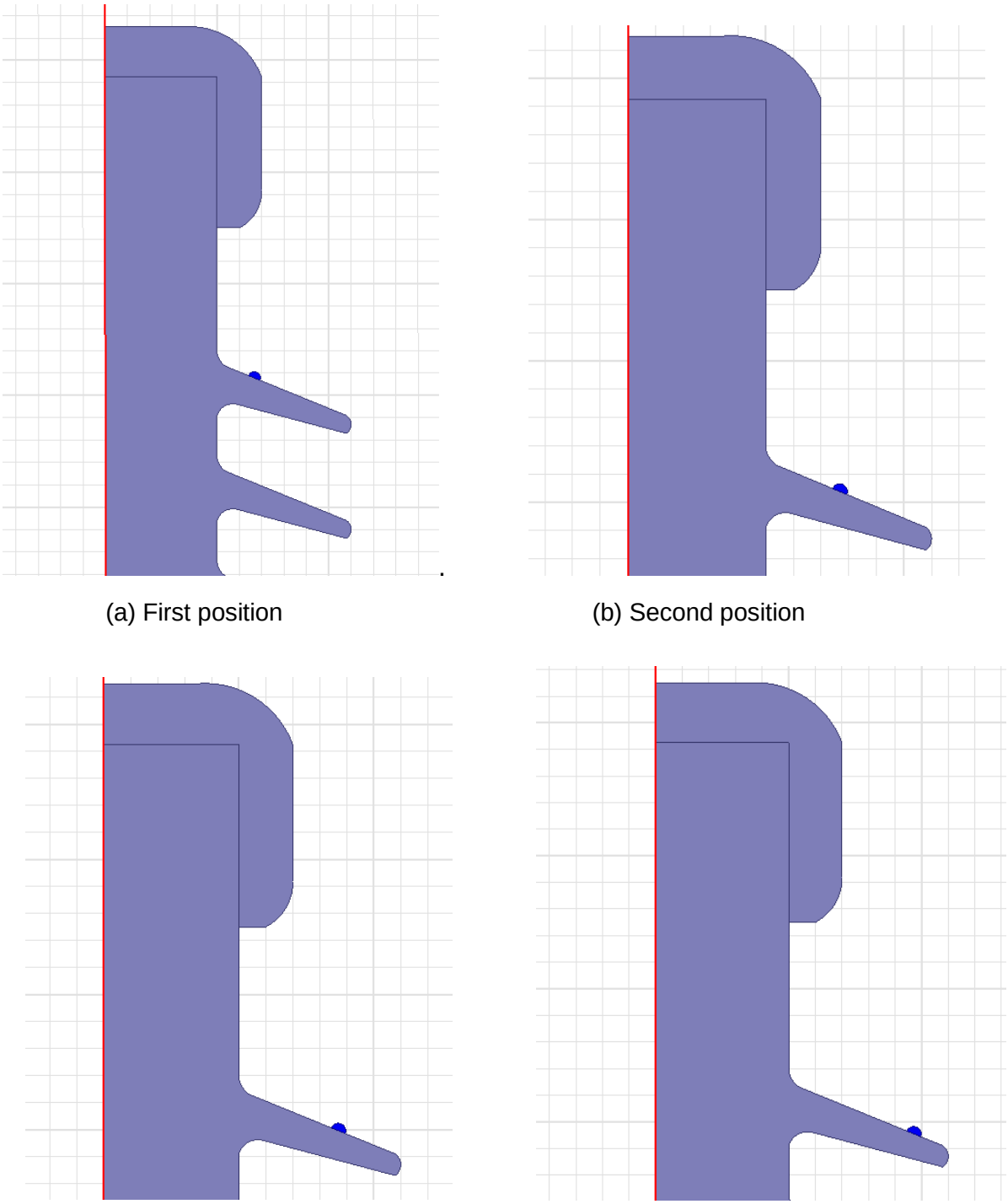

(a) First position

(b) Second position

(c) Third position

(d) Fourth position

Figure 6.5: Water drop at different positions

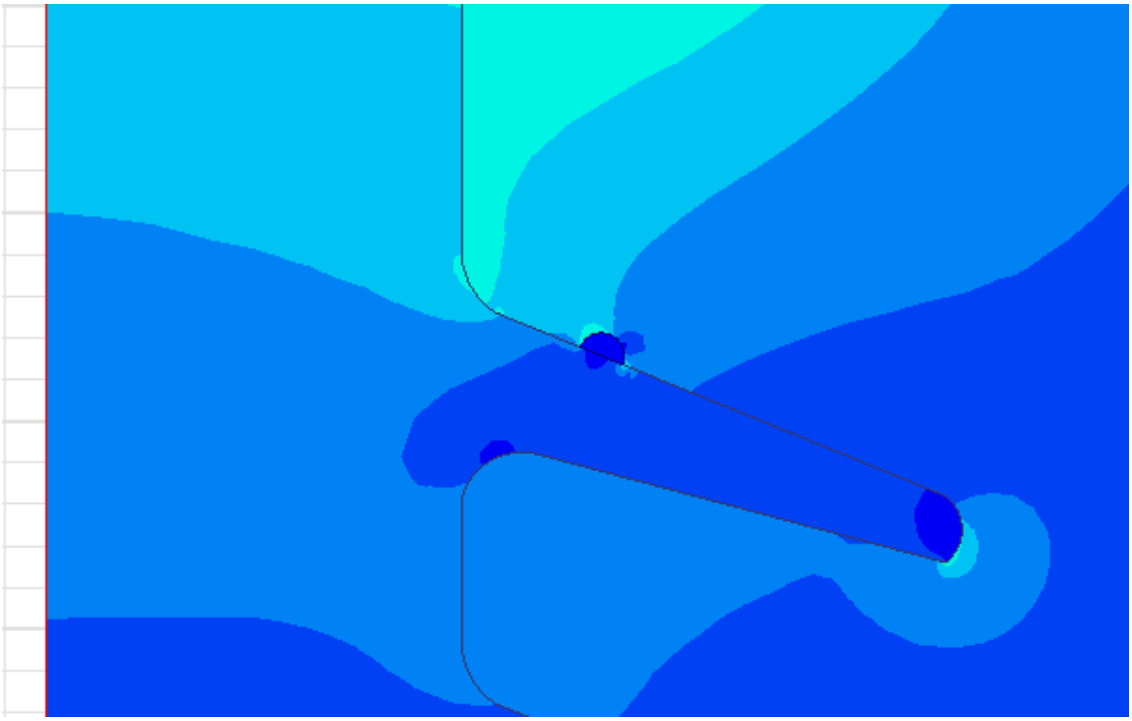

Figure 6.6: Electric field distribution along the shed with a water drop

Electric field distribution along the first shed including water drop is shown in figure 6.6. It is observed that the electric field inside the water drops is zero. Therefore, it is important to investigate the behavior of the electric field around the surface of a water drop. In simulation software the electric field values are calculated from the nodes of the mesh triangles created inside the boundary. This issue is clearly explained in the chapter “Mesh & Boundary Settings” (Chapter 3.1.2). If the measurement has taken place exactly on the surface of insulator shed, the calculated electric field values would be wrong as there might a be a connection of mesh triangles created inside the porcelain shed and outside the shed which are in air. It is the same situation over the water drop as well. To avoid inappropriate results one reference line is considered to observe the electric field values over the water droplet and along the surface of the first shed. This line is shown in figure 6.7.

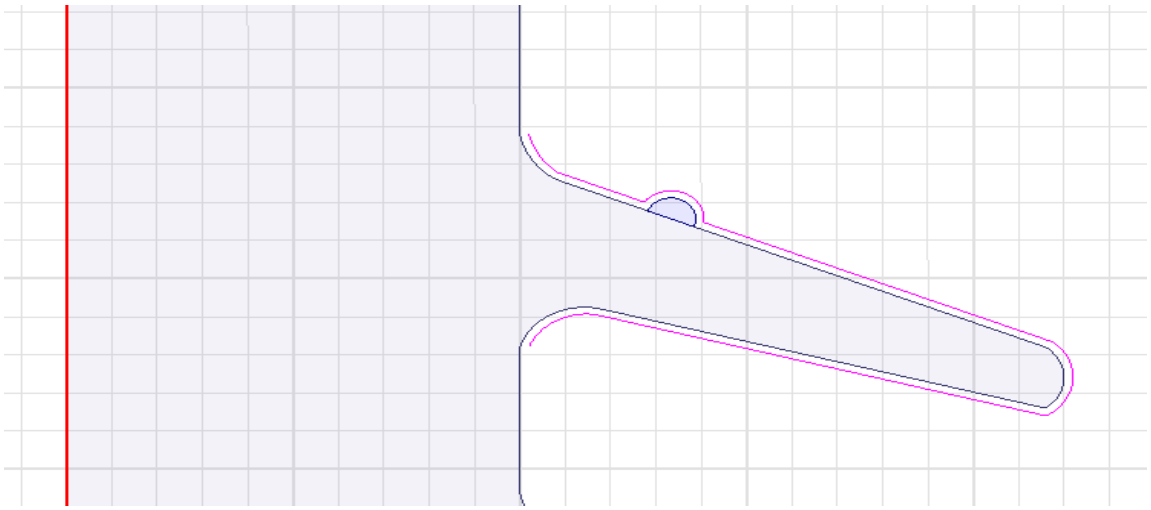

Figure 6.7: Reference line along the insulator shed with a water drop

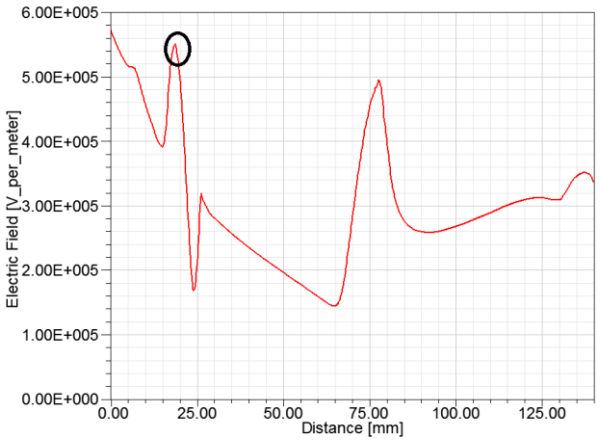


a) Water drop at 1st position

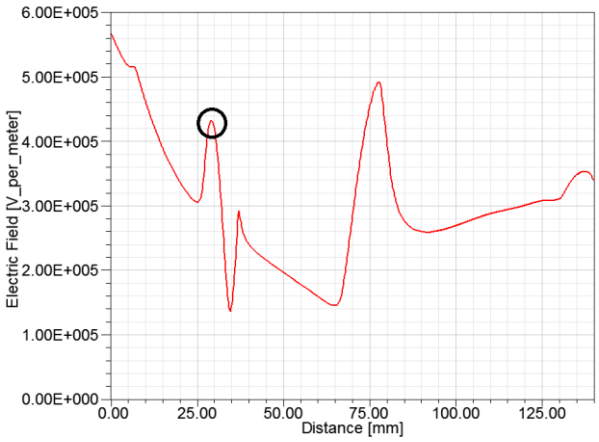


b) Water drop at 2nd position

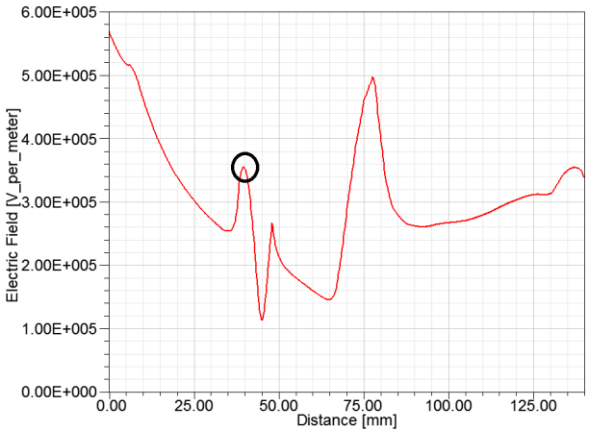


c) Water drop at 3rd position

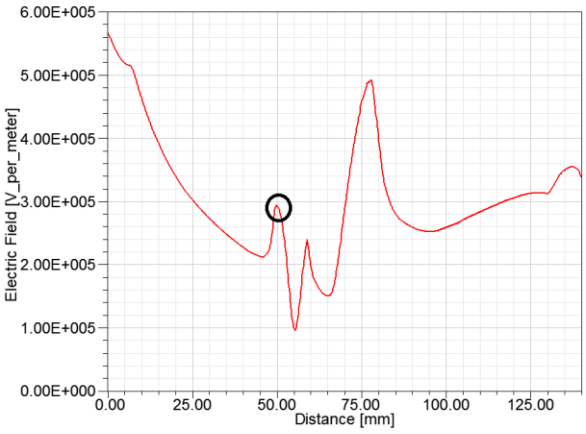


d) Water drop at 4th position

Figure 6.8: Highest values of the electric field near the water drop

The maximum values of electric field near the water drop (value in the black rings shown in the figure 6.8) are considered for analysis. There are significant changes in the electric field distribution near water drop. Peak values of the electric field near a water drop are shown in table 4.

| Water drop position | Maximum Electric field value near the water drop (kV/cm) |
|---|---|
| 1 | 5.51 |
| 2 | 4.31 |
| 3 | 3.55 |
| 4 | 2.96 |

Table 4: Maximum electric field values near the water drop at different positions in 2D

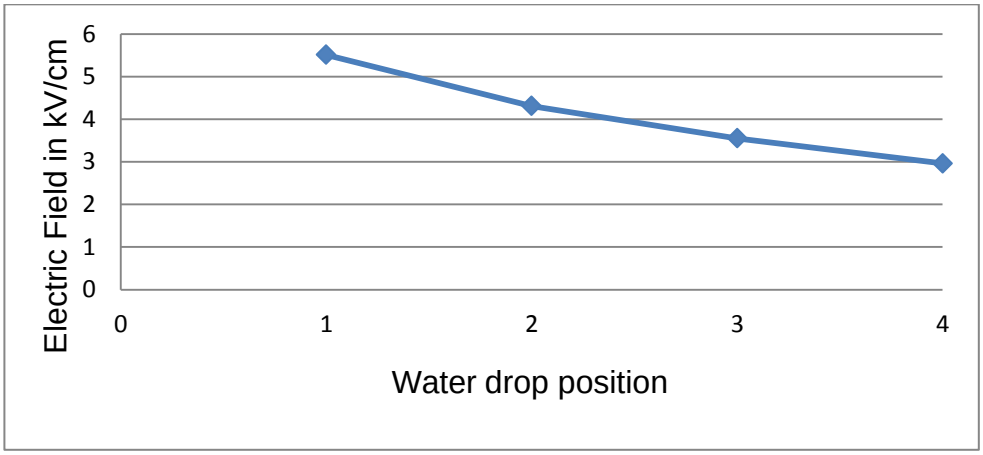


Figure 6.9: Graph of electric field value vs water drop position

Before considering the presence of a water droplet, the electric field is enhanced at the sharp edges of the insulator shed due to the accumulation of charges. These edges are outer edge of the shed and where the shed join the core of the insulator. The highest value of the electric field is at the edge near the HV electrode. When a water droplet is present the electric field is also higher at the contact angle between water drop and insulator. Only one water droplet was considered to find the behavior of the electric field near to it.

The simulation of the electric field distribution due to the presence of a water droplet on an insulator surface has been carried out based on the finite element method [FEM].

A sufficiently large number of triangular elements have been created in mesh to produce accurate results of electric field distribution. When the water droplet changes its position along the shed the electric field around the water droplet evidently changes. The results from the figure 6.9 show that the value of the maximum electric field E gradually decreases along the shed. The maximum E value changed from 5.51kV/cm to 2.96kV/cm.

### 6.2.1.2 Hanging Water Drop

The above chapter contained a discussion about the water drop moving along the surface of the first shed. This chapter deals with the water drop hanging at the edge of the first shed. It is shown in figure 6.10.

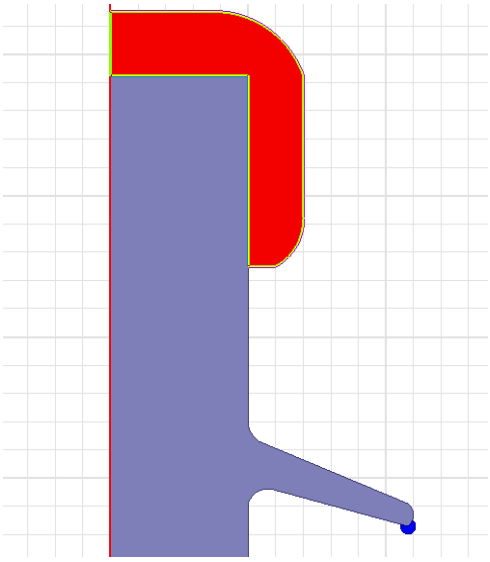

Figure 6.10: Hanging water drop

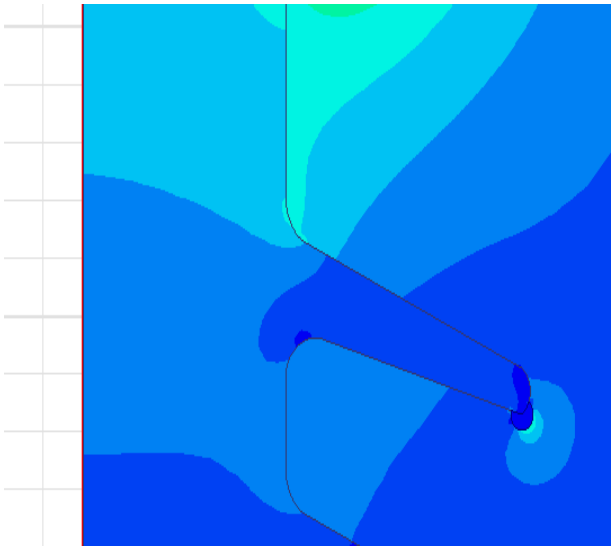

Figure 6.11: Electric field near the hanging drop

The electric field plot along the shed including the hanging water is shown in figure 6.11. The results without water drop and with hanging drop have been considered for investigation of results. These results are shown in figure 6.12

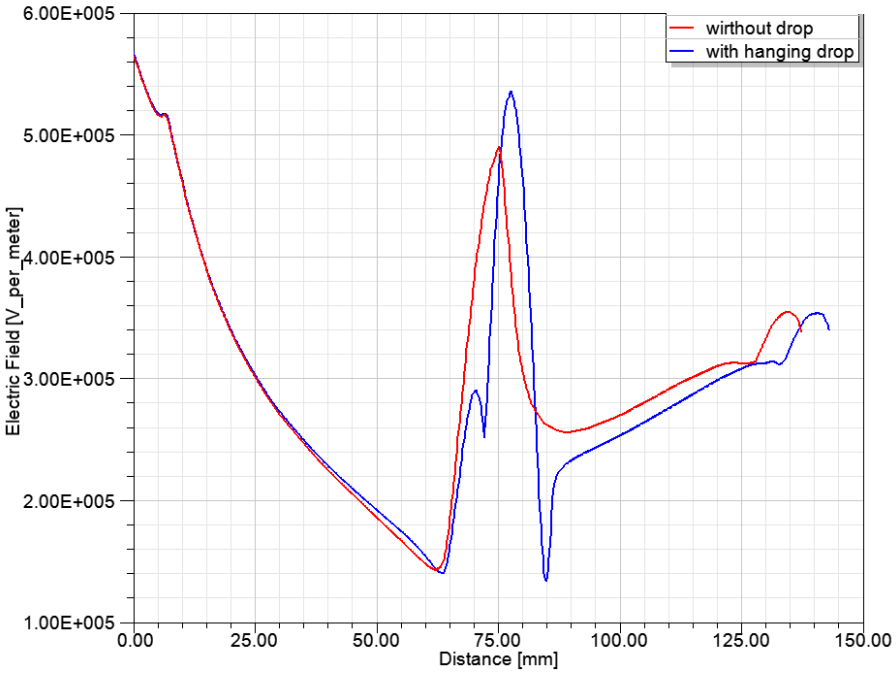


Figure 6.12: Electric field plots with and without hanging water drop

There is a change in electric field from 4.8 kV /cm (without hanging drop) to 5.3 kV/cm (with hanging drop).

### 6.2.2 Understanding the Results

In the above chapters the simulation work has done only in 2D. To create the model of insulator and water drop I applied Ansys 2D axisymmetric configuration which many people use for simple simulation work instead of the complex creation of models in 3D. But there is a misunderstanding when it comes to water drop modeling over the shed of the insulator surface. Here I explain in my dissertation so that in future no one might make the same mistake. Everyone knows that a single insulator is an axisymmetric model. There is a possibility to do any kind of simulation over it. When it comes to a water drop representation it is not any more a 2D axisymmetric model. It is a 3D object which has certain volume. 2D - modelled water drop on the insulator shed is a ring along the whole shed diameter. Therefore it is by no way possible to create a water drop in 2D axisymmetric configuration. Of course it is not even possible to create different shapes

of water drops with electrical simulation software. It is easy and simple to create such models in design software like Auto CAD or SolidWorks. Because of these reasons this research work is further continued in 3D.

## 6.3 Simulations in 3D

To simulate the water drop on the insulator surface in 3D, porcelain and composite insulators have been created.

### 6.3.1 Porcelain Insulator

The porcelain insulator with the same parameters showed in the chapter 6.2.1 has been modelled. Figure 6.13 shows the model of the insulator designed in 3D.

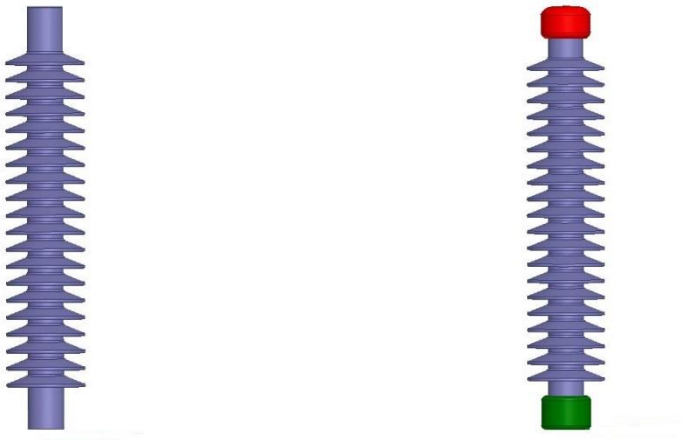

(a) (b)

Figure 6.13: Insulator models without(a) and with(b) flanges

#### 6.3.1.1 Different Positions of a Water Drop

After modeling the insulator, a water drop is modelled with the parameters mentioned in the chapter 6.1. The water drop is placed on the first shed of the insulator surface and it

is moved to different positions to study the behavior of the electric field near the actual water droplet. The drop at different positions in 3D is shown in figure 6.14.

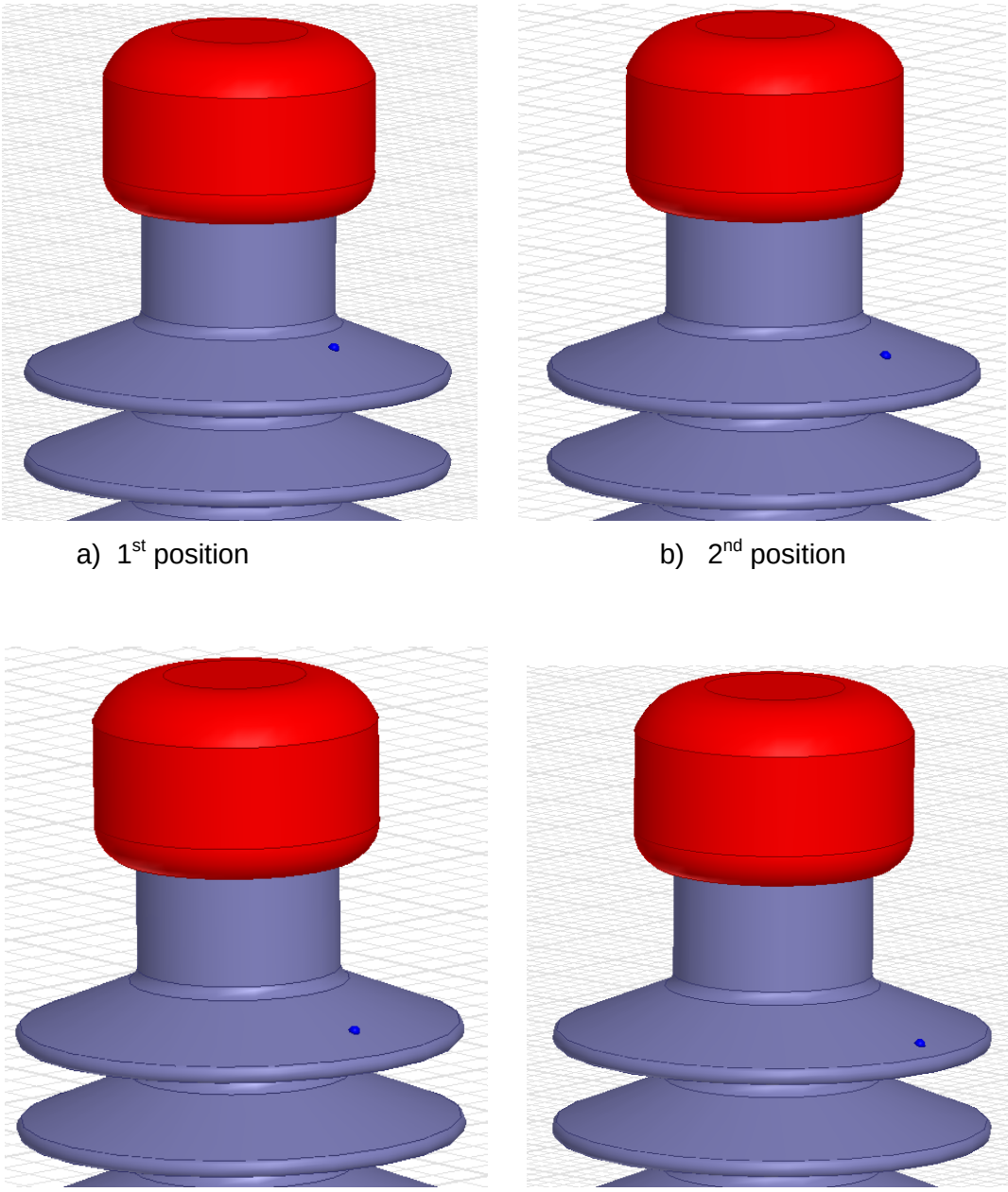

a) 1st position

b) 2nd position

C) 3rd position

d) 4th position

Figure 6.14: Water drop at different positions on the insulator shed

The example for the electric field near the water drop in 3D is shown in the figure 6.15.

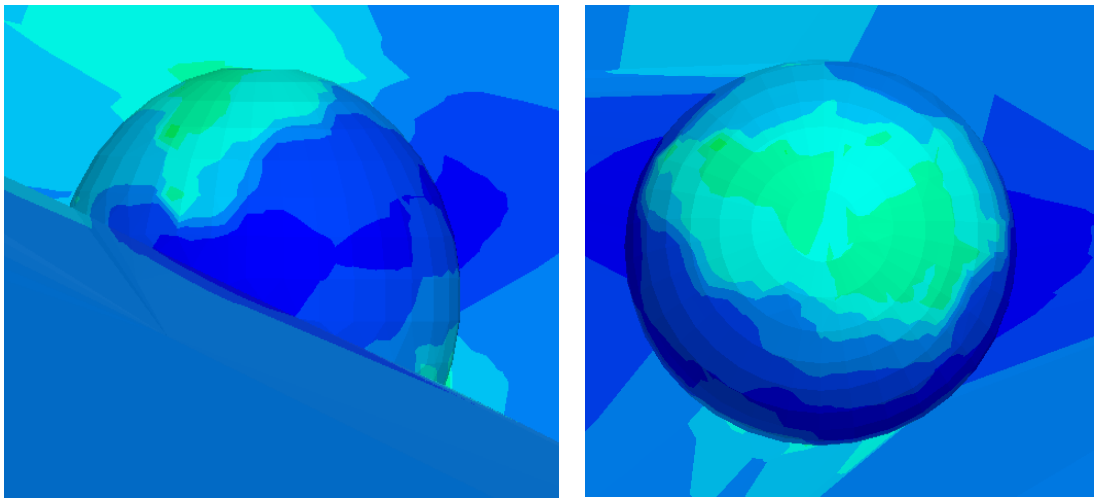

(a) Side view (b) Top view

Figure 6.15: Electric field near the water drop in different views

Simulations in 2D can mislead the understanding of the electric field near water droplet. As per theory it is assumed that the highest values of the electric field occur near the triple junction (between air, insulator surface and water drop surface). After clear observations from figure 6.15, one could say that the highest electric field is occurring near the surface top of the water droplet and is decreasing its value towards down and again increasing near the triple junction. However the highest value occurs near the surface top.

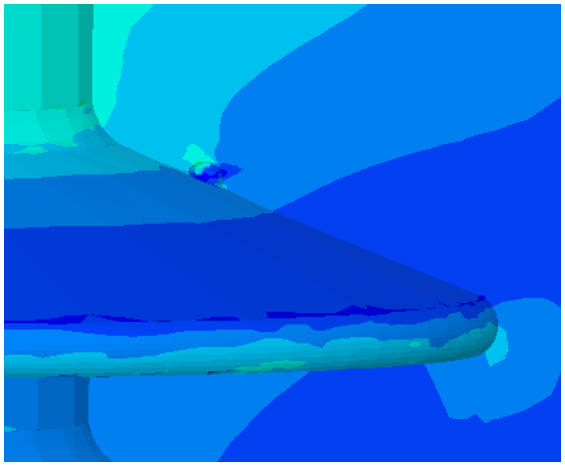

Figure 6.16: Electric field along the shed

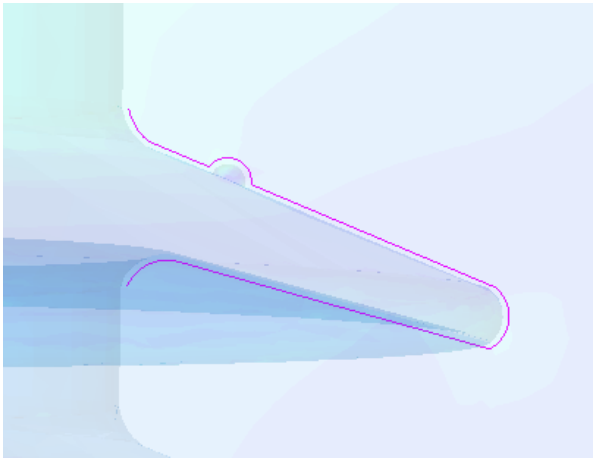

Figure 6.17: Reference line along the water drop and shed surface

As it is mentioned in chapter 6.2.1.1 here also a reference line is considered to measure the electric field values along the shed surface including water drop. The following

graphs in figure 6.18 represent the electric field along the first shed. The values are taken along the line shown in the figure 6.17.

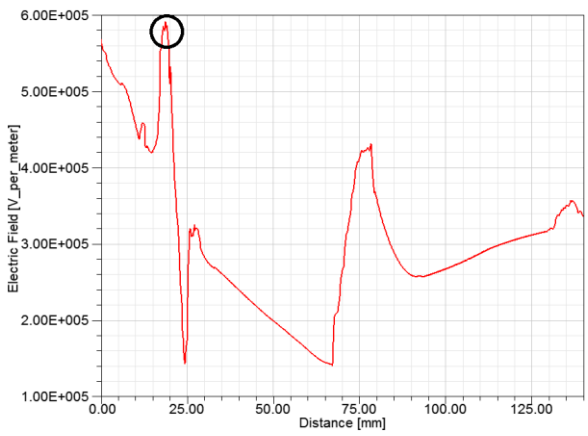


a) 1st position

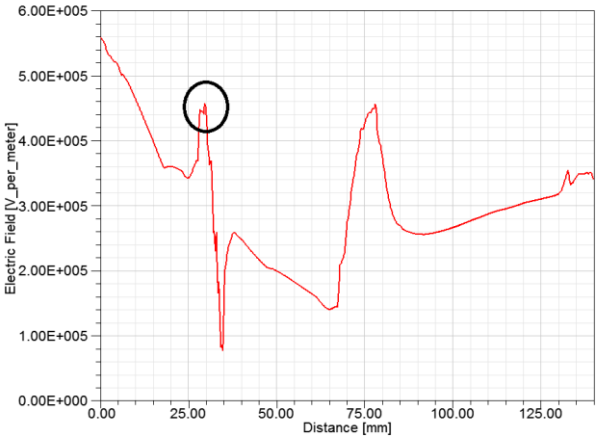


b) 2nd position

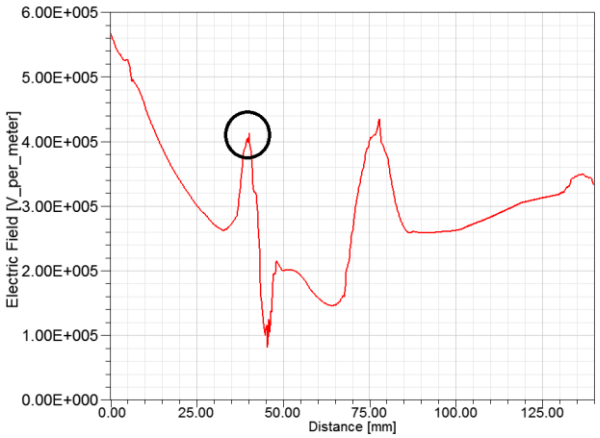


c) 3rd position

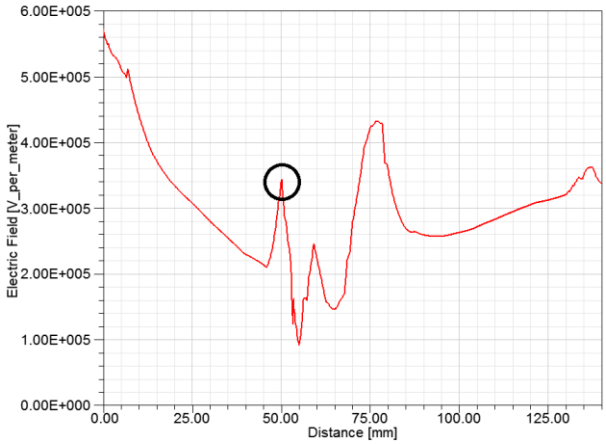


d) 4th position

Figure 6.18: Highest values of the electric field near the water drop along a shed

The electric field values near the water drop (value in the black rings shown in figure 6.18) are considered for investigation. Because of the shape of the shed, there are certain variations in the electric field values along the shed surface. Let us consider figure 6.18(a). If we avoid the starting point in the graph, there is a highest value in the graph other than the highest value near the water droplet. This happens because of the outer curved shape of the insulator shed. This highest value at the edge of the shed could be avoided if there is an optimization in the shed shape. There are substantial

variations in the electric field distribution near the water drop and along the insulator shed. The electric field values obtained at certain positions with and without water drop are shown in table 5.

| position | Maximum Electric field near the water drop (kV/cm) | Electric field without water drop (kV/cm) |
|---|---|---|
| 1 | 5.84 | 3.63 |
| 2 | 4.48 | 2.91 |
| 3 | 4.04 | 2.26 |
| 4 | 3.43 | 1.92 |

Table 5: Electric field values at different positions in 3D (porcelain insulator)

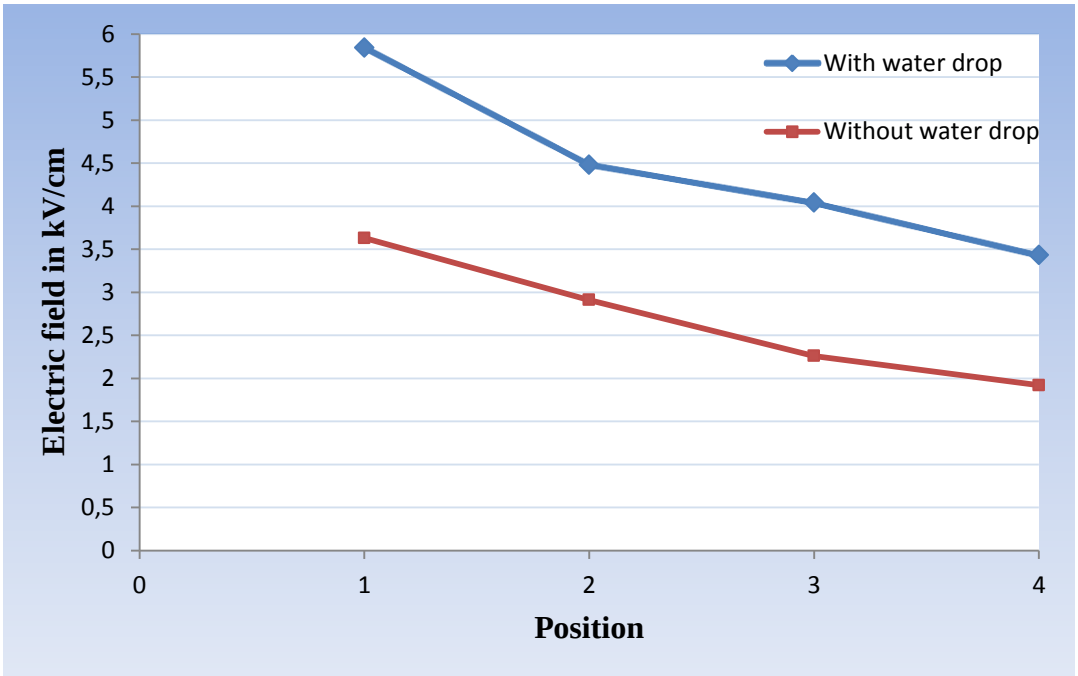


Figure 6.19: Electric field graphs at different positions (porcelain insulator)

The graphs in figure 6.19 have been drawn from the values in table 5. These are the values obtained in the simulation done in 3D. Here, also, the tendency of the electric field near the water drop along the surface of the shed is the same as in 2D. But the values are different and it is clear that the highest values occur not only at the triple

points but also at the top of the surface of the water drop. There is an average of 68% increase in the electric field values with the presence of water droplet compared the values without water drop. It must be noted that due to the behavior of a porcelain surface actually no surface discharges occur due to the water drop. The considerations in this research on porcelain insulators have been carried out solely for reasons of comparison between porcelain and composite insulators.

### 6.3.1.2 Hanging Water Drop Effect

In the above chapter there was a discussion about the moving water drop along the surface of the insulator shed. It described clearly the behavior of the electric field near the water drop when it is on the surface of the shed. This chapter deals with the water drop which is hanging at the edge of the shed. Figure 6.20 shows the position of this water drop. The electric field around the hanging water drop is shown in figure 6.21.

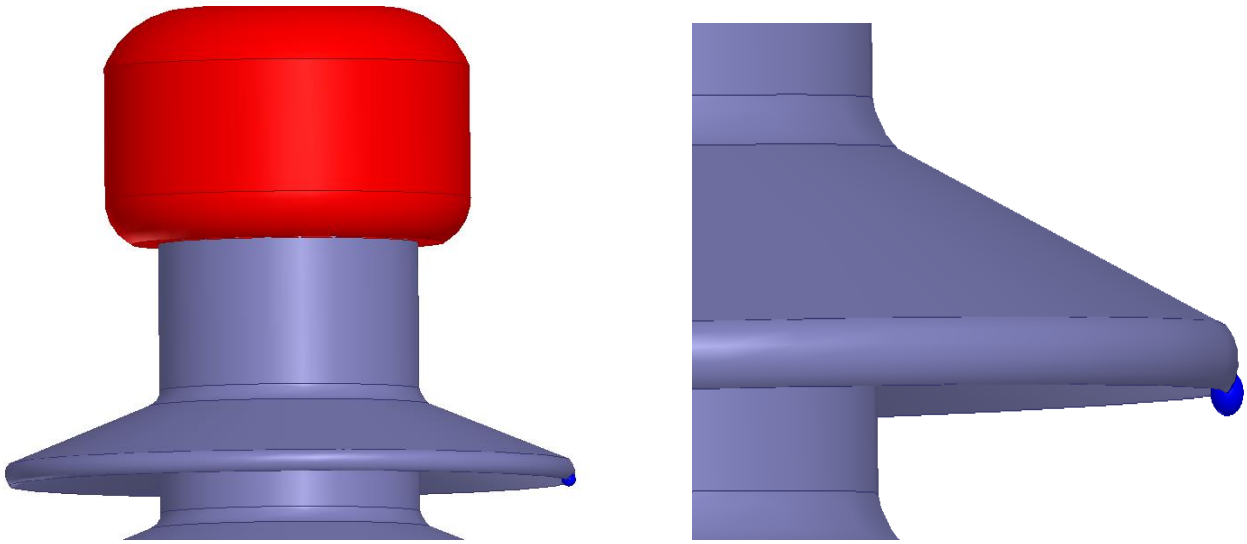

(a) (b)

Figure 6.20: Water drop hanging at the edge of the shed in far(a) and near(b) view

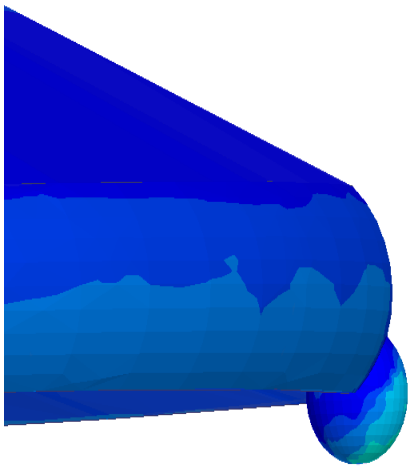

Figure 6.21: Electric field near the hanging water drop

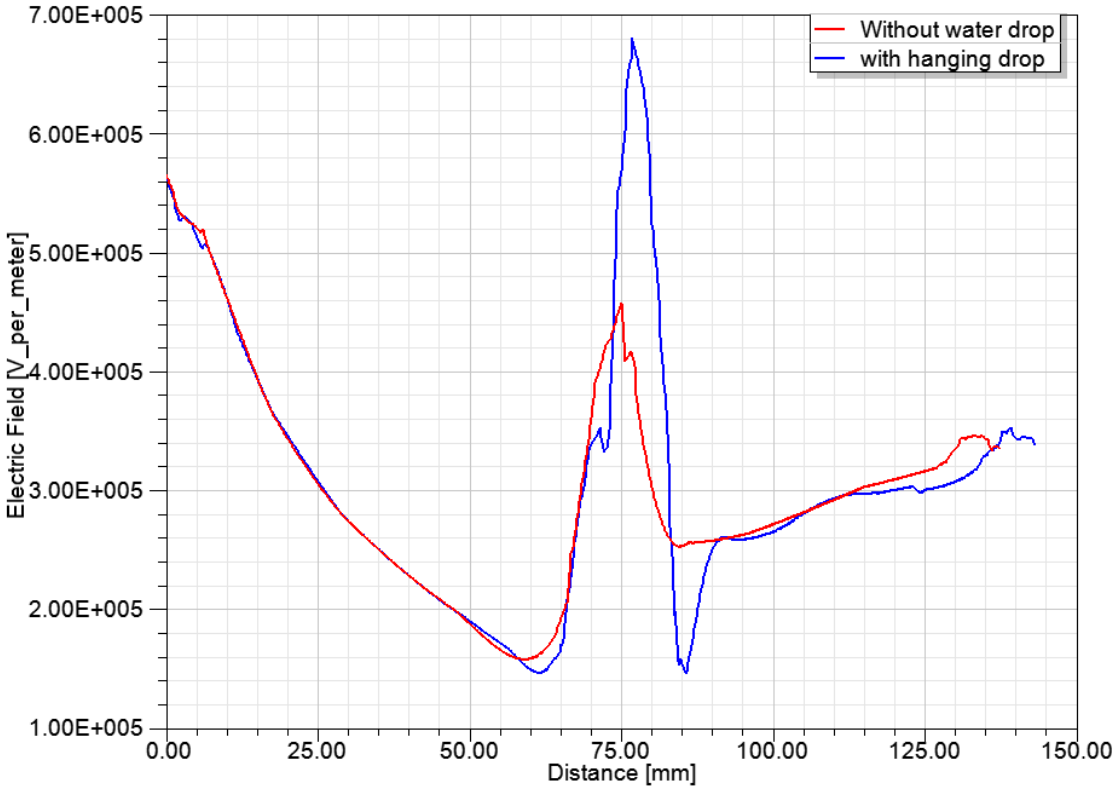


Figure 6.22: Electric field graph with and without hanging water drop along the shed surface

Figure 6.22 shows the deviation in the electric field when the water drop is hanging at the edge of the insulator shed. There is a 51% increase in the electric field with the hanging water drop when compared with the electric field value without water drop. Therefore, it is obvious that there is an effect of a hanging drop at the edge of the insulator shed. This situation has to be considered while designing the shape of the insulator sheds. Specifically in case of DC more precautions should be considered. One suggestion could be optimizing the edge of the shed in such a way that no water drop is hanging to it.

### 6.3.2 Composite Insulator

The previous chapters contain a discussion on the behavior of a water drop on the surface of a porcelain insulator shed. These days the use of composite insulators has been increased. Composite insulators are made of organic materials. Silicon rubber has become the material of choice for the casings of high voltage composite insulators because of the hydrophobicity. After some years in service there is a possibility that the hydrophobicity decreases. The water drops on the insulator sheds can have an effect on the electric field and lead to partial discharges. The surface of the silicon rubber will be able to initiate the surface discharges if the electric field values are in the range of 5 kV/cm [BAO 2014]. It is necessary to study the behavior of water drops on the composite insulator sheds. For this purpose one composite insulator model has been created to understand the water drop behavior over the insulator shed surface.

To avoid complexity in modeling and simulation a simple structure of composite insulator with only two sheds is considered in the investigation of water drop. First a fiber reinforced plastic rod with diameter of 10mm and height of 100mm has been considered. Then silicon rubber sheds with diameter of 70mm are modeled and joined to the FRP rod. These models are shown in figure 6.23.

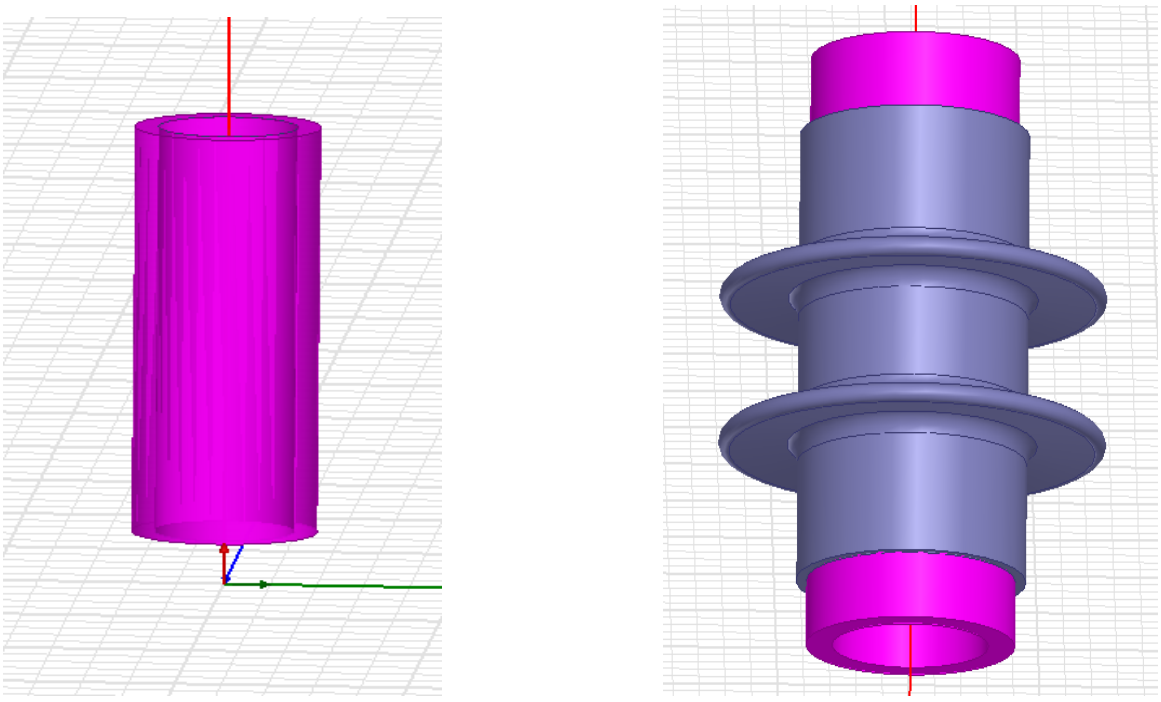

a) Without sheds b) With composite sheds

Figure 6.23: Composite insulator modelled in Ansys Maxwell

Finally aluminium flanges with diameter of 60mm are modelled and joined at the top and bottom of the FRP rod. The fully created model is shown in figure 6.24.

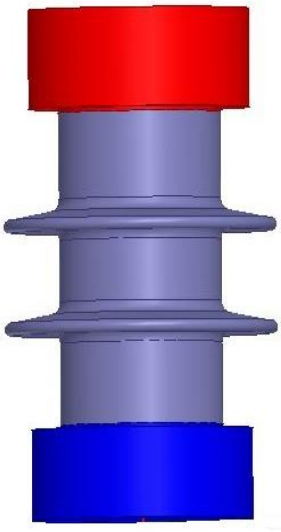

Figure 6.24: Composite insulator model

### 6.3.2.1 At Different Positions of a Water Drop

The water drop is placed on the first shed of the composite insulator and moved towards the end of the shed to study the effect of it on the electric field under DC. The changing positions of the water drop are shown in figure 6.25 (zoomed).

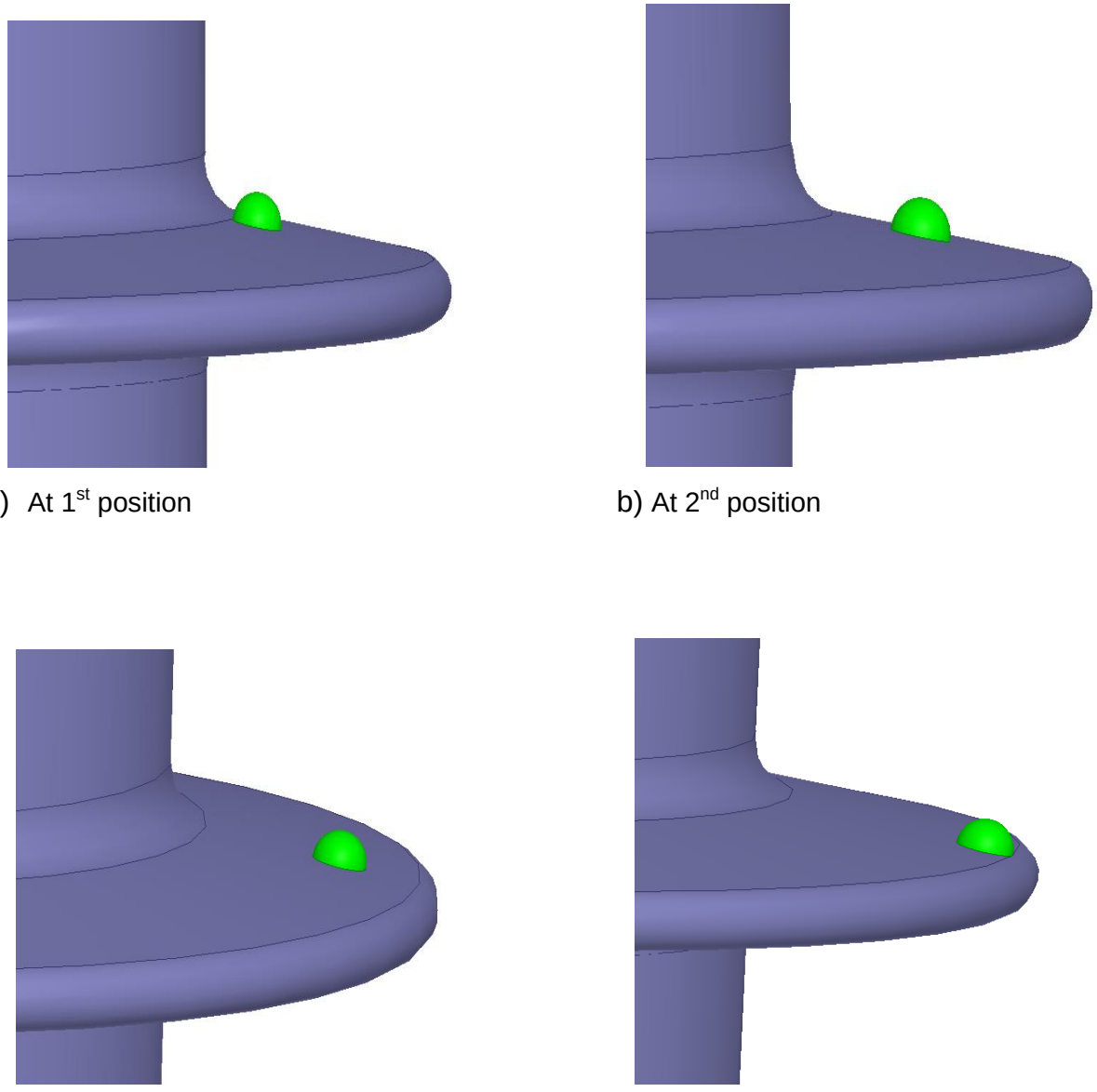

a) At 1st position

b) At 2nd position

c) At 3rd position

d) At 4th position

Figure 6.25: Water drop at different positions on the composite insulator

Figure 6.26 shows the electric field near the water drop on the composite insulator shed. This chapter is dedicated to study the electric field near the water drop. Therefore, the values of the electric field are considered only near the water drop.

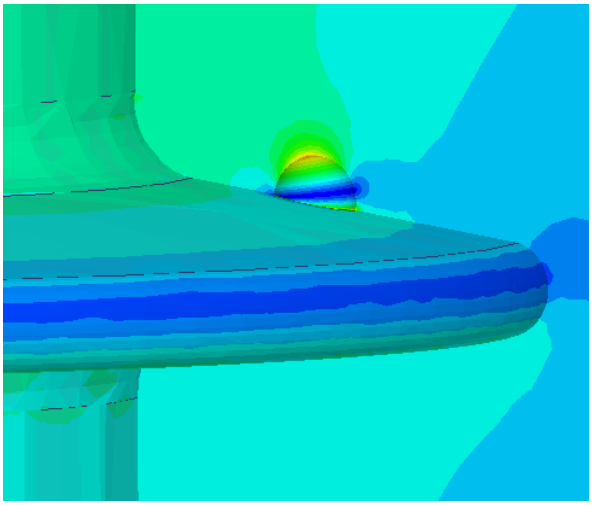

Figure 6.26: Electric field plot near the water drop

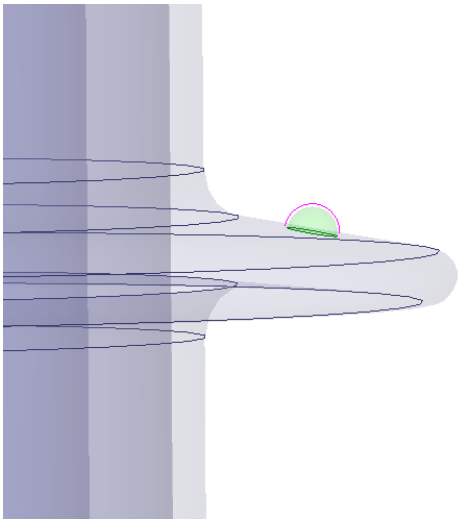

Figure 6.27: Reference line over the water drop

As it is explained in the chapter 6.2.1.1 one reference line is considered to avoid the inappropriate calculations of the electric field. A line 1mm away from the water drop surface is drawn to take the values of the electric field over the water drop which is shown in figure 6.27. The graphs in figure 6.28 show the electric field values near water

drop. The distance given on the x-axis follows the reference line. The 0.00 is where the reference line touches the upper surface of the shed near the water drop.

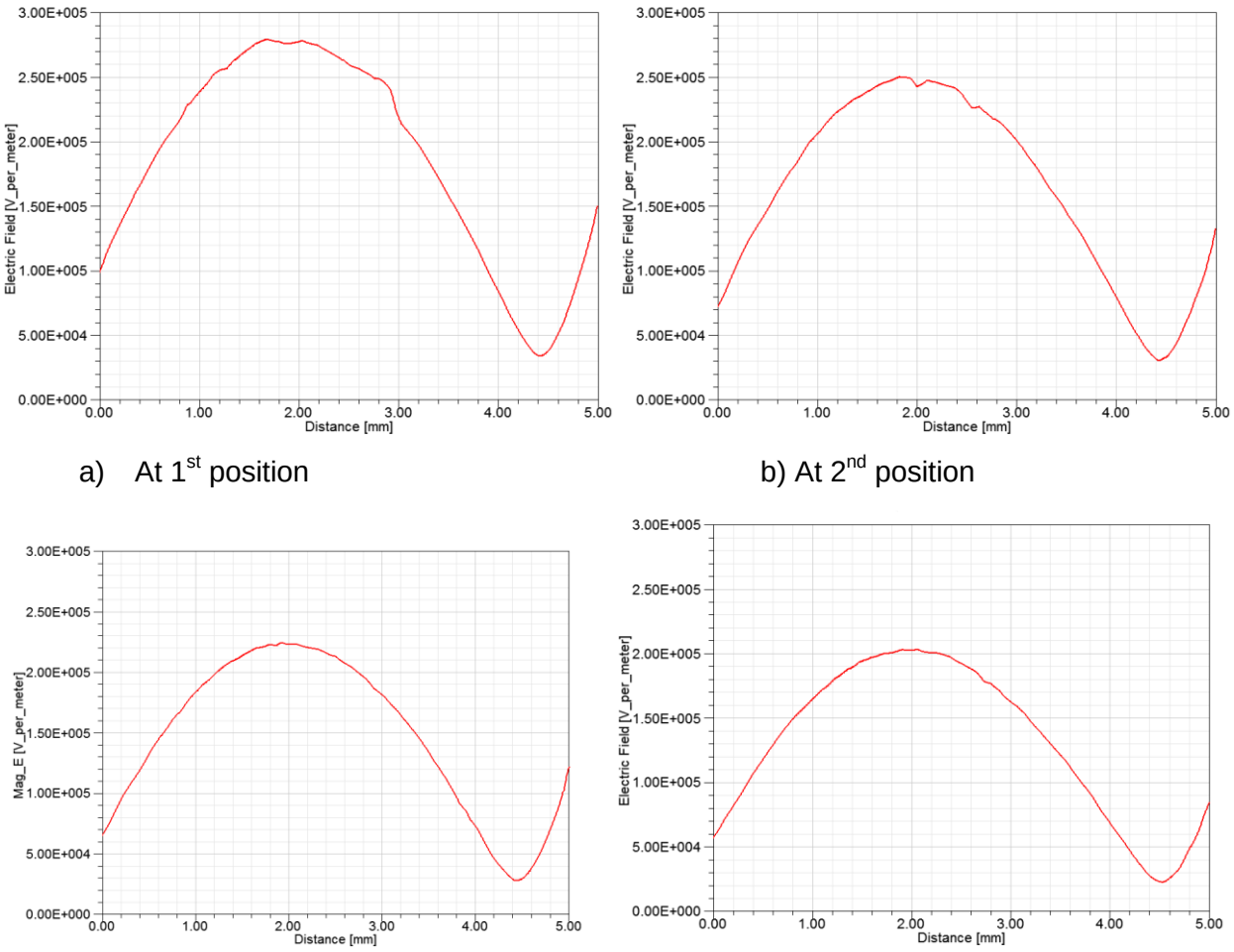


a) At 1st position

b) At 2nd position

c) At 3rd position

d) At 4th position

Figure 6.28: Electric field graph along the water drop at different positions

The table 6 shows the highest values of the electric field obtained near the water drop on the composite insulator shed and the electric field values without water drop at different positions.

| Water drop position | Maximum Electric field value near the water drop (kV/cm) | Electric field without water drop (kV/cm) |
|---|---|---|
| 1 | 2.81 | 0.98 |
| 2 | 2.50 | 0.71 |
| 3 | 2.25 | 0.64 |
| 4 | 2.03 | 0.58 |

Table 6: Electric field values near the water drop at different positions (composite insulator)

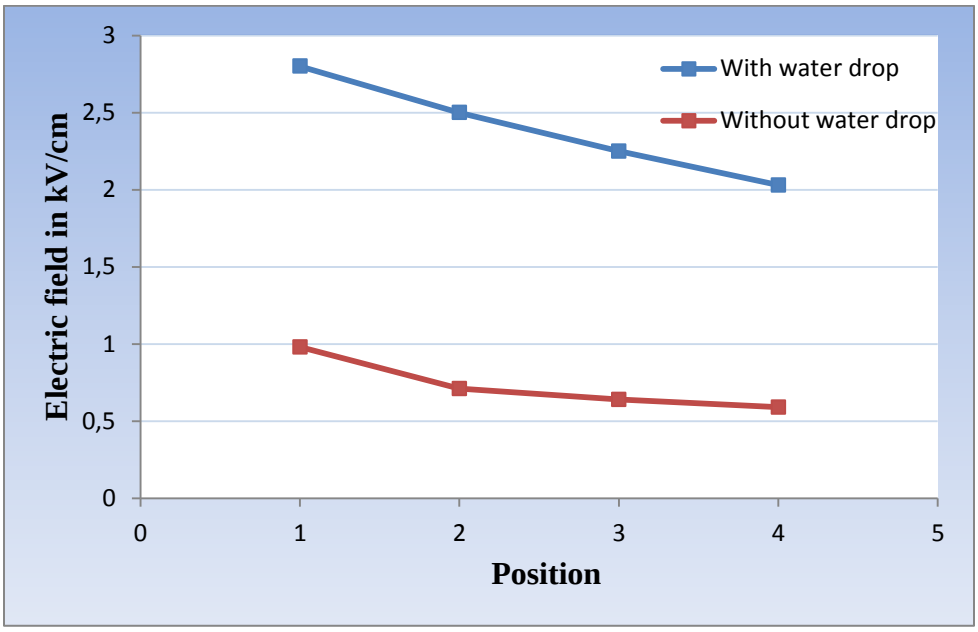


Figure 6.29: Graph of electric fields at different positions (composite insulator)

From the graph in figure 6.29 it is clear that even in the case of a composite insulator the electric field values near the water drop are decreasing as the drop moves towards the end of the shed. The main difference is in the values of decrease. In case of composite insulators there is a constant reduction in the electric field values while the drop is moving to the end of the shed. The electric field values with the water drop have more than 100% increase compared to the values without water drop. These simulation results are too low to initiate surface discharges on the composite insulator because the discharges are possible only if the electric field stress is higher than 5 kV/cm.

### 6.3.2.2 Hanging water drop

This chapter discusses the situation of a hanging water drop at the edge of the composite insulator shed. The hanging water drop is shown in figure 6.30 and the electric field over the surface of drop is shown in figure 6.31.

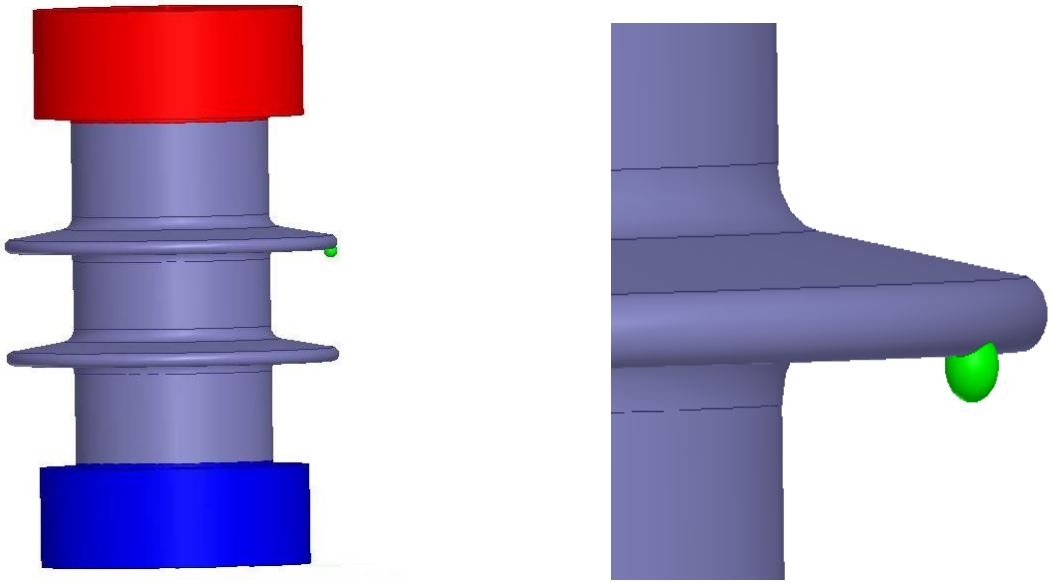

(a) (b)

Figure 6.30: Far(a) and near(b) view of hanging water drop on composite insulator

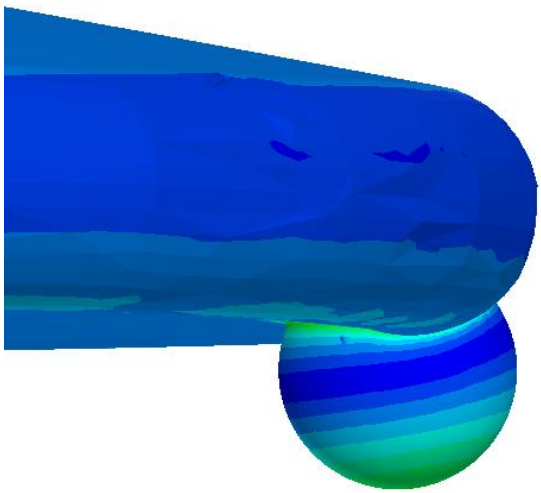

Figure 6.31: Electric field near the hanging water drop on composite insulator

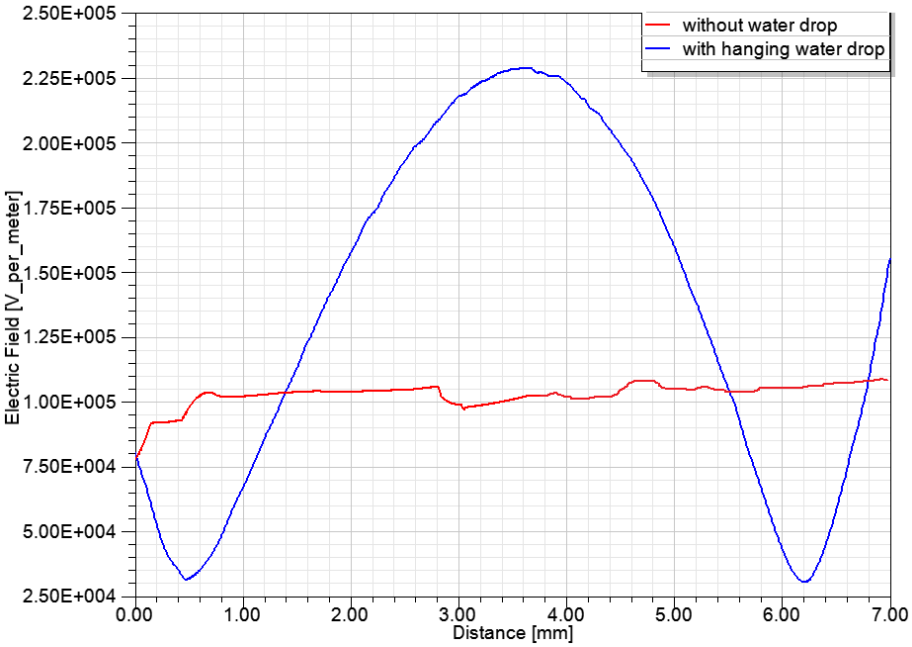


Figure 6.32: Electric field on the composite insulator with and without hanging water drop

The value of the electric field with the hanging water drop is 2.3 kV/cm, and the value at same position without drop is around 1 kV/cm. Therefore, there is an increase of more than 100% with the hanging water drop. This observation has to be considered while designing the polymer sheds for the polluted areas.

### 6.3.3 Comparison of Porcelain and Composite Insulator Results

According to the chapters 6.3.1 and 6.3.2 (figures 6.19 and 6.29) it is clear that the tendency of the electric field values near the moving water drop on porcelain and composite insulators is same. The main difference is in the values of decrease. The applied voltages for the modelled insulators are based on the conditions given in the IEC standard 60815[IEC 2008]. The main parameters considered to apply the voltage are length of the insulator, creepage distance and diameter of the sheds.

Results show that there are virtually no flashovers along the wet upper surface of porcelain sheds. Although as stated in 6.3.2 the electric field on a composite insulator shed with water drops may obtain locally higher values which should be kept below 5 kV/cm in order to avoid surface discharges.

## 6.4 Behavior of Electric Field by Change in Contact Angle between Water Drop and Insulator Surface

As per the theory, the contact angle between the insulator surface and water drop has an impact on the electric field. Therefore it is important to observe the simulation results for it. For this purpose four different angles are considered and observed in the simulation results. At first the angle between the shed surface and the water drop is maintained at 30 degrees. Then it is changed to 60, 90 and 120 degrees. These differences are shown in figure 6.33.

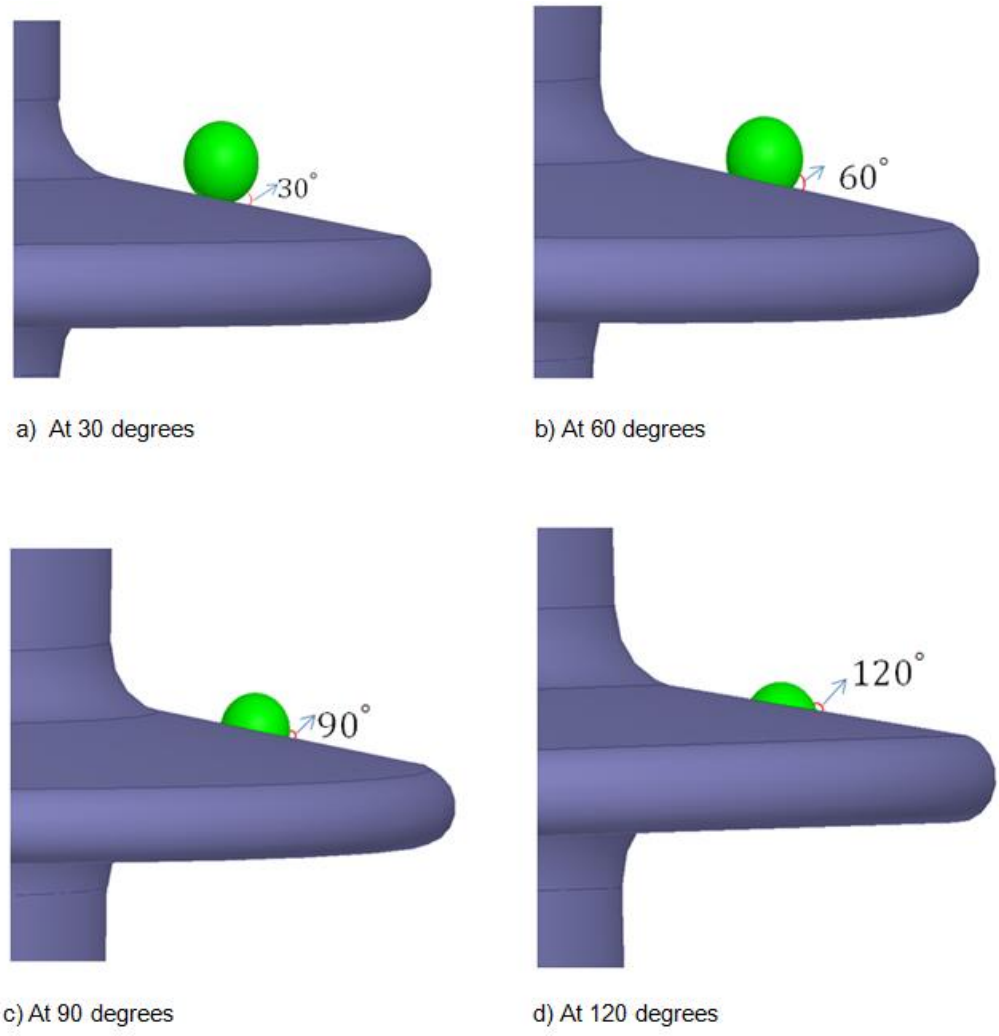


Figure 6.33: Different contact angles between insulator surface and a water drop

The electric field is measured at the contact angle between the shed surface and the water drop. Values of the electric field for each angle are represented figure 6.34.

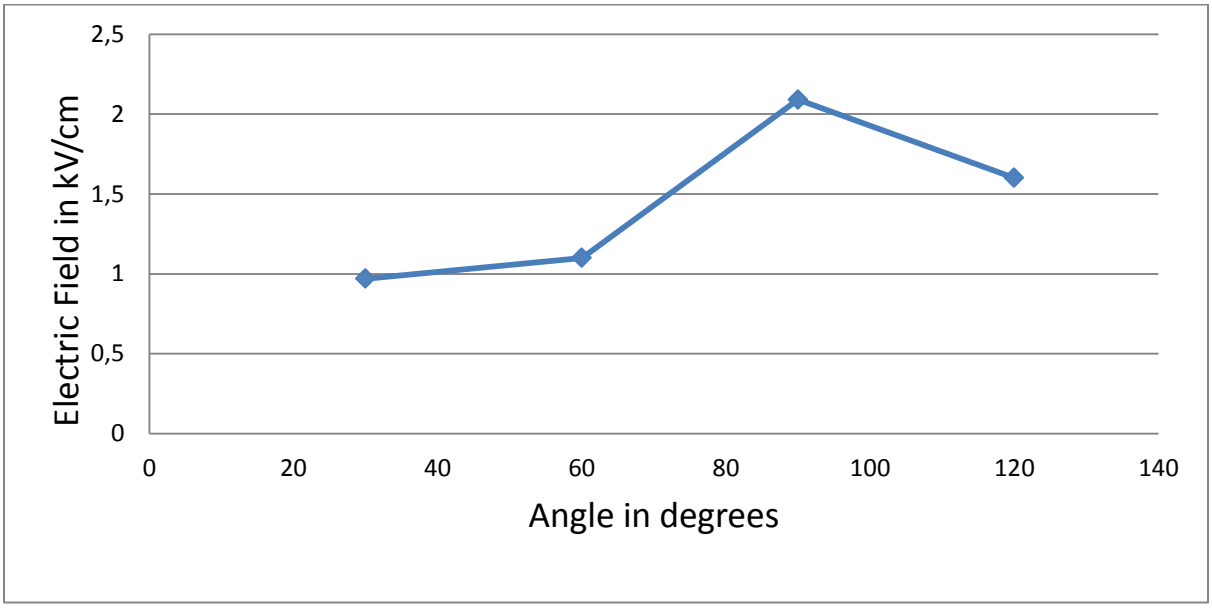


Figure 6.34: Maximum electric field enhancement at water drops

The results show that there is an increasing value of the electric field while changing the contact angle from 30 to 90 degrees. Then there is a certain decrease at greater than 90 degrees. The electric field value determined without water drop is 1.1 kV/cm which is near the value with the water drop at the contact angle of 60 degrees. These results showed how the changing contact angle affects the electric field. The angle above 120 degrees is not considered for simulation as it does not happen in real situations.

# 7 Behavior of DC Electric Field on Parallel Insulators

The behavior of parallel insulators under electric field stress is one of the problems encountered on transmission as well as distribution networks in power systems. The aim of this work is to analyze the electric field stresses between parallel or double insulator assemblies under stresses of DC voltage. Some insulator assemblies used in substations and on transmission lines have to be designed with two parallel insulators due to the structural or mechanical requirements. One example is the double insulator assembly used in disconnectors or on overhead transmission lines.

Electric field characteristics on the surface of parallel insulators have an obvious influence on corona generation, surface discharge and flashovers. The distance between the insulators is the key parameter which must be considered in the design of the structure of double insulator assembly. Based on the finite element method, this chapter illustrates the electric field behavior of parallel insulators under DC.

## 7.1 Difference in Behavior of Electric Field on Single and Parallel Insulators

### 7.1.1 Single Insulator

It is easy and sufficient to simulate the simple models instead of complex models which usually take so much random access memory and time. Here insulator without sheds is considered as the simple model. For comparison and to know the behavior it is sufficient to use the simple models. Single insulator with the following parameters is considered to compare the results with the parallel insulators behavior and shown in figure 7.1.

| | |
|---|---|
| Length of the insulator | : 1000 mm |
| Core diameter | : 100 mm |
| Diameter of top and bottom flanges | : 120 mm |
| Material of the insulator | : Porcelain |

Relative permittivity : 5.7

Conductivity : 0 Siemens/m

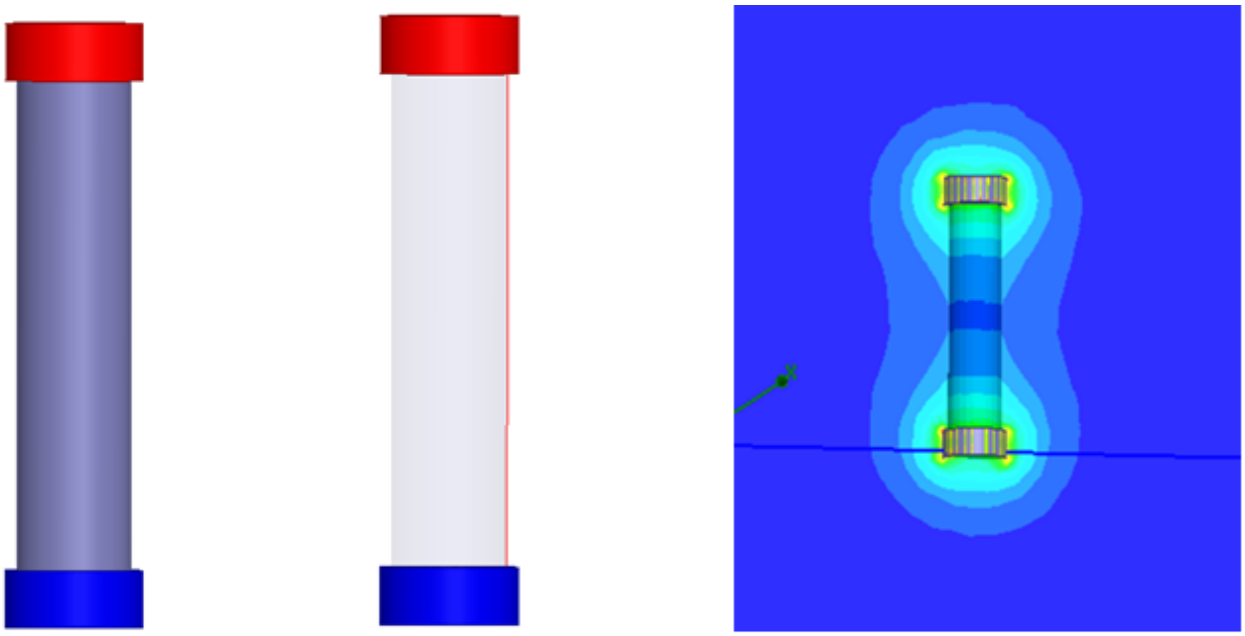


Figure 7.1: Single insulator model (a) with reference line (b) and electric field distribution (c)

In order to minimize discretization errors with mesh statistics, a reference line is considered 1 mm away from the insulator surface (figure 7.1(b)). In mathematics discretization means the process of transferring continuous models and equations into discrete counterparts. This process usually is carried out as a first step for numerical evaluation and implementation on digital computers. More explanation on this regard is given in chapter 6.2.1.1.

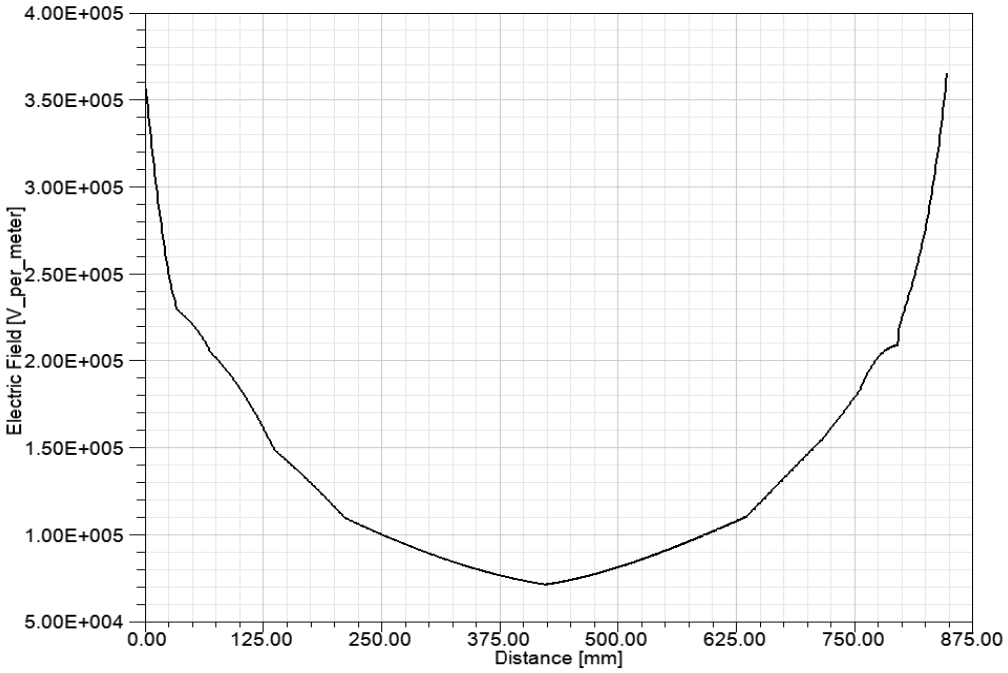


Figure 7.2: Electric field along the reference line of single insulator

The graph (figure 7.2) indicates the electric field along the reference line which is obtained 1mm away from the surface of the insulator. The distance in x-axis represents the length of reference line from top to bottom (Distance: 0.00, top of the reference line). It is clear that there is a gradual decrease in the electric field from top of the insulator till it reaches the middle and then there is a gradual increase till the bottom of the insulator (position 875.0mm).

### 7.1.2 Parallel Insulators

It is not possible to simulate the parallel insulator models with two dimensional axisymmetric solution types as a double insulators structure is not axisymmetric. Because of this reason three dimensional solution types with simple models are considered to show the behavior of parallel insulators with and without pollution. Two insulators with the same diameter of 100mm in parallel are considered for the simulation. The same parameters shown in chapter 7.1.1 are considered for both

insulators. For simulation purpose, the distance of 300 mm is maintained between the axes of the parallel insulators (figure 7.3).

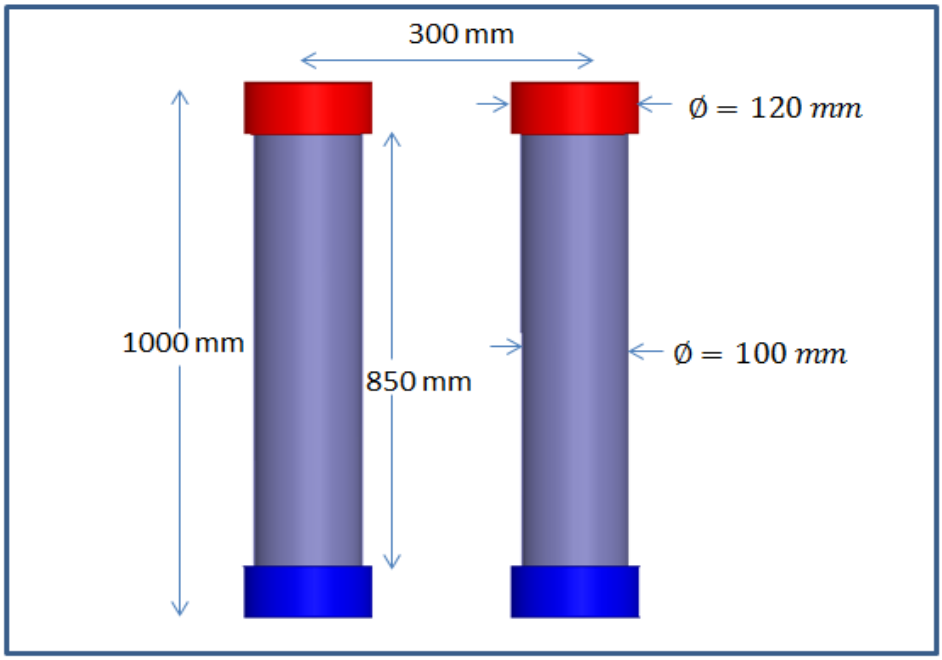


Figure 7.3: Double insular assembly

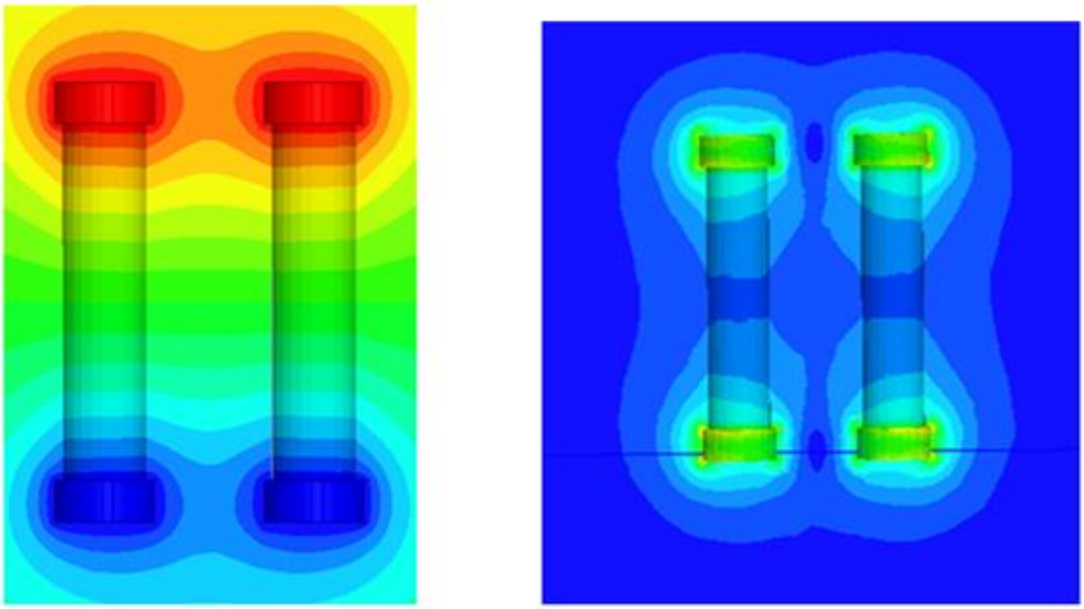


Figure 7.4: Voltage (a) and electric field (b) distribution of clean parallel insulators

Figure 7.4 shows the electric potential and field distributions between the parallel clean insulators. The graph in figure 7.5 indicates the electric field along the reference line on the same left side insulator as in figure 7.1(b) but with an another insulator next to it.

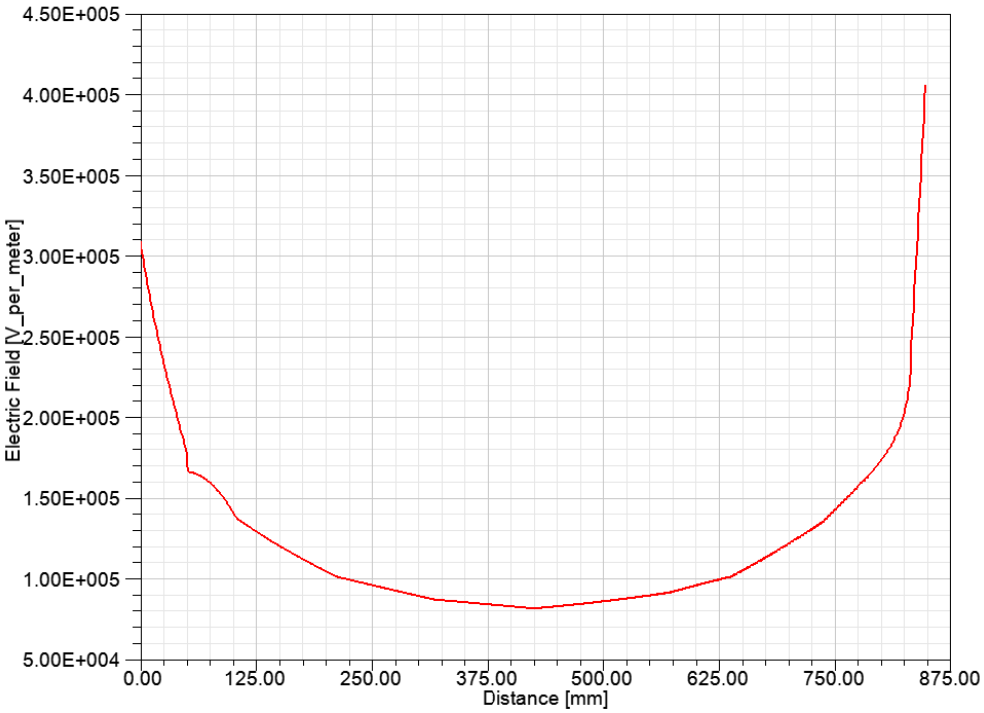


Figure 7.5: Electric field along the inner surface of the first insulator

Here also it is clear that there is the same tendency in the graph compared with single insulators, except the values. To observe the actual difference in values with single and parallel insulators it is better to combine both graphs (figure 7.2 and figure 7.5). Figure 7.6 compares the electric field distribution along the surface of a single insulator and along the same insulator surface with existence of a parallel insulator.

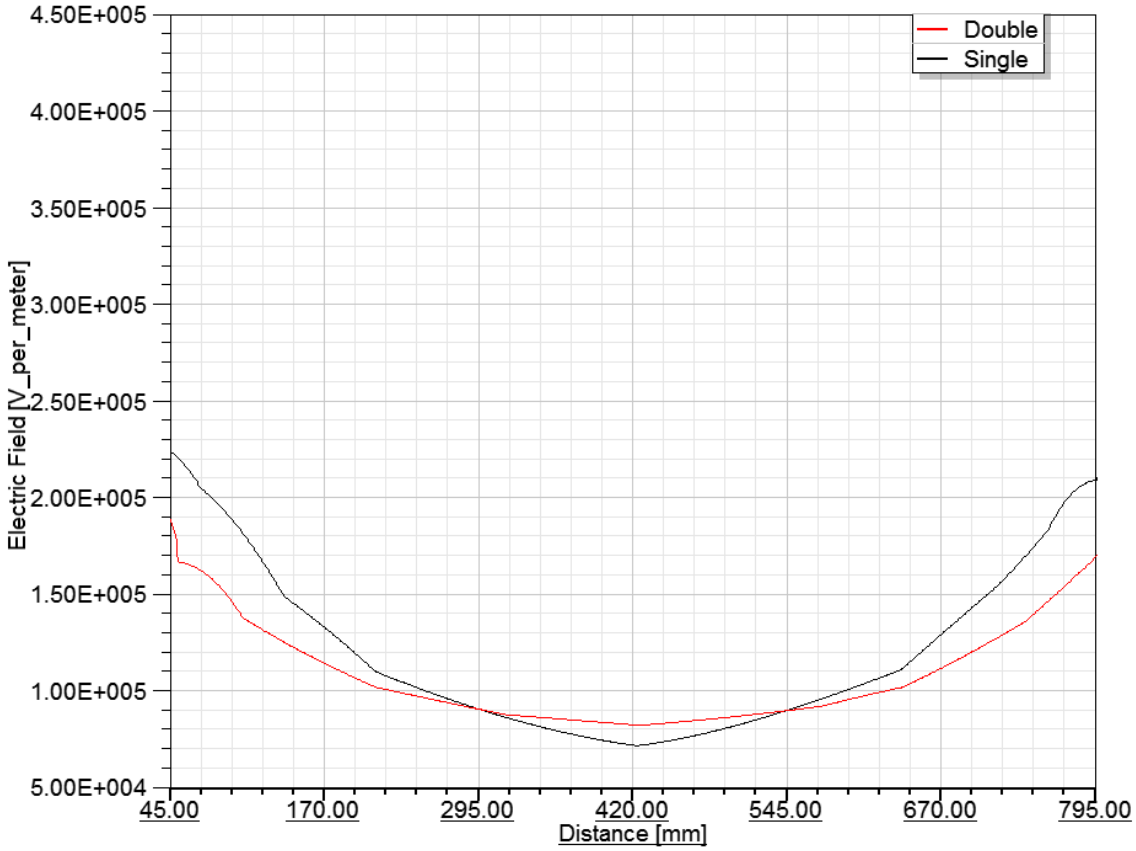


Figure 7.6: Electric field comparison with single and parallel clean insulators

The red line indicates the graph with parallel insulators and the black line indicates the single insulator graph.

After observing the combined graphs in figure 7.6 one could say that there is a reduction in the electric field values with the double insulator assembly when compared to a single insulator. We can observe this phenomenon except in the middle region. There is an explanation for this exception region in the chapter 7.3.1. If we exclude this exceptional region there is an average of 24.5% decrease in the electric field because of the existence of a parallel insulator. These two insulators have an effect like a conductor bundle with virtually enlarged surface and thus reduced electric field.

To avoid confusion at the ends of the insulator material (especially at the triple point region: the contact junction of insulator material, aluminium flanges and air) the electric

field values are not considered for the length approximately 50 mm at the ends of the insulators.

Parallel clean insulators result in a virtual enlargement of the electrode areas (upper and lower flange) (figure 7.4) and thus in a more equal electric field distribution over the length of the insulators as in figure 7.6 shows.

## 7.2 Electric Field between and outside of Parallel Insulators

Before approaching to study the behavior of the electric field on the surfaces of the parallel insulators with pollution, it is better to look at the behavior of insulators without pollution. Here we can observe the potential and electric field distributions between the parallel insulators.

### 7.2.1 Insulators with 100mm Diameter

The parameters for the parallel insulator are considered to be same as from the figure 7.3. Top and bottom flanges made of aluminum alloy with a diameter of 120mm are considered in the simulation. The core diameter of insulators is 100mm and the distance between the insulator axes is 300mm. The balloon boundary is taken 1000 mm away from the test object. It is maintained at the same distance along the three axes.

In order to minimize discretization errors with mesh statistics while calculating the electric field along the surfaces of the insulators, the reference lines 1 to 4 (Figure 7.7) are considered 1mm away from the insulator surface. The electric fields are calculated along these four reference lines and shown in figure 7.8. Lines 1 and 2 are inner surfaces( between the insulator configeration) and lines 3 and 4 represent outer surfaces (outside of the insulator configeration) of the parallel insulators.

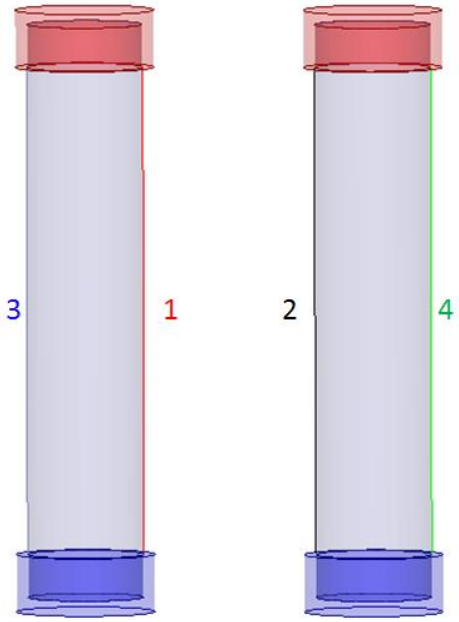


Figure 7.7: Reference lines representation along the insulator surface

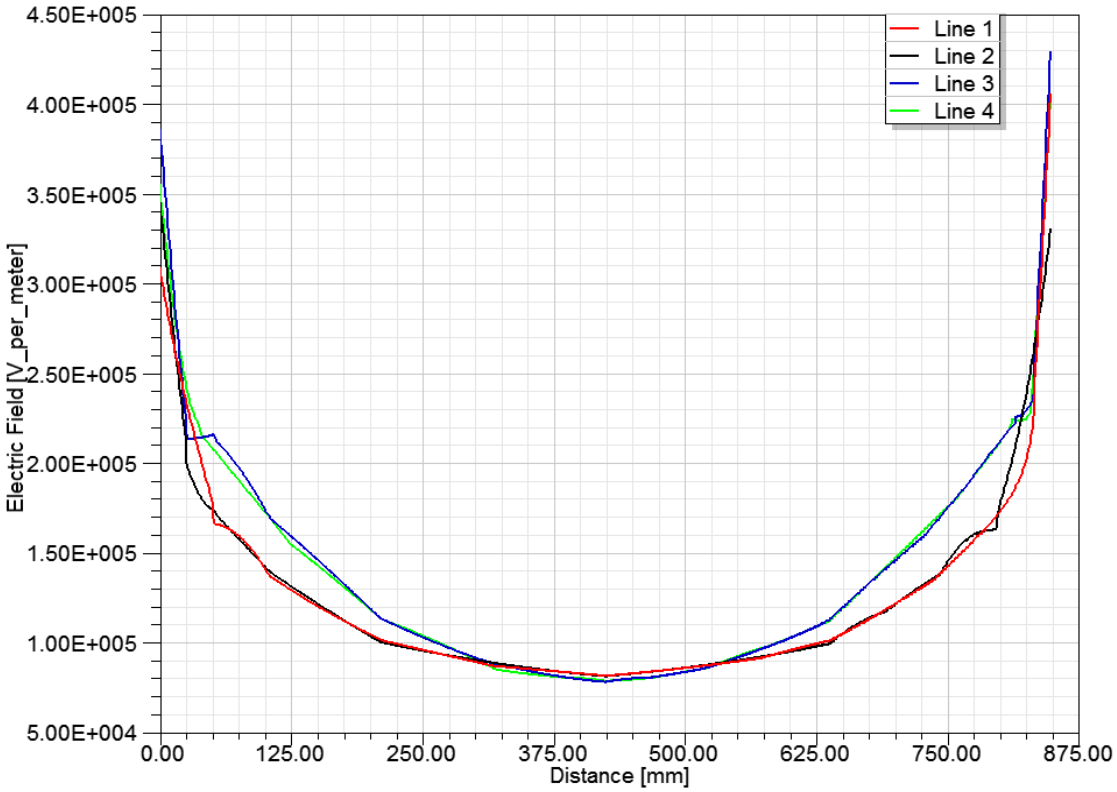


Figure 7.8: Electric field along the inner and outer surfaces of the insulators

### 7.2.2 Insulators with 200mm Diameter

Now insulators with 200mm diameter are considered to compare the inner and outer electric field behavior of the parallel insulators. The distance between the insulator axes and the length of the insulators are maintained to be the same as before shown in the figure 7.3. The diameter of the flanges is 220mm. Parallel insulators with these parameters are shown in figure 7.9.

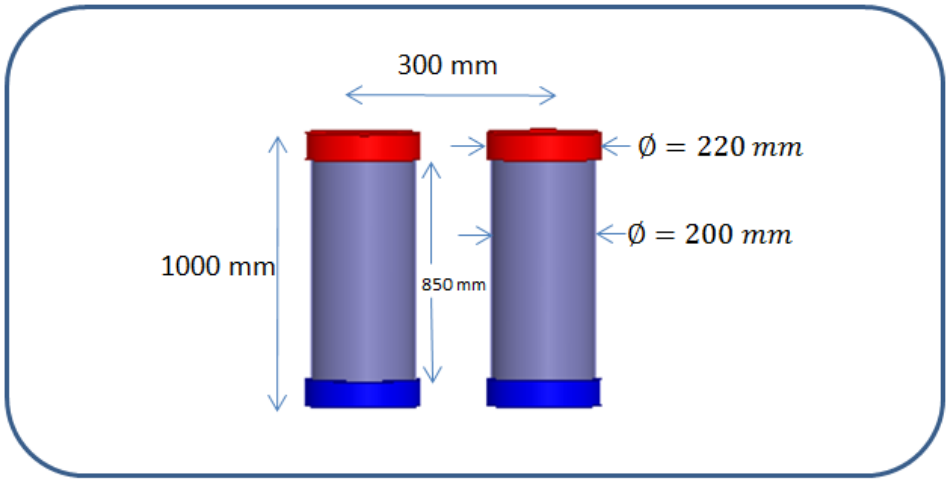


Figure 7.9: Insulator models with 200mm diameter

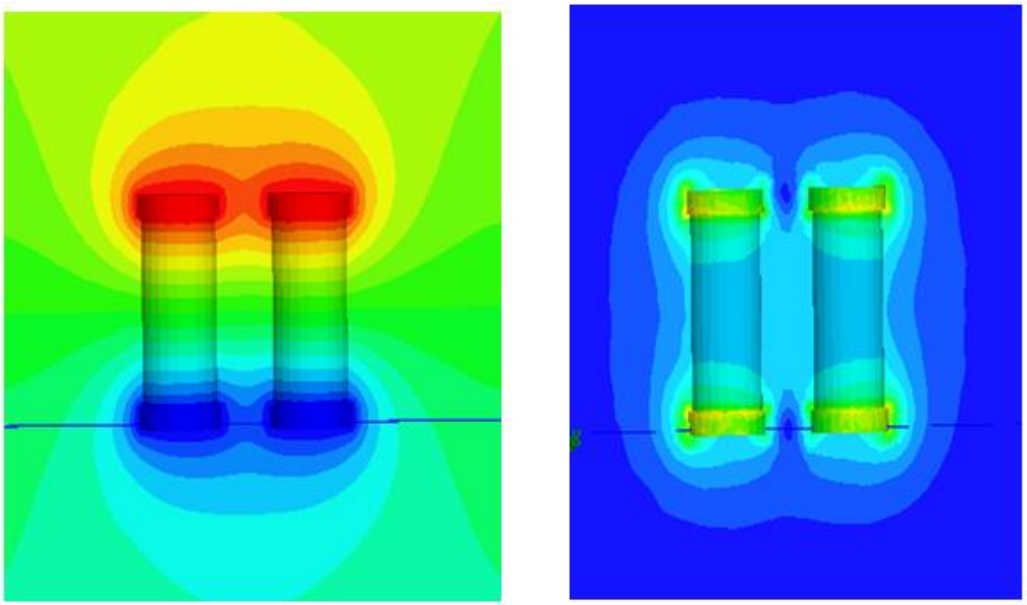


Figure 7.10: Voltage (a) and electric field (b) distribution of parallel insulators of 200mm diameter

The voltage and electric field distributions (figure 7.10) of insulators with 200mm diameter from the high potential terminal to ground are similar to insulators with 100 mm diameter (figure 7.4).

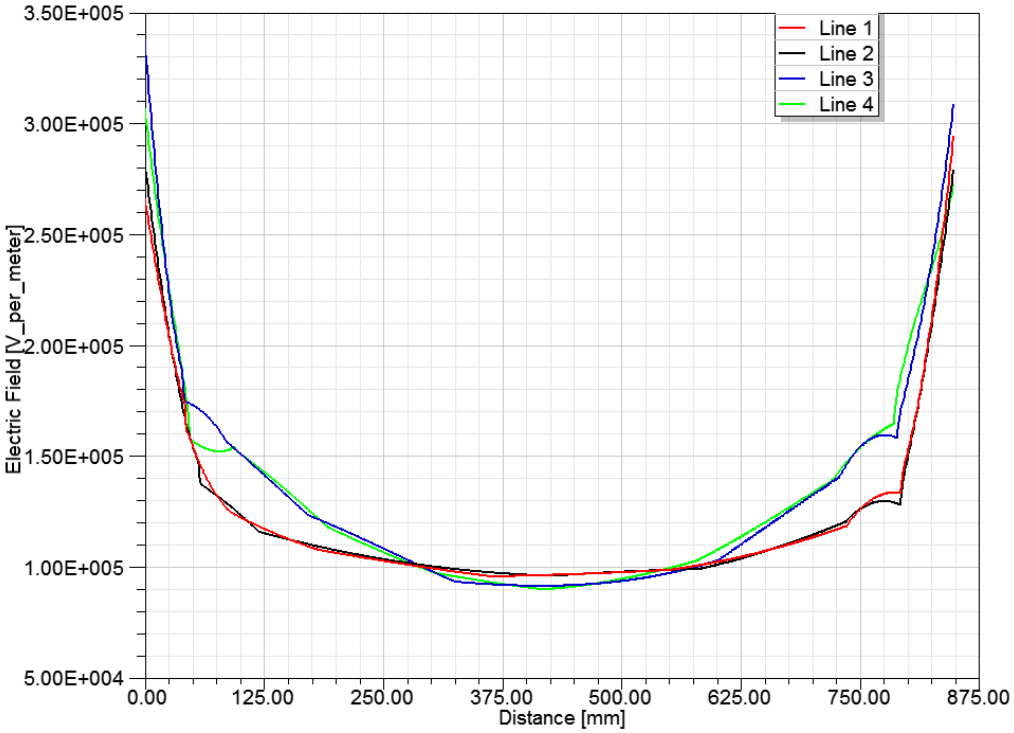


Figure 7.11: Electric field along the inner and outer surface of 200mm diameter insulators

The electric field values along the four reference lines are measured. These reference lines are to be considered to be same as in figure 7.7 but on the surface of insulators with 200 mm diameter. The electric field graphs are shown in figure 7.11.

### 7.2.3 Insulators with Different Diameter

In the previous section, the behavior of the electric field along the inner and outer surfaces of the parallel insulators with the same diameter has been studied. It is found that the behavior is the same in two cases. It is shown in chapters 7.2.1 and 7.2.2, respectively.

This chapter explains the behavior of the electric field over the surfaces of the parallel insulators with different diameters (figure 7.12). This type of double insulator assembly is observed in vertical and pantograph disconnectors. Two insulators with diameters of 200mm and 100mm are considered to show the effect on the inner and outer surfaces of the insulators. The voltage and electric field distributions are shown in figure 7.13.

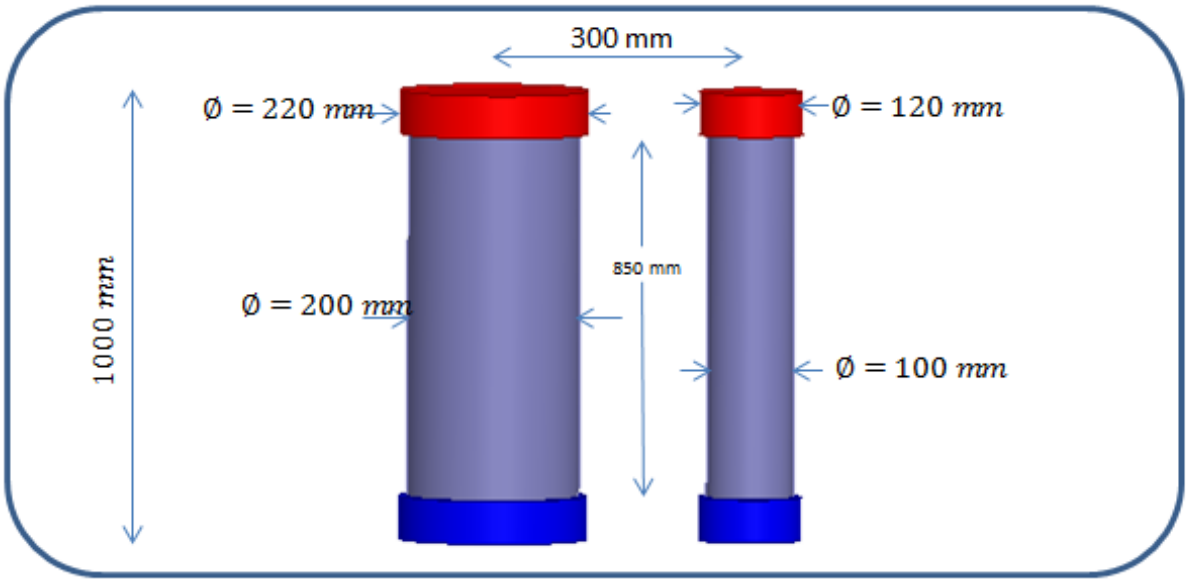


Figure 7.12: Insulator models with different diameter

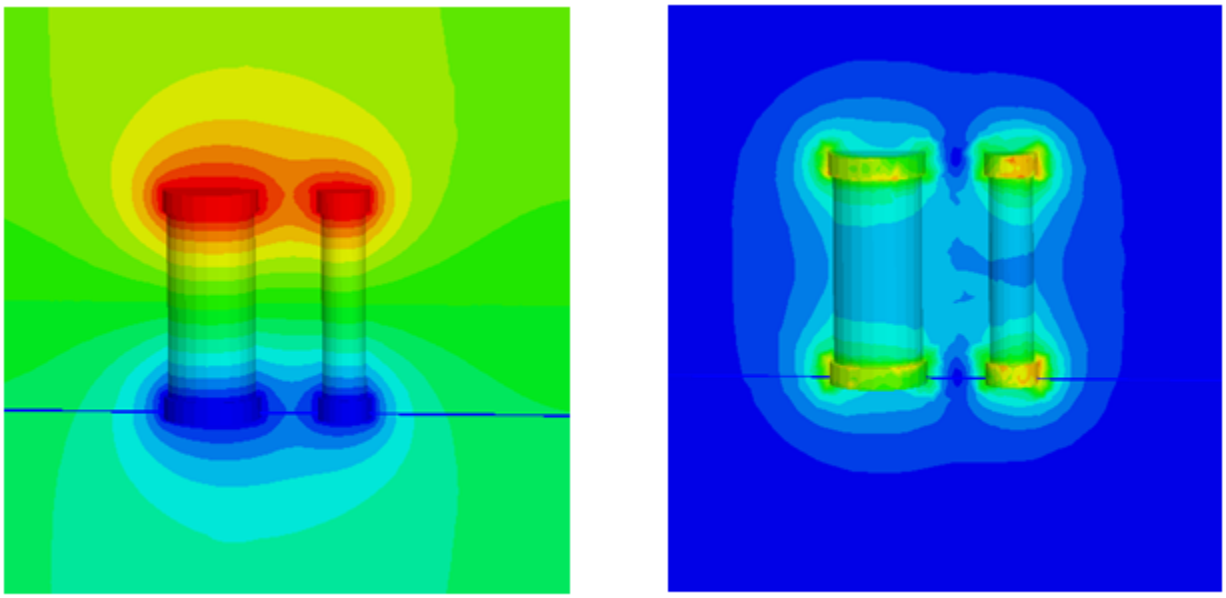

(a) (b)

Figure 7.13: Voltage (a) and Electric field distribution (b) over insulators with different diameter

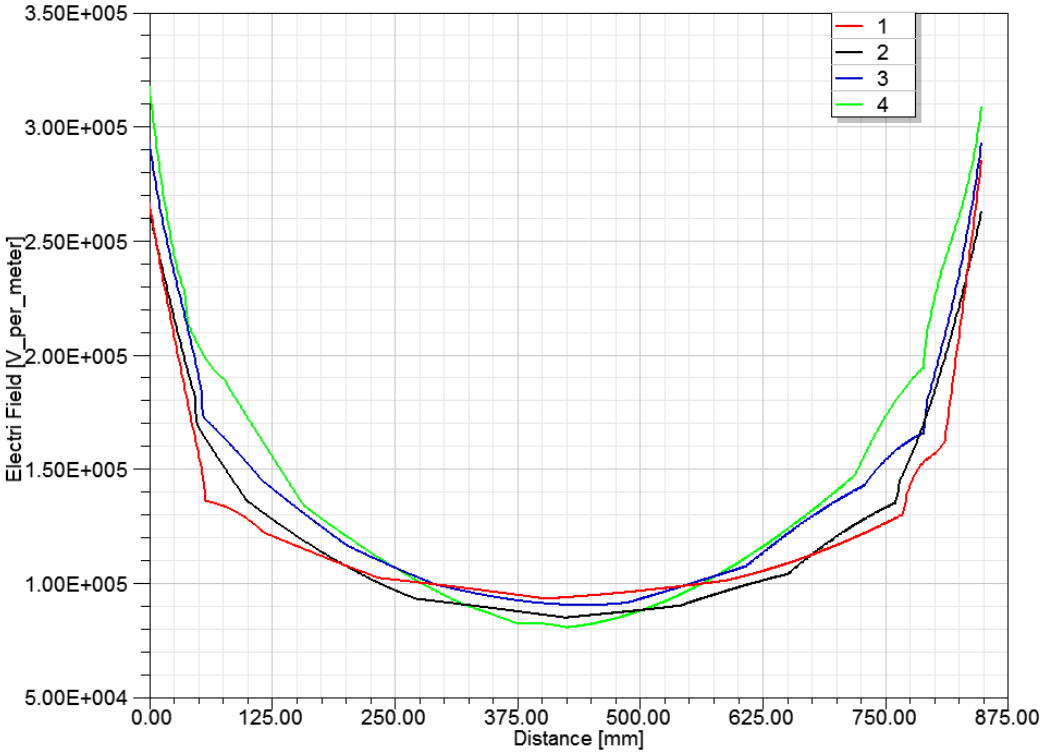


Figure 7.14: Electrical field distribution along the inner and outer surfaces of insulators with different diameter

The electric field values along the reference lines (see in figure 7.7) but on the surface of insulators with different diameter are shown in figure 7.14. The graphs with different colors indicate different surfaces of the insulators. Because of the difficulty in creation of fine mesh the graphs are not changed gradually. However, the behavior or tendency of the electric fields over the inner and outer surfaces of the parallel insulators with different diameters is the same as the parallel insulators with same diameter.

## 7.3 Study of Electric Field on Parallel Insulators with and without Pollution

In this chapter, a study of the behavior of the electric field between parallel insulators with and without pollution is presented. The electric field distribution on the surfaces of parallel clean insulators is already described in chapter 7.1.2. In this chapter the

behavior of the electric field distribution in the middle between parallel clean insulators will be studied. Later a uniform pollution layer is applied over the surfaces of single and parallel clean insulators to study the electric field distribution on the surface of parallel polluted insulators.

### 7.3.1 Electric Field without Pollution

The aim of this chapter is to describe the behavior of the electric field between parallel insulators without pollution and to illustrate some of the key reasons for the difference in the behavior of the electric field in the middle between parallel insulators. In practice it is usually easy to investigate the behavior of the electric field on a single insulator without pollution. For parallel insulators the knowledge of electric field vectors (E- vector) is required. Parallel clean insulators considered in this chapter have the same parameters as of 100mm diameter insulators (figure 7.15 (a)) which are shown in previous chapters. The electric field distribution on the clean parallel insulators is shown in figure 7.15(b).

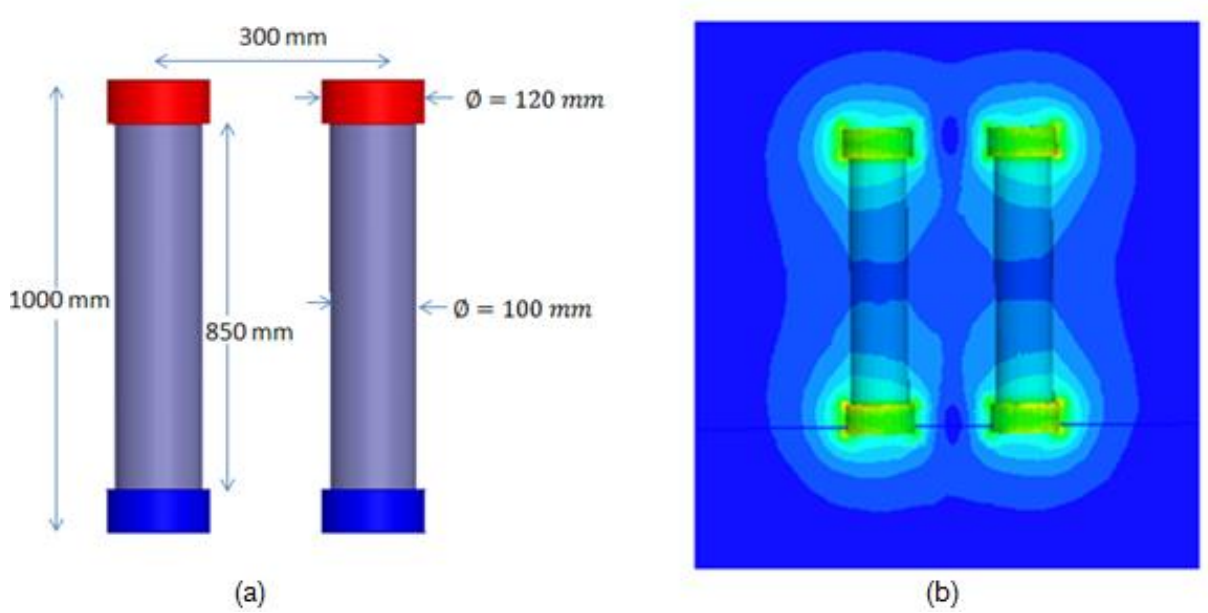


Figure 7.15: Clean insulators (a) and electric field distribution (b) over their surfaces

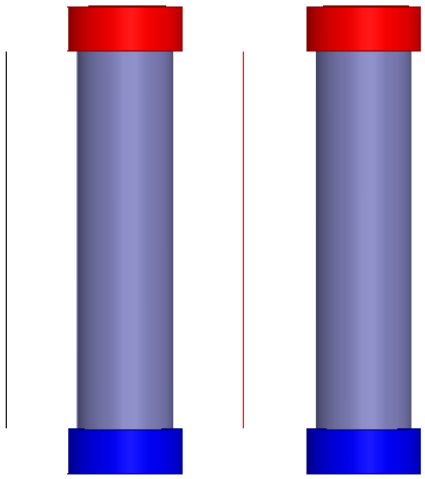

Figure 7.16: Clean parallel insulators with reference lines

To interpret the electric field vectors two lines are considered as shown in figure 7.16. The inside (red) line represents the symmetry axis between the two insulators. The position of the outside line (black) is chosen at the same distance to the outside surface as between the inside surface and the symmetry axis. The electric field values along the reference lines are shown in figure 7.17.

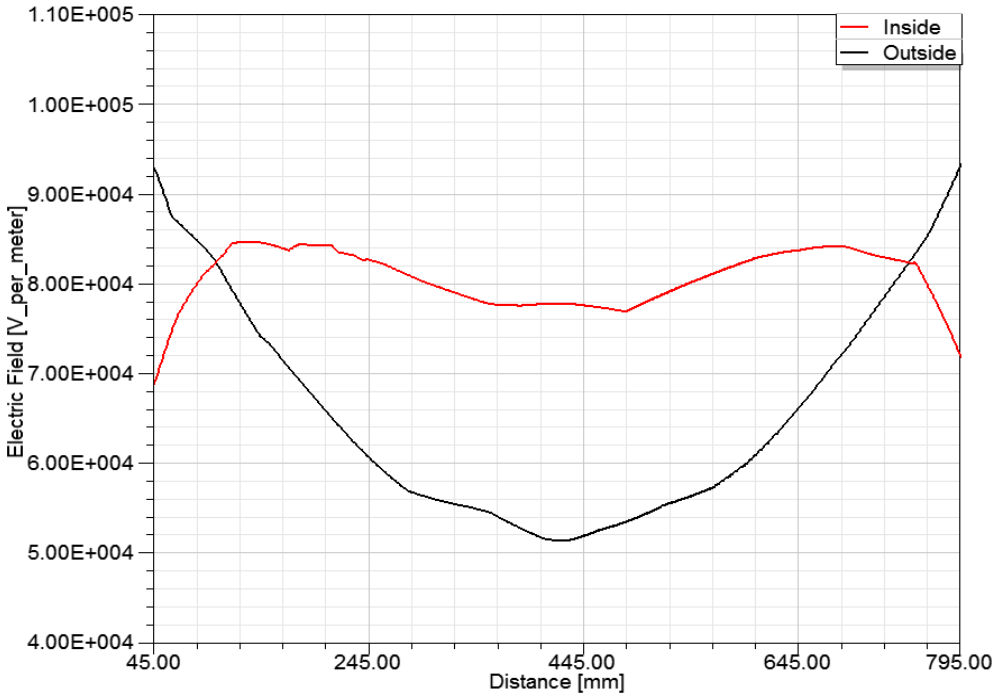


Figure 7.17: Comparison of electric fields along the reference lines

The graphs in the figure 7.17 show there is a reduction in the electric field values for the line outside of the parallel insulators compared to inside values except at the starting and ending of the graphs. This is totally a different behavior as compared to the results in the previous chapter 7.2. Thus in this area between the insulators it is more important to investigate the results. The more precise graphs, taken from figure 7.17 which represent the reduction in the electric field values outside the insulators compared to inside the parallel insulators are shown in figure 7.18.

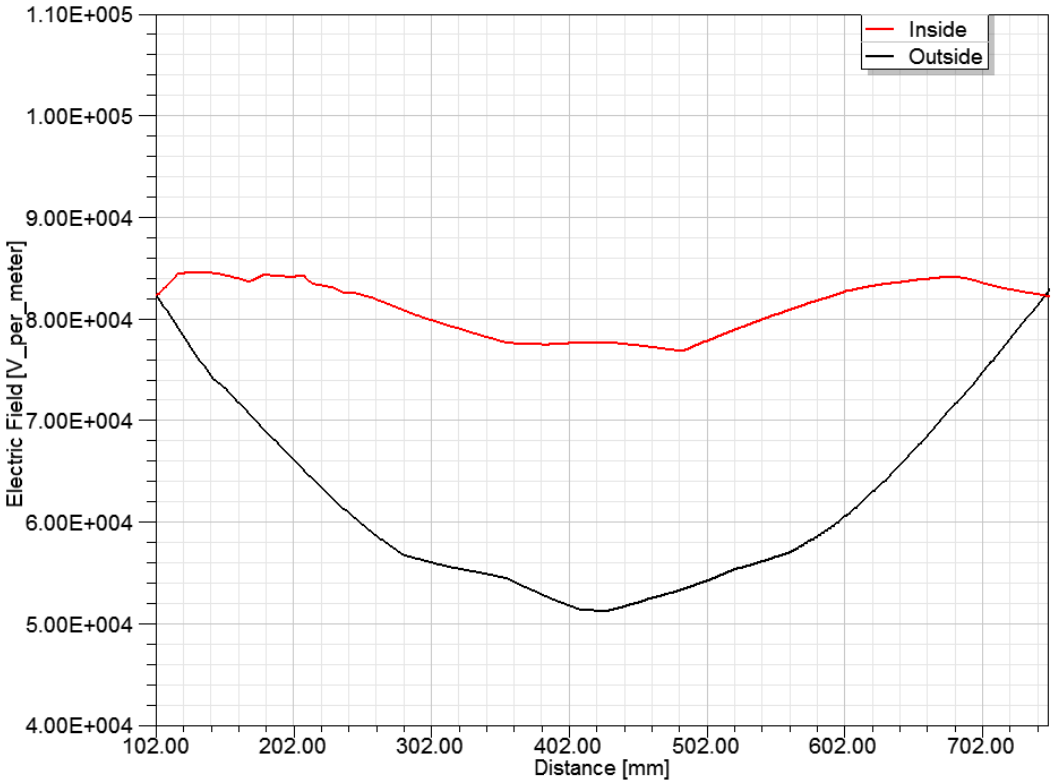


Figure 7.18: Comparison of the electric fields at certain region along the reference lines

It is obvious that the magnitude or strength of an electric field in the space surrounding a source charge is related directly to the quantity of charge on the source and it is inversely proportional to the distance from the source charge. Since the electric field is a vector quantity, it can be represented by vector arrows. For any given location, the arrows point in the direction of the electric field and their length is proportional to the

strength of the electric field at that location. To analyze the behavior of the electric field in figure 7.18 electric field vector arrows are shown in figure 7.19.

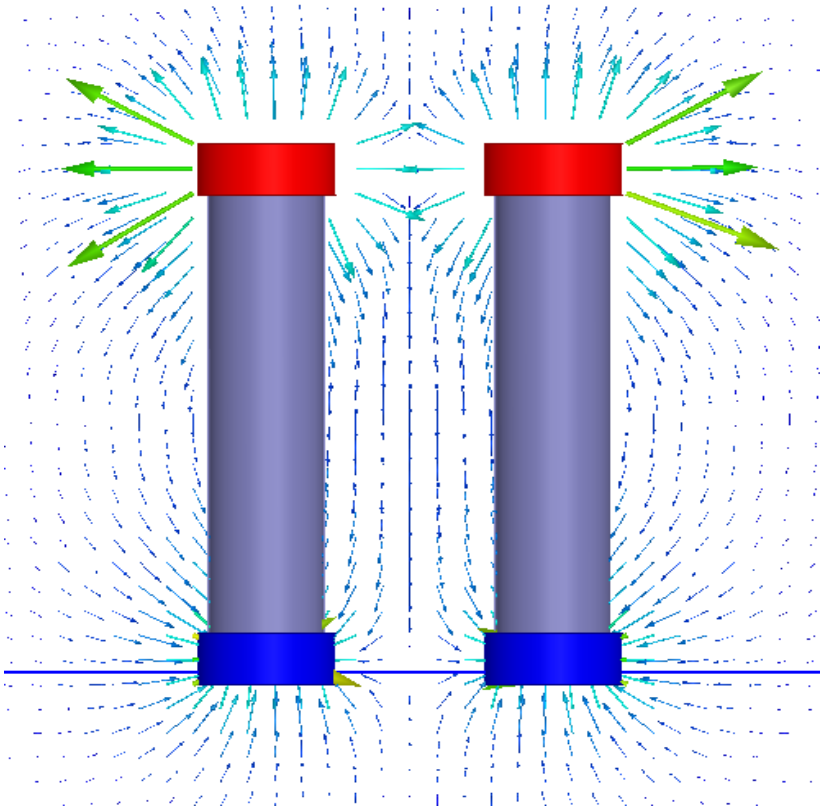

Figure 7.19: Electric field vectors representing field strength over clean insulators

Let us first consider the electric field vectors outside the insulators. It is clear that there is a maximum electric field near the top flange as high voltage is applied to it. When one is moving away downward from the flange there is a reduction in vectors. If one move further away there will be more reduction in the vectors magnitude and there will be no opposing or same direction vectors compared to the existing vectors. So there is a gradual decrease in the electric field values when one moves away from top flange to the middle of the insulators.

Now the observation and explanation is given for the reference line (in figure 7.16) existing between the parallel insulators. Here it is important to remember that this line is far from the insulator surfaces. To be specific one could say it is at the middle of the parallel insulators. On this line the electric field vectors exist from the both insulators and

they add up each other. Consequently the resulting electric field near the flanges is reduced. In the middle area between the insulators the vectors are in the same direction (figure 7.19) and therefore the electric field is higher compared to the outside of the insulators.

### 7.3.2 Electric Field with Pollution

To observe the electric fields on the polluted insulators, the pollution considered in this research is Kaolin. Main components in Kaolin pollution are silicon oxide, aluminium oxide and water. It contains 40 to 50 % of silicon oxide, 30-40% of aluminium oxide and 7 to 14% of water [IEC 1993]. Normally tap water which has a conductivity of maximum value 0,05 S/m is considered in this mixture. The relative permittivity of the pollution is determined by using the formula (7.1) and applied in Ansys Maxwell software to see the effect of pollution layer on insulators.

$$\ln \varepsilon_{r,res} = v_1 . \ln \varepsilon_{r1} + v_2 \ln \varepsilon_{r2} + v_3 . \ln \varepsilon_{r3} \qquad (7.1)\ [\text{KÜC 2005}]$$

Where

$v_1$ - Volume (in %) of silicon oxide

$v_2$ - Volume (in %) of aluminium oxide

$v_3$ - Volume (in %) of water

$\varepsilon_{r1}$ - Relative permittivity of silicon dioxide

$\varepsilon_{r2}$ - Relative permittivity of aluminium oxide

$\varepsilon_{r3}$ - Relative permittivity of water

$\varepsilon_{r,res}$ - Resultant relative permittivity of the pollution layer

Different combinations of silicon oxide, aluminium oxide and water are considered to find the resultant relative permittivity of pollution. These combinations are shown in table 7.

| Volume of silicon oxide in % $(v_1)$ | Volume of aluminium oxide in % $(v_2)$ | Volume of water in % $(v_3)$ | Resultant relative permittivity of pollution $(\varepsilon_{r,res})$ |
|---|---|---|---|
| 50 | 40 | 10 | 7,48 |
| 50 | 38 | 12 | 7,81 |
| 50 | 36 | 14 | 8,15 |
| 48 | 40 | 12 | 7,94 |
| 46 | 40 | 14 | 8,44 |
| 48 | 38 | 14 | 8,29 |

Table 7: Relative permittivity of pollution with different volumes of inert materials

The average value of the resultant relative permittivities obtained in table 7 is used as the relative permittivity of pollution. A pollution layer with a relative permittivity of 8 and conductivity of 2.5 S/m (according to IEC 60815 conductivity of medium pollution) is applied over the insulator surface.

### 7.3.2.1 Pollution on Single Insulator

To show the effect of pollution on the electric field an insulator with 100mm diameter is considered. This insulator has the same parameters as presented in chapter 7.1.1. A uniform pollution layer is applied along the surface of the insulator as shown in figure 7.20. Black color in figure 7.20(b) indicates the pollution layer of 2mm thickness over the surface of the insulator. The voltage and electric field distributions over the single polluted insulator are shown in figure 7.21. The maximum electric field strengths are observed at the edges of the top and bottom flanges. The lowest electric field stress is observed at the middle of the insulator.

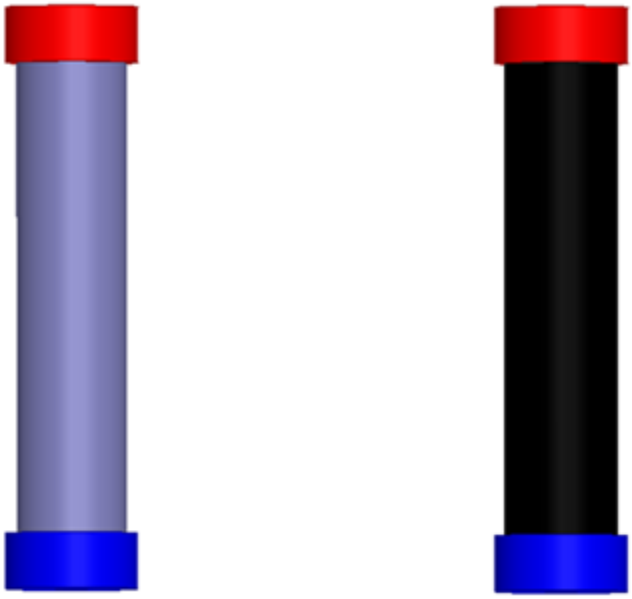


Figure 7.20: Clean (a) and polluted (b) single insulator

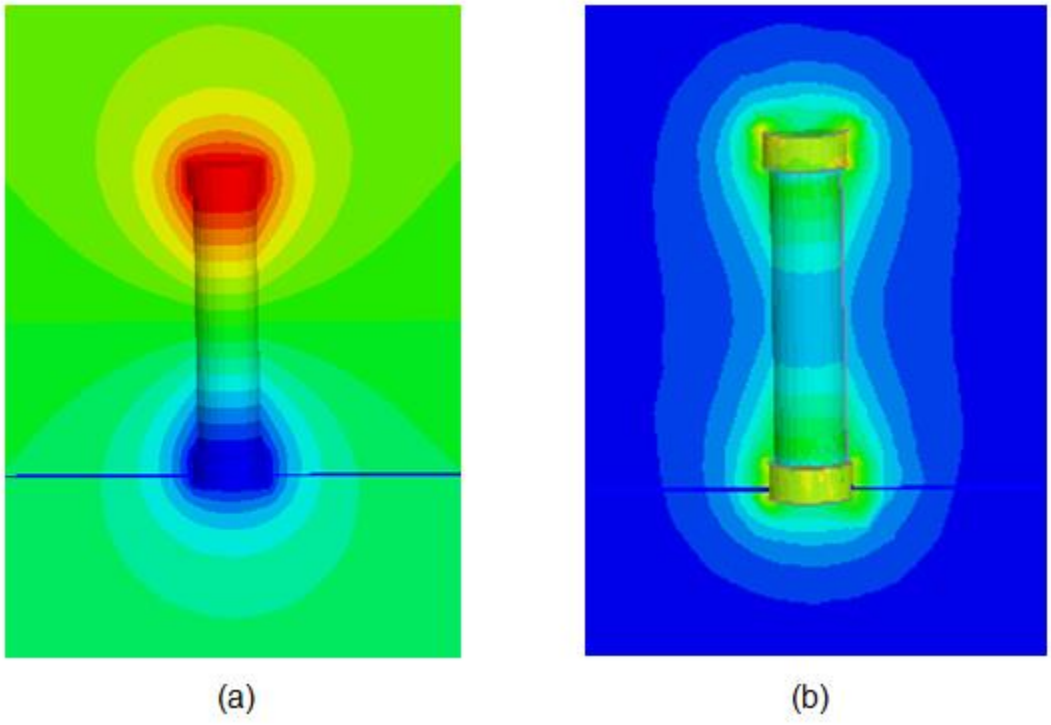


Figure 7.21: Voltage (a) and electric field (b) distribution over polluted insulator

The pollution layer on the surface of the insulator can be analyzed in the following way. It is clear that there is a linear distribution of voltage along the length of the insulator in the presence of a pollution layer. We consider a length of the insulator as 'L' with a radius 'r', covered with a thin pollution layer of thickness 'd' which is very small compared to insulator radius 'r'. The insulators section with this configuration can be represented by an equivalent circuit as shown in figure 7.22.

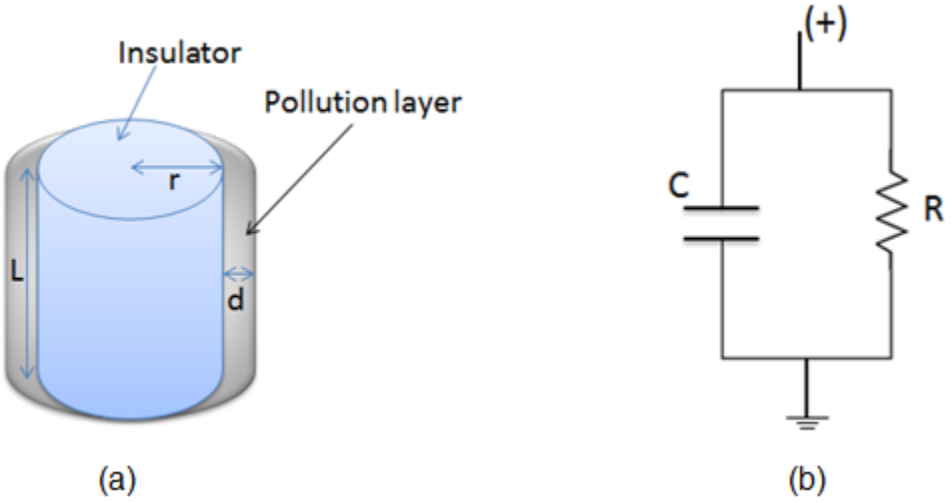


Figure 7.22: Equivalent diagram (a) and circuit (b) of polluted insulator

In the circuit the resistance R is given by

$$R = \frac{\rho L}{A_1} = \frac{L}{\sigma 2\pi (r+d)^2} \qquad (7.2)$$

Where

$\sigma$ - Conductivity of the pollution layer

$\rho$ - Resistivity of the pollution layer

L - Length of the insulator

r - Radius of the insulator

$A_1$ - Surface area covered by pollution layer

d - Thickness of the pollution

The capacitance C is given by the following equation

$$C = \frac{\varepsilon A_2}{L} = \frac{\varepsilon_r \varepsilon_0 2\pi r^2}{L} \quad (7.3)$$

Where

$\varepsilon_r$ - Permittivity of insulator

$A_2$ - Surface Area of the insulator

$\varepsilon_0$ - Permittivity of a free space / Vacuum permittivity

The formula for capacitive reactance at a frequency f (Hz) is

$$X_c = \frac{1}{2\pi f C} \quad (7.4)$$

The ratio between the reactance and resistance is given by

$$\frac{X_c}{R} = \frac{\sigma(r+d)^2}{2\pi r^2 f \varepsilon_r \varepsilon_0} \quad (7.5)$$

Where

$X_c$ - Reactance of the capacitance

f – Frequency

If there is a thin pollution layer of thickness 2mm (conductivity 2.5 S/m, medium pollution) accumulated on the surface of the insulator (with diameter 100mm), we get the ratio ($X_c$ /R) of approximately 1, 94*$10^8$ at 50 Hz. Even if one changes the frequency value from 50 Hz to near 0, the resistance value is always lower than the capacitive reactance. Both factors play a role in establishing the potential and electric field distribution over the polluted insulators under AC. The resistance R is very low in DC and therefore, more leakage current flows over the insulator surface. Partial discharges that cause damages are high since there is no current zero at DC stress. DC cannot flow through the capacitance therefore, even stray capacitances will not affect flashover on the polluted insulators.

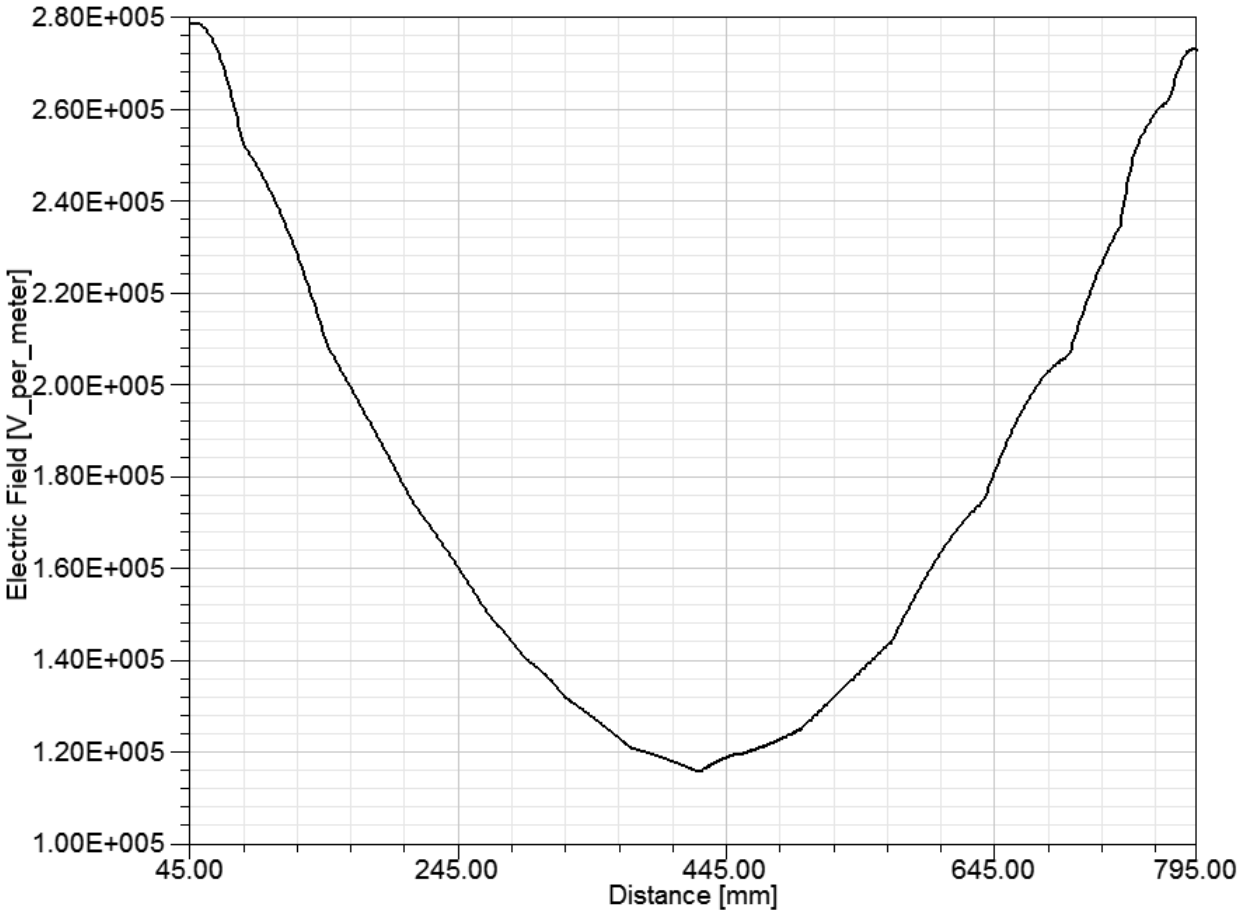


Figure 7.23: Electric field along the surface of a polluted single insulator

The electric field along the surface of the single polluted insulator is shown in figure 7.23. The distance in X axis indicates the length of the insulator surface from top to bottom except at the triple points. To avoid confusion at the triple points the electric field values at the ends of the insulator are not considered in the graph (see in chapter 7.1.2). It is clear that there is a gradual decrease from the top to the middle of the insulator and then gradual increase till the bottom of the insulator. Here the electric field on the flanges is not considered for evaluation.

### 7.3.2.2 Parallel Insulators with Pollution on only one Insulator

Parallel insulators with the same diameter of 100mm are considered. To know the effect of the second insulator which is next to the polluted insulator a pollution layer of 2 mm thickness is applied only on one insulator as shown in figure 7.24(a). Both insulators are connected to voltage. The voltage and electric field distributions are shown in figure 7.25.

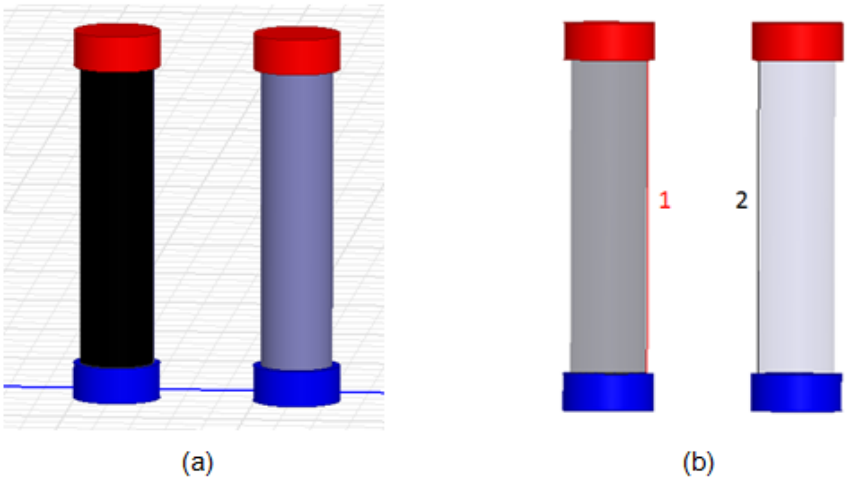


Figure 7.24: Parallel insulators with pollution on only one insulator (a) and reference lines

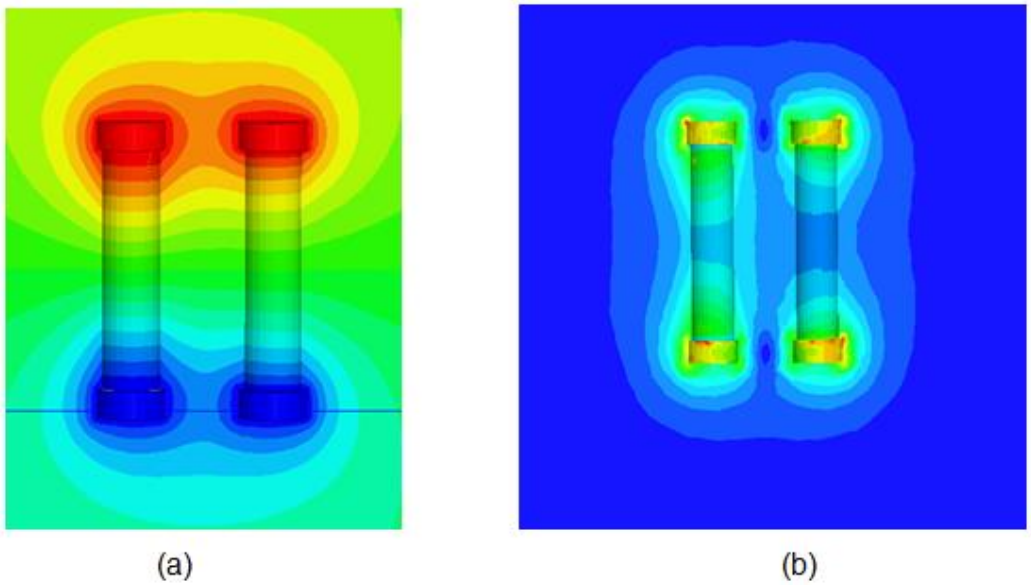


Figure 7. 25: Voltage (a) and electric field (b) distributions over parallel insulators with pollution on only one insulator

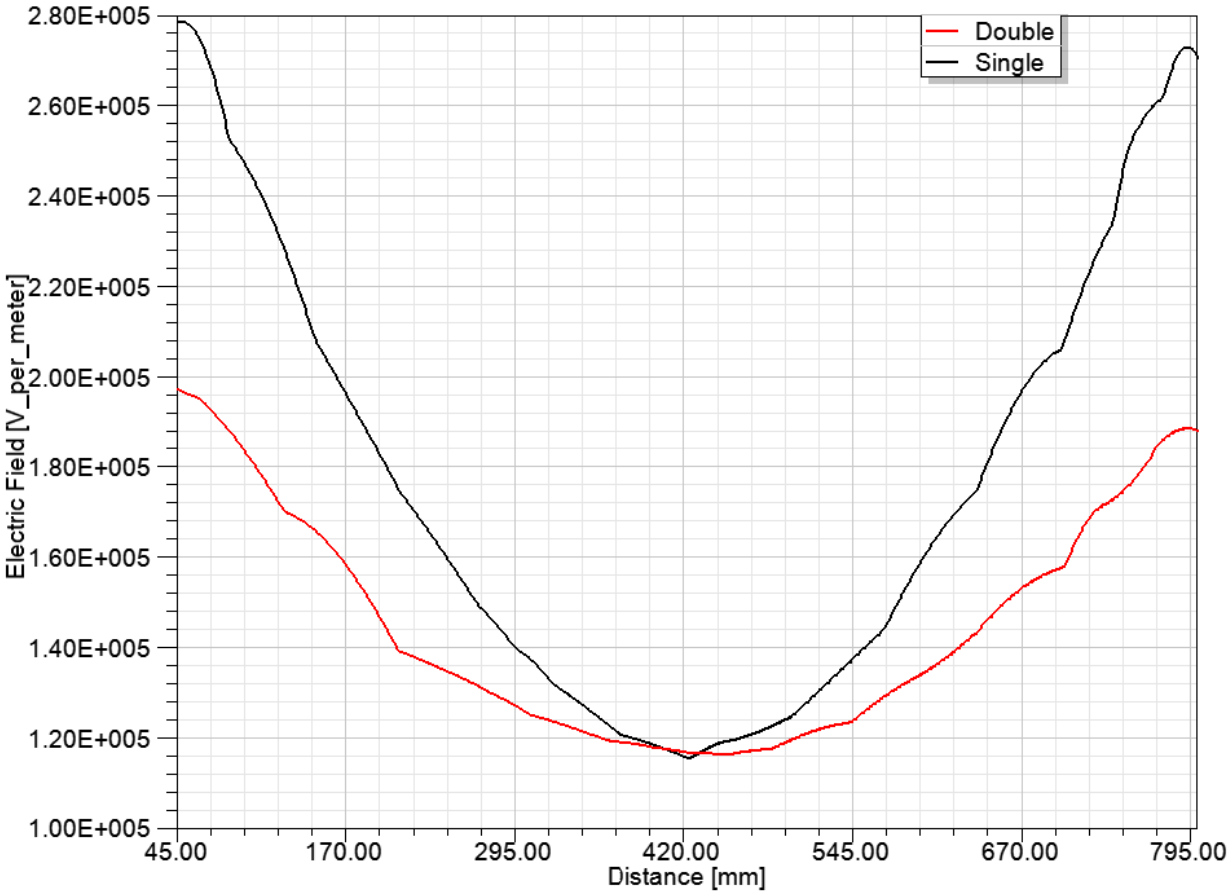


Figure 7.26: Electric field comparison with single and parallel polluted insulators (only one insulator polluted)

The red line in figure 7.26 indicates the graph with parallel insulators of which one being polluted as in figure 7.24(a), and the black line indicates the graph with the presence of only one single polluted insulator (figure 7.20(b)).

The electric field distribution on the polluted insulator has been taken along the reference line number 1 according to figure 7.24(b) and compared to the electric field distribution of a single polluted insulator according to figure 7.23.

The figure 7.26 shows that there is a reduction in the electric field values with the double insulator assembly when compared to a single insulator. There is a decrease in the electric field because of the existence of the parallel clean insulator. This decrease can

be explained in the following way. At starting near the top flange(45 mm) there is a 40% reduction of the electric field on the polluted insulator when comparing single and parallel insulators. After 100mm down the flange, there is a 24% decrease in value, then in the middle of the insulator we have almost the same electric field values, and after that there is an average reduction of values when we go from the middle of the insulator to the down flange (795 mm).

To compare the effect of a polluted insulator on a non polluted insulator the electric field values on the reference lines 1 and 2 (figure 7.24(b)) are considered and shown in figure 7.27.

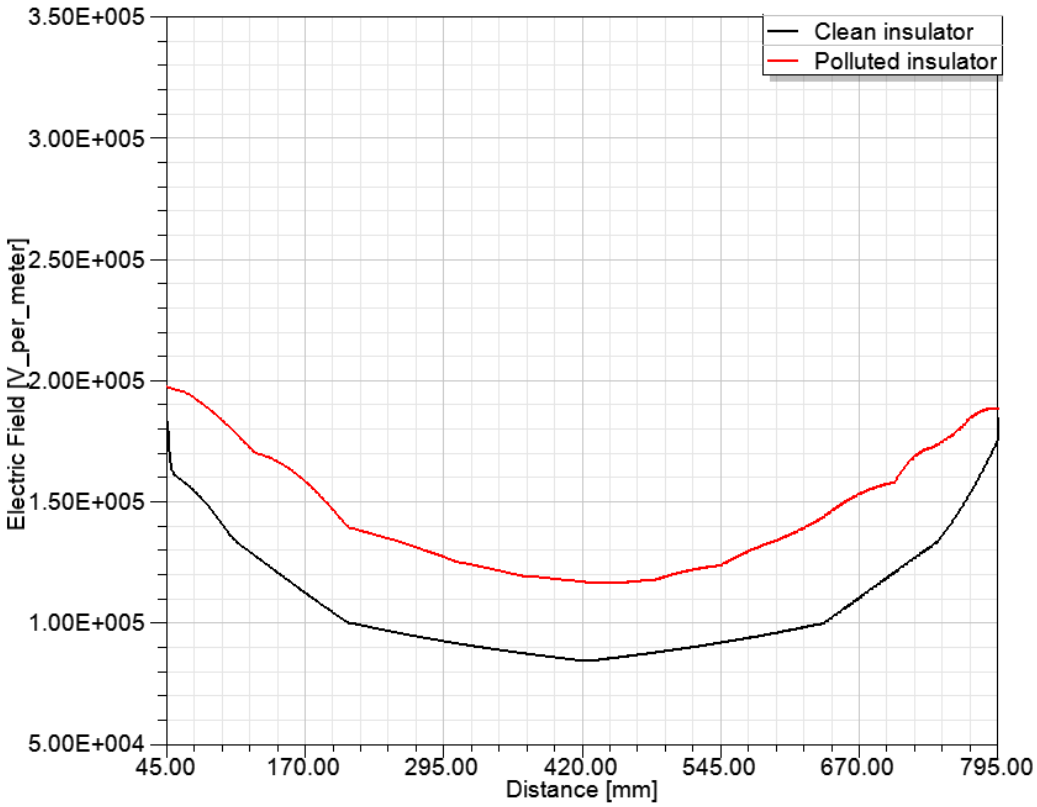


Figure 7.27: Electric field comparison on the surfaces of polluted and non polluted insulators in parallel insulator combination

By observing the graph in figure 7.27 one may say that the electric field stress on the surface of the non polluted insulator (black line) is lower than on the surface of the polluted insulator (red line). Distance in x-axis shows the length of the reference lines 1 and 2 except at the ends approximately 50mm. There is an average of 34% decrease in

the electric field values on the surface of the non polluted insulator due to the polluted insulator existing next to it or vice versa. Therefore it is determined that there is a mutual effect of parallel insulators even though one is polluted and other is non polluted.

### 7.3.2.3 Parallel Insulators with Pollution on both Insulators

In this chapter uniform pollution on both insulators is considered. This is the generally happening case when compared with the pollution on only one insulator. If there is humidity or moisture in the atmosphere the chances are higher to accumulate a uniform pollution on both the insulators. To simulate that kind of situation, a uniform pollution layer is applied on both insulators. As shown in the previous chapters two insulators with the same 100mm diameter are considered and a pollution layer with 2mm thickness is applied over the insulators surface. In figure 7.28 black color represents the pollution layer. Voltage and the electric field distributions for this configuration are shown in figure 7.29.

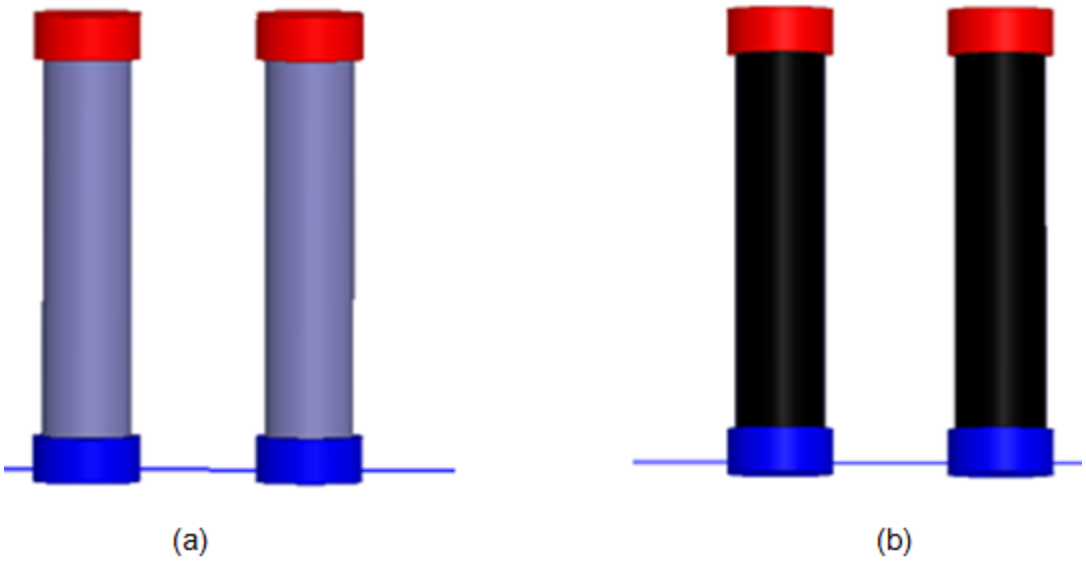


Figure 7.28: Clean (a) and polluted (b) insulators

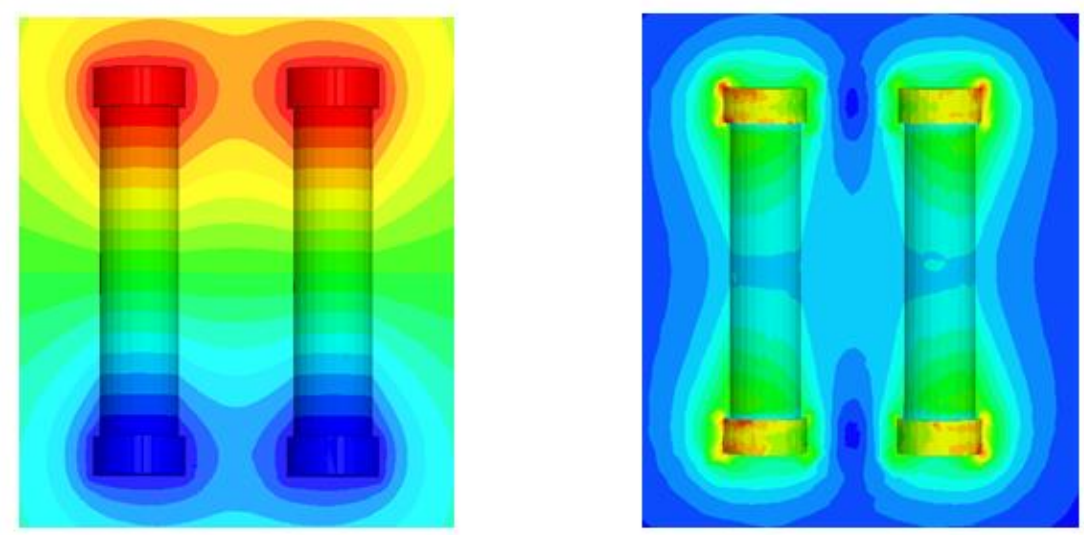


Figure 7.29: Electric potential (a) and field distribution (b) over the polluted insulators

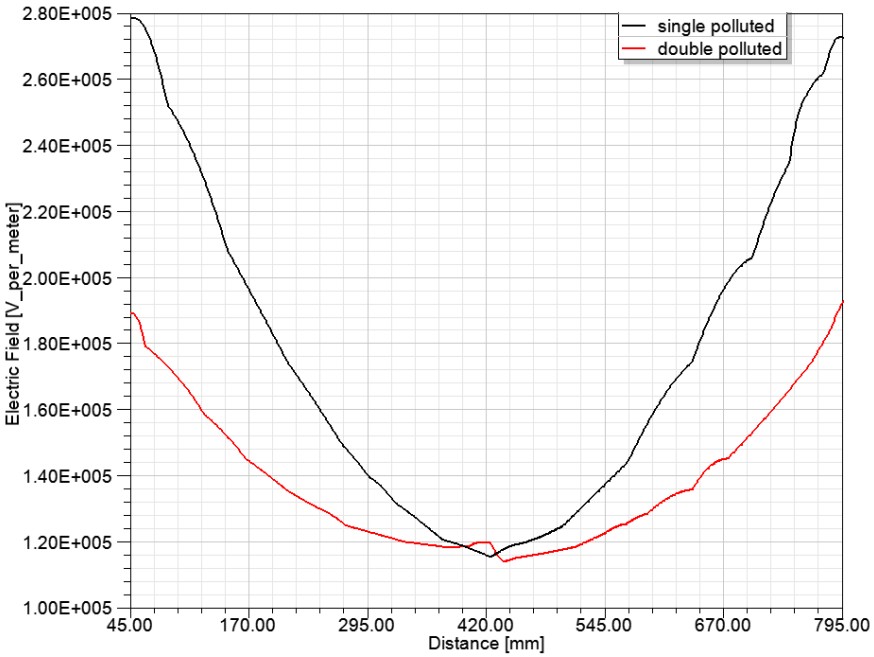


Figure 7.30: Electric field comparison with single and double polluted insulators

The graphs in figure 7.30 show the same tendency which we have seen in the previous chapter except of the changing values. The graph shows that near the top flange there is a 41% decrease in the electric field value of the double insulators over the single polluted insulator because of the second polluted insulator next to it.

The electric field distribution of two parallel insulators, both polluted, is practically the same as that of one polluted insulator (figure 7.26) in parallel to non polluted insulator. This tendency towards equalization of the electric field distribution on the polluted insulators is caused by the leakage current along the pollution layer.

## 7.4 Critical Area between Parallel Insulators

Here the break down position between the parallel insulators where breakdown may occur is explained. Based on the finite element method, this chapter also uses Ansys Maxwell software to calculate the electric field characteristics of the critical area between the parallel insulators which is shown in figure 7.31. This chapter explains the dependence of the electric field behavior of parallel insulators on the distance between the axes of two parallel insulators when partial pollution layers occur on their surfaces.

The black color in the figure 7.31 indicates the pollution layer on the parallel insulators. Figure 7.32 shows the position where the larger electric field between the two insulators makes it more probable to become the breakdown point. However, the electric field at the individual flanges is also higher relative to that of other positions.

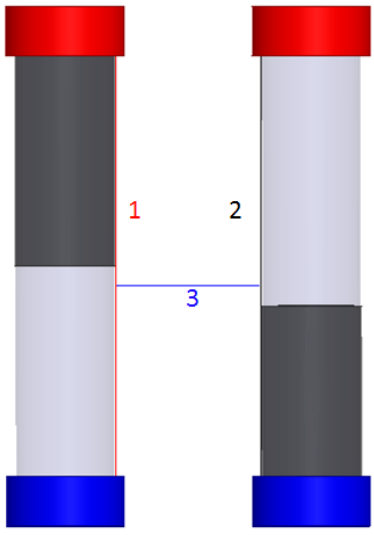


Figure 7.31: Partially polluted parallel insulators with reference lines

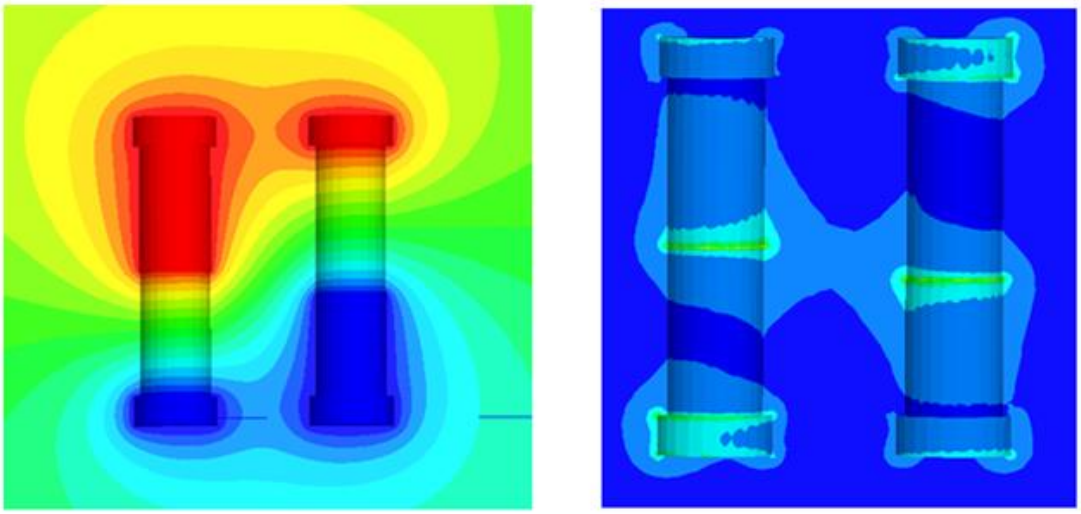

(a) (b)

Figure 7.32: Electric potential (a) and field distribution (b) between the insulators

Figure 7.32 shows the potential and electric field distributions which could happen with uneven polluted parallel insulators. The voltage distribution is shifted due to the polluted area on the insulators in such manner that the electric field between the insulators becomes higher, thus may cause a flashover. The electric field values along the reference lines 1 and 2 (figure 7.31) are shown in figure 7.33.

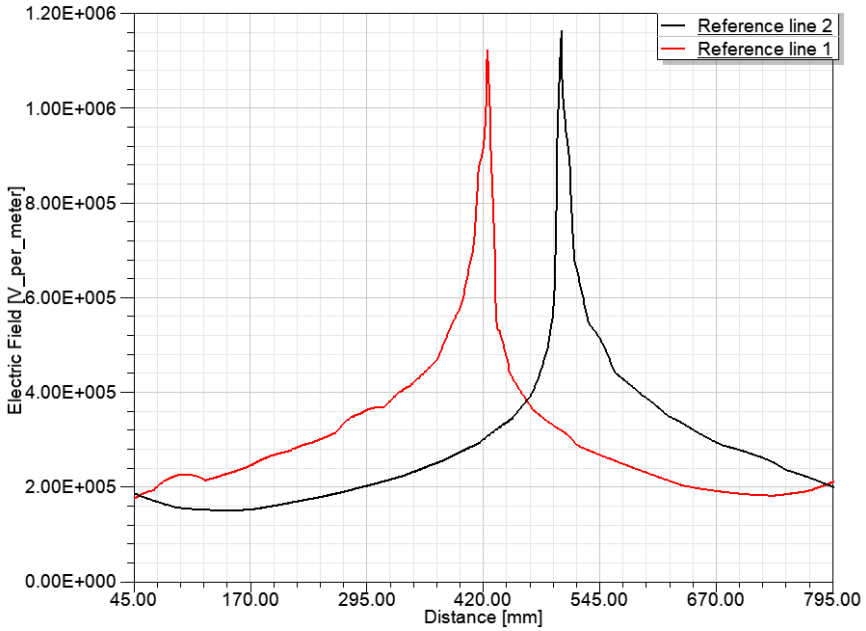


Figure 7.33: Electric field values along the reference lines 1 and 2 on partially polluted insulators

It is determined that the highest electric fields are obtained at the distance of 420mm and 503mm on the reference lines 1 and 2 respectively. The distance on the x-axis shows the length of the reference lines from top to bottom except at the ends. The highest electric fields are at the ends of pollution layer which are at the middle of the insulator surfaces. The electric field values between the insulators (along the reference line 3) are shown in figure 7.34.

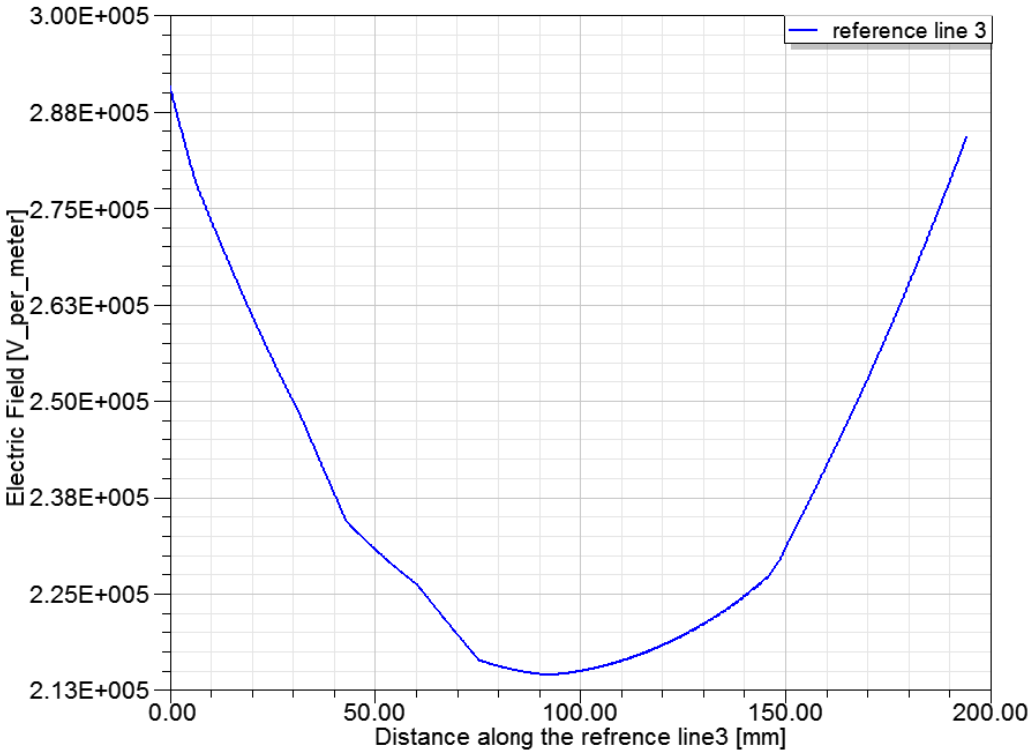


Figure 7.34: Electric field values along the reference line 3

It is observed that the electric field values are decreasing from the surface of the insulator till the center of the line and then increasing towards the surface of the other insulator. Here the minimum electric field between the insulators obtained is 2.15 kV/cm. If one is able to avoid aforesaid situation, there is a less possibility for the flashover to occur between the parallel insulators.

The distance between the insulators is varied in different steps to observe the effect of it over the electric field. At a certain distance between the insulators, the electric field strength between them is less than 1kV/cm. This is the area which does not connect the

pollution layers with the electric field being not more than 1 kV/cm between the two insulators. This happens for these insulators of 100mm diameter at a distance of the axis above 390mm. From this observation it is obvious that there is an influence of the distance between the parallel insulators on the electric field between them. The voltage and electric field distributions after changing the distance are shown in figure 7.35.

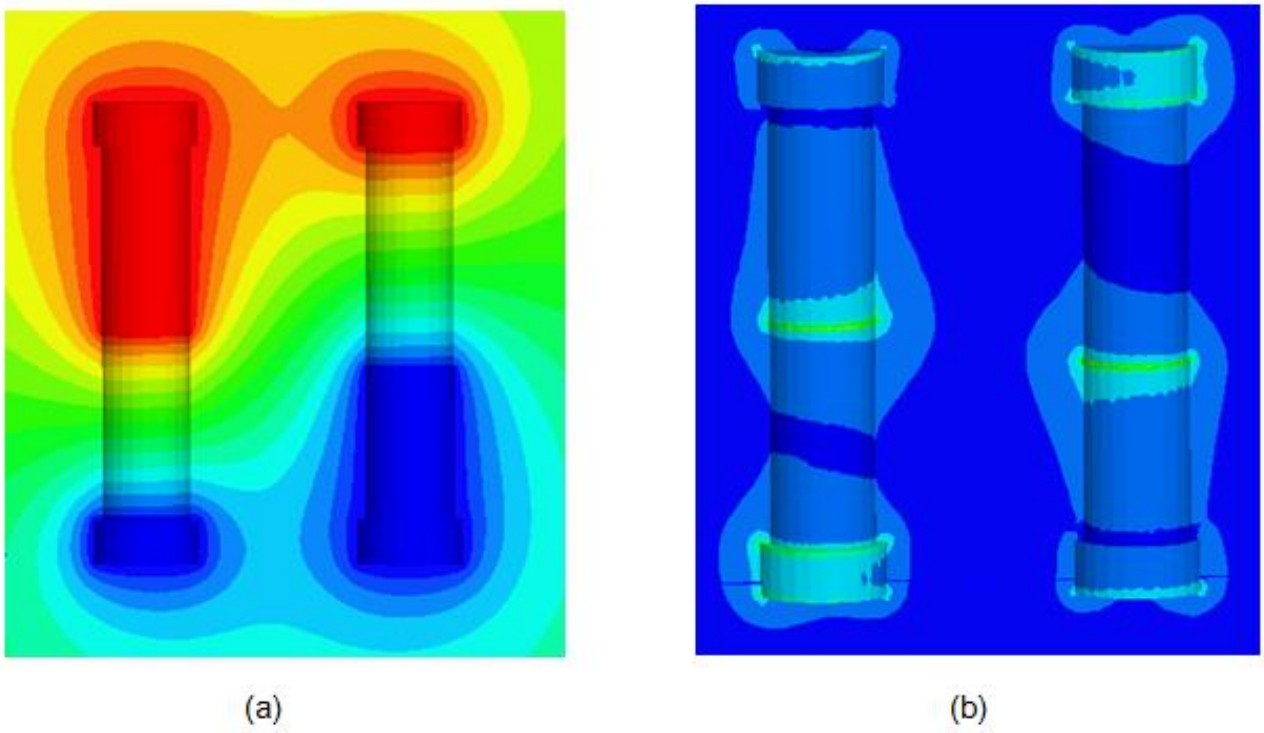


Figure 7.35: Electric potential (a) and field distribution (b) over a critical area after increasing the distance between the insulators

Comparing the figures 7.32 and 7.35 shows that an enlargement of the distance between the parallel insulators reduces the electric field (the color indicating the electric field changes from light blue, i.e. high electric field, to dark blue, i.e. low electric field) and thus increases the flashover voltage withstand. The electric field values between the insulators with distance enlargement (along the enlarged reference line 3) are shown in figure 7.36.

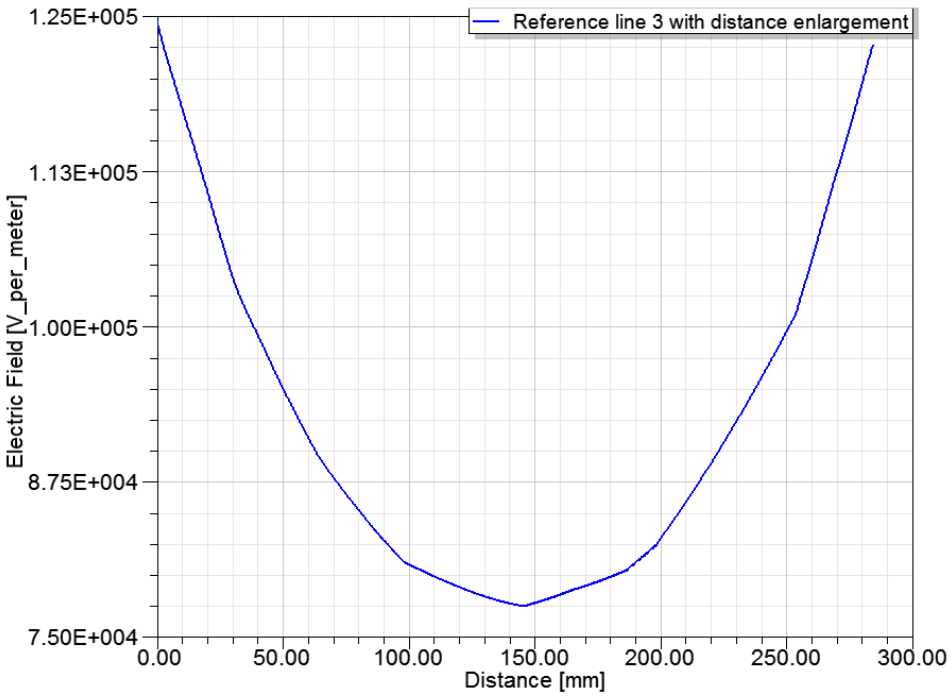


Figure 7.36: Electric field values along the reference line 3 after the distance enlargement

The graph in figure 7.36 shows that the minimum electric field value obtained after changing the distance is 0.77 kV/cm which is less than the value 1 kV/cm. These results show that the parallel insulators with a small distance between them have a reduction in flashover voltage compared to the flashover voltage of parallel insulators with a larger distance. This situation has been proved for AC as well. The AC flashover voltage of a double insulator set decreases with a reduction of distance between the two parallel insulators [SKL 1999].

## 7.5 Conclusions on Parallel Insulators

Based on the model created in the simulation software, the simulation results for electric potential and field plots over the clean and polluted insulators are shown in different figures in chapter 7. The results demonstrate that the electrical field stresses are highest in the areas near the top and bottom flanges. The chapter 7.1 shows the stresses near the insulator surface do not exceed the stress near the flanges. The results from the

same chapter 7.1 describe the effect of one insulator over the other insulator which is placed next to it. There is a 24.5% reduction in the electric field caused by the adjacent insulator with same parameters except in the middle region between the insulators. In chapter 7.3.1, it is explained why in this region the inner field stresses are higher compared to the outer field stress.

The graphs (figure 7.8) indicate that the electric field between and near to the surface of insulators is lower compared to the electric field near the outer surface of the parallel insulators. This is the same situation which was proved by using different insulator diameters (figure 7.12).

An electric potential plot on the insulator with uniform pollution layer shows that the voltage is linearly distributed over the insulator surface from the live flange to the dead end flange (figure 7.21(a)). This is likely to happen across a uniform resistive layer. However, the electric field plots indicate that the highest electric field stresses are present on the flange surfaces (figure 7.21(b)).

In case of a critical area between the parallel insulators, the voltage is transferred from the live end flange to the dry band, and the ground potential is transferred from the dead end flange to the dry band (figure 7.32). The electric field analyses show that higher stresses are present at the critical region where partial discharges can start and further lead to a flashover. The flashover voltage will decrease with the reduction of the distance between the parallel insulators. To avoid this situation a certain distance between the parallel insulators should be maintained. The distance between the insulators is varied in different steps to know the position where the connection of the electric field between the insulators is less than 1 kV/cm. As an example the distance ≥ 390mm is measured for the insulators of 100mm diameter as per simulation results. These results need to be confirmed by practical experiments.

# 8 Conclusions and Future Work Suggestions

In this dissertation, the electric field behavior of a water drop on the insulator shed surface and parallel insulators were analyzed by simulation methods. This chapter discusses the conclusions drawn from the simulation results and suggestions for future work.

## 8.1 Conclusions

Different types of environments and pollution are explained. This report presents simulation results which contribute to a better understanding of the behavior of water drops on the insulating surface under DC electric field stress. This work states that partial discharges under DC condition are absolutely different from AC conditions. The theory which gives an insight about the discharge process near the water drop can be explained with avalanche and streamer discharges.

The simulation of a water drop on the insulator shed surface is not accurate from 2D simulations, and it is not a good idea to use axisymmetry even though the insulator is cylindrical. Simulation results from 3D are considered to show the behavior of water drops on an insulating surface under DC stress. The electric field values near the water drop are determined for analysis. Certain variations in the electric field values along the shed surface are observed because of the shape of the shed. One of the highest values of the electric field is obtained near the edge of the shed. The tendency of the electric field near the water drop is demonstrated along with its behavior by changing the position of the water drop on the insulator shed surface.

It is observed that the highest stress near the water drop is originated near the top surface of the water drop. At the triple point the electric field is lower compared with top surface.

Simulation results show that there is a considerable change in the electric field values near the water drop when it is hanging at the edge of the shed. Additionally the effect of

different insulator materials on the electric field values near the hanging water drop is also simulated. It shows the percentage change in the electric field with the hanging water drop compared to without hanging drop. There is a noticeable change in the electric field values when the contact angle of the water drop is changing. Results show that there is an increasing tendency in the electric field when the angle of contact is changing from 30 to 90 degrees. All these considerations must be taking into account while designing the insulators for polluted conditions especially in case of DC stress.

To know the behavior of the electric field on parallel insulators a simple structure without sheds has been considered. Simulation work has been carried out using “DC Conduction” solver in Ansys Maxwell software to simulate the insulators under DC condition. Simulation results on parallel insulators show that the electric field between and near to the surface of insulators is lower compared to the electric field near to the outer surfaces of outside of the parallel insulators. This was even proved by considering insulators of different diameters. There is an exceptional case between the parallel insulators which is explained by pictorial representation of the electric field vectors.

There is a certain percentage of reduction in the electric field when an insulator is placed next to the existing insulators. This reduction is different for polluted and for clean insulators. In case of parallel polluted insulators the voltage is more uniformly distributed over the insulators surfaces from the live flange to the dead end flange than on clean insulators. The critical part between the parallel insulators is derived when they show a non-uniform pollution layer over the surfaces.

## 8.2 Future Work Suggestions

Behavior of a water drop on the insulator surface is explained by considering a simple structure of it. For further research the following considerations are worthy to be recommended:

- There is a chance of water drop deformation with the electric field stress. It should be captured with high speed cameras.

- It is better to use some special designed software like Solid Works to simulate the precise water drop.
- Practical experiments are necessary to compare the simulation results.
- There should be a mathematical relationship between flashover voltage gradient and water drops by using the artificial neural network (ANN) or regression based modeling.
- Simulations should be done using boundary element method (BEM) to compare the results with finite element method (FEM).

Behavior of parallel insulators is explained by considering a simple structure. For further work the following considerations are recommended:

- It is important to use software like Comsol Multiphysics to avoid solution type confusions for 2D and 3D simulations on polluted insulators.
- Simulation work on parallel insulators with sheds.
- Comparison of simulation results with practical experiments.
- Artificial neural network or regression based modeling should be used to have a mathematical relationship between flashover voltage gradient and pollution on parallel insulators.
- Simulations on parallel insulators should also be done by using BEM to compare the results with FEM.
- For better understanding the electric field behavior at the ends of an insulator further research has to be done near the triple points.

# References


[ALS 1968] L. L. Alston
*High Voltage Technology*
Oxford University Press, 1968

[ANS 2014] Ansys Maxwell 16.0, Help System, ANSYS® 2014

[BAR 2002] R. Bartnikas
*Partial Discharges, Their Mechanism, Detection and Measurement*
IEEE Trans. Diel. Elect. Insul., Vol. 9, pp.763-808, 2002

[BRA 1971] Brazier-Smith, P. R
*Stability and shape of insolated and pairs water drops in an electric field*
The physics of fluids, Vol.14, No. 1, 1971

[BAO 2014] Han Bao
*Optimal Design of 245kV $SF_6$ Bushing by Using Genetic Algorithm*
Dissertation at TU Cottbus-Senftenberg, Germany, 2014

[CHA 1999] D. C. Chaurasia
*Scintillation modelling for insulator string under polluted conditions*
11th Int. Symp. High Voltage Eng., Aug. 23-27, 1999 vol. 4, pp. 224-227

[CIG 2012] Alexander Levinzon, Daniel Kottick
*On-Line Wireless PD Monitoring System for Contamination Detection on High Voltage Overhead Transmission Lines Insulators*
Paper B2 – 205, CIGRE 2012

[CWG 2012] CIGRE Working Group C4.303
Outdoor Insulation in Polluted Conditions
Technical Brochure No: 518, 2012

[COB 1958] J. D. Cobine
*Gaseous Conductors*
Dover, New York, 1958

[DRA 1996] P.J. Drallos, V.P. Nagorny, D.D. Ryutov and W. Williamson
*Effective Secondary Emission Coefficient for Rough Cathode Surfaces*
Department of Physics and Astronomy, The University of Toledo, 1996

[ENG 1984] English, W. N
*Corona from a water drop*
Phys. Review, Vol. 74, No. 2, 1984

[ENG 1965] A. von Engel
*Ionized Gases*
Oxford: Clarendon Press, 1965

[FRE 2000] Fred Padgett ; Walter P. Ruedrich
Wood Amongst the Wires, The Temporary Solution
Mary Anne Ruedrich 2000, Lorne Way, Sunnyvale, CA 94087

[FRO 1995] U. Fromm
Interpretation of Partial Discharges at DC Voltages
IEEE Trans. Diel. Elect. Insul, Vol .2 No 5, October 1995

[FRA 1960] G. Francis
*Ionization Phenomena in Gases*
London: Butterworths Scientific Pub, 1960

[FRI 1992] Friedrich, G. H
*Die physikalischen Entladungsparameter der synthetischen Luft unter dem Einfluss der Feuchte und Temperatur*
Dissertation Zürich, 1992

[FRO 1995] U. Fromm, and P. H. F. Morshuis
*Partial discharge classification at DC Voltage*
5th ICSD, Leicester, paper 7.1.9, 10-13 July 1995

[FRO 1995] U. Fromm
*Partial Discharge at High DC Voltage*
Diss. TU Delft University Press, ISBN 90-407-1155-0, 1995

[HAR 1984] Hartmann, G
*Theoretical evaluation of Peek's law*
IEEE Transactions on Industry Applications, Vol. IA 20, No 6, Dec 1984

[IEC 1993] IEC Technical Report No 1245
*Artificial pollution tests on high- voltage insulators to be used in d.c. systems*

[IEC 2008] IEC Technical Report No 60815
*Selection and dimensioning of high-voltage insulators intended to use in polluted conditions*

[INMR 2014] *DC Versus AC Pollution Flashover*
INMR's Weekly Technical Review, June 3, 2014

[INM 2014] *Insulator Pollution in Desert Environments*
INMR's Weekly Technical Review, February 18, 2014.

[IWA 1998] K. Iwai, Y. Hase, E. Nakamura, and H. Katsukawa
*Development of a new apparatus for contamination measurements of overhead transmission line insulators*
IEEE Trans. Power Del., vol. 13, no.4, pp. 1412-1417, Oct 1998

[KAM 1993] Kamra, A. K., Bhalwankar, R. V., Sathe, A. B.
*The onset of inhomogeneous and corona in water drops falling as terminal velocity in horizontal electric fields*
J. Geophysics. Res., No. 98, D7, 1993

[KIN 1985] Kind, D., Kärner, H
*High voltage insulation technology*
Friedr. Vieweg & Sohn, 1985

[KOB 2000] Stoshi Kobayashi ´; Yutaka Matsuzaki, Hiroshi Masuya
*Development of Composite Insulators for Overhead Lines*
Furukawa Review, No. 19, 2000

[KOR 1998] Korolev, Yu. D; Mesyats, G. A
*Physics of pulsed breakdown in gases*
ISBN 5769107790; URO-PRESS 1998

[KÖN 1993] König, D.; Rao, Y. N. ;
*Partial discharges in electrical power apparatus*
VDE Verlag Berlin Offenbach; 1993

[KUN 1983] E.E. Kunhardt and L.H. Luessen
*Electrical Breakdown and Discharges in Gases*
New York: Plenum Press, 1983

[KUF 2000] E. Kuffel, W. S. Zaengl, and J Kuffel
*High Voltage Engineering Fundamentals*
Boston: Newnes, 2000

[KÜC 2005] Küchler, A
*Hochspannungstechnik Grundlagen - Technologie – Anwendugen*
Springer Science & Business Media, 2005

[KÜP 1990] Küpfmüller, K
*Einführung in die theoretische Electrotechnik*
Springer Verlag, 1990

[LAG 1994] A.N. Lagarkov and I.M. Rutkevich
*Ionization Waves in Electrical Breakdown of Gases*
New York: Springer – Verlag, 1994

[LLE 1957] F. Llewellyn-Jones
*Ionization and Breakdown in Gases*
London: Methuen & Co. LTD, 1957

[LLE 1967] F. Llewellyn-Jones
*Ionization Avalanches and Breakdown*
London: Methuen & Co. LTD, 1967

[MAC 1931] Macky, W.A
*Some Investigations on the Deformation and Breaking of Water Drops in Strong Electric Fields*
Proc. R. Soc. Lond. Vol.A133, London,1931

[MAC 1990] J. Macur, K. Domansky, and J. Sikula
*Stochastic Character of Partial Discharges in Insulators*
Appl. Phys., Vol. 67, No. 1, pp.540-542, 1990

[MAL 1987] N. H. Malik, and A.A. Alrainy
*Statistical Variation of DC Corona Plus Amplitudes in Point to Plane Gaps*
IEEE Trans. on EI, Vol. 22, No. 6, pp. 825-829, 1987

[MAT 1999] H. Matsuo, T. Fujishima, and T. Yamashita
*Relation between leakage impedance and equivalent salt deposit density on an insulator under salt water spray*
IEEE Trans. Dielectr. Elect. Insul., vol. 6, no.1, pp. 117-121, Feb. 1999

[MEE 1978] J.M. Meek and J.D. Craggs
*Electrical Breakdown of Gases*
New York: John Wiley & Sons, 1978

[MON 2004] G. Montoya, I. Ramirez, and J. I. Montoya
*Correlation among ESDD, NSDD and leakage current in distribution insulators*
Proc. Inst. Elect. Eng.-Gener. Transmiss. Distrib.,Vol. 151,no3, May 2004

[MOR 2005] Peter H.F. Morshuis and Johan J. Smit
*Partial Discharges at DC Voltage: Their Mechanism, Detection and Analysis*
IEEE Trans. Diel. Elect. Insul., Vol. 12, No. 2; April 2005

[MÜL 1976] K.B. Müller
*Über Das Verhalten Extrudierter PE-Kabel bei Hoher Gleichspannungs-Langzeit belastung*
Diss. TH Darmstadt, Germany, 1976

[NAS 1971] E. Nasser
*Fundamentals of Gaseous Ionization and Plasma Electronics*
Wiley series in plasma physics, 1971

[NOL 1926] Nolan, J. J.
*The breaking of water drops by electric field*
Proc. Roy. Irish Acad. No. 37, 1926

[PEE 1915] F. W. peek
*Dielectric phenomena in High Voltage Engineering*
New York: McGraw- Hill Book Co, Inc 1915

[RAI 1997] Y.P. Raizer
*Gas Discharge Physics*
New York: Springer – Verlag, 1997

[RAO 1971] Rao, C. R; Raju, G. R. G
*Growth of ionization currents in dry air at high values of E/N (E is the electric field strength and N is the gas number density)*
Journal of Physics D: Applied Physics, Vol. 4, 1971

[RAV 2011] Ravindra Arora, Wolfgang Mosch
*High Voltage and Electrical Insulation Engineering*
IEEE Press Series on Power Engineering, 2011

[SAL 1966] B. Salvage, and N. R. Steinberg
*Discharge Repetition in an Air-filled Cavity in a Solid Dielectric under Direct –Voltage Conditions*
Electronics Letters, Vol. 2, No. 11, pp. 432-433, 1966

[SHE 1988] Sherwood, J. D
*Breakup of fluids droplets in electric and magnetic fields*
The Jornal of Fluids Mechanics, Vol. 188, 1988

[SHI 1972] S. Shihab
*Teilentladungen in Hohlräumen von Ploymeren Isolierstoffen bei hoher Gleichspannung*
Diss. TU Braunschweig, Germany, 1972

[SIN 1995] Singer, H
*Present and Future Topics of HV Field Calculation and Measurement*
Proceedings of the 9th International Conference on High Voltage Engineering, September 1995

[TAY 1964] Taylor G
*Disintegration of the water drops in an electric field*
Proceedings of the Royal Society, Vol. A280, London, 1964

[VAN 1992] R. J. Van Brunt, K. L. Stricklett, J. P. Steiner, S. V. Kulkarni
*Recent Advances in Partial Discharge Measurement Capabilities at the National Institute of Standards and Technology*
IEEE Trans. on EI, Vol.27, No. 1, pp. 114-129, 1992

[WIL 1925] Wilson, C. T. R., Taylor, G. I.
*The bursting of sopat bubbles in a uniform electric field*
Proc. Camb. Phil. Soc., No. 22, 1925

[WIN 1994] Windmar, D
*Water drop initiated discharges in air*
Dissertation Uppsala 1994

[WOL 2010] Wolfgang Hauschild
*High-Voltage Test and Measuring Techniques*
A Tutorial on the Fundamentals and the Actual IEC Standards, 2010

# List of Tables

# List of Figures

# List of Abbreviations

| | |
|---|---|
| AC | Alternating current |
| DC | Direct current |
| FRP | Fiber-reinforced plastic |
| CSM | Charge simulation method |
| FEM | Finite element method |
| BEM | Boundary element method |
| ANN | Artificial neural network |
| CAD | Computer aided design |
| E | Electrical field strength |
| $E_{peak}$ | Peak value of electrical field strength |
| $E_{max}$ | Maximum value of electric field strength |
| USCD | Unified specific creepage distance |
| SPS | Site pollution severity |
| NSDD | Non soluble deposit density |
| SDD | Salt deposit density |
| IEC | International Electrotechnical Commission |
| IEEE | Institute of Electrical and Electronics Engineers |
| HV | High voltage |
| PD | Partial discharge |